Classification: Social Sciences – ANTHROPOLOGY

Early modern human settlement of Europe north of the Alps occurred 43,500 years ago in a cold steppe-type environment

Short title: Europeans occupied 43,500 years ago a cold steppe

Philip R. Nigst[1,2*], Paul Haesaerts[3], Freddy Damblon[3], Christa Frank-Fellner[4], Carolina Mallol[5,6], Bence Viola[1,4,7], Michael Götzinger[8], Laura Niven[1], Gerhard Trnka[9], Jean-Jacques Hublin[1]

Affiliations:
[1]Department of Human Evolution, Max-Planck-Institute for Evolutionary Anthropology, Deutscher Platz 6, 04103 Leipzig, Germany.

[2]Division of Archaeology, Department of Archaeology and Anthropology, University of Cambridge, Downing Street, Cambridge CB2 3DZ, UK.

[3]Department of Paleontology, Royal Belgian Institute of Natural Science, 29 Rue Vautier, 1000 Brussels, Belgium.

[4]Department of Anthropology, University of Vienna, Althanstrasse 14, A-1090 Vienna, Austria.

[5]Departmento de Geografia e Historia, Universidad de La Laguna, Campus de Guajara, La Laguna-38071, Tenerife, Spain.

[6]Instituto Universitario de Bio-Orgánica Antonio Gonzáles, Campus de Guajara, La Laguna-38071, Tenerife, Spain.

[7]Department of Evolutionary Genetics, Max-Planck-Institute for Evolutionary Anthropology, Deutscher Platz 6, 04103 Leipzig, Germany.

[8]Institute of Mineralogy and Crystallography, University of Vienna, Althanstrasse 14, A-1090 Vienna, Austria.

[9]Institute for Prehistoric and Historic Archaeology, University of Vienna, Franz-Klein-Gasse 1, A-1190 Vienna, Austria.

*Corresponding author – contact details:
Dr Philip R Nigst
Division of Archaeology, Department of Archaeology and Anthropology, University of Cambridge, Downing Street, Cambridge CB2 3DZ, UK.
Email: prn25@cam.ac.uk
Tel: +44 (0)1223-333531

Keywords: archaeology - modern humans - climate – Europe

Abstract

The first settlement of Europe by modern humans is thought to have occurred between 50,000 and 40,000 calendar years ago (cal BP). In Europe, modern human remains of this time period are scarce, often not associated with archaeology or originating from old excavations with no contextual information. Hence, the behavior of the first modern humans in Europe is still unknown. Aurignacian assemblages—demonstrably made by modern humans—are commonly used as proxies for the presence of fully behaviorally and anatomically modern humans. The site of Willendorf II (Austria) is well known for its Early Upper Paleolithic horizons, which are among the oldest in Europe. However, their age and attribution to the Aurignacian remain an issue of debate. Here, we show that archaeological horizon 3 (AH 3) consists of faunal remains and Early Aurignacian lithic artifacts. Using stratigraphic, paleoenvironmental, and chronological data, AH 3 is ascribed to the onset of Greenland Interstadial 11, around 43,500 cal BP, and thus is older than any other Aurignacian assemblage. Furthermore, the AH 3 assemblage overlaps with the latest directly radiocarbon-dated Neanderthal remains suggesting that Neanderthal and modern human presence overlapped in Europe for some millennia possibly at rather close geographical range. Most importantly, for the first time we have a high-resolution environmental context for an Early Aurignacian site in Central Europe, demonstrating an early appearance of behaviorally modern humans in a medium cold steppe-type environment with some boreal trees along valleys around 43,500 cal BP.

Significance Statement

Modern humans dispersed into Europe and replaced Neanderthals at least 40,000 years ago. However, the precise timing and climatic context of this dispersal are heavily debated. Therefore, a new project combining paleoenvironmental and archaeological fieldwork has been undertaken at Willendorf II (Austria), a key site for this time period. This project has concluded that modern humans producing Aurignacian stone tools occupied Central Europe about 43,500 years ago in a medium cold steppe environment with some boreal trees along valleys. This discovery represents the oldest well-documented occurrence of behaviorally modern humans in Europe and, in turn, demonstrates contemporaneity with Neanderthals in other parts of Europe, showing that they shared this region longer than previously thought.

\body

Introduction

Modern humans dispersed out of Africa and into western Eurasia at least 50,000 calendar years ago (cal BP) and subsequently replaced all previous hominin species on our planet (1–4). While the route and number of modern human dispersal(s) are an issue of ongoing debate (5), the fact that modern humans and older hominins (including Neanderthals in western Eurasia and Denisovans in Central Asia) met and mixed is strongly suggested by genetic studies (6). For Europe, it is debated when and under which climatic conditions the first anatomically and behaviorally modern humans colonized the continent (2, 7–9).

Fully anatomically modern human fossils older than 35,000 cal BP outside Africa are scarce, often not associated with any archaeology (4) or originating from old excavations with no (or highly biased) contextual information (10, 11). Therefore, their behavior remains unknown. The Aurignacian technocomplex is associated exclusively with modern human remains (12) and therefore can be used as a proxy for modern human presence in Europe (7, 13). Modern humans might have entered Europe earlier, since Bohunician stone tools in Central Europe are considered by some as the material culture correlate of a modern human dispersal into Europe (14–17). However, until now no Bohunician assemblage in Europe is associated with modern human remains. Similarly, Uluzzian stone tools in Italy are claimed to be associated with modern human remains (18), although this association has been questioned (19). Therefore, the Aurignacian is used here as a proxy for anatomically modern human presence. Moreover, the Aurignacian is generally accepted as showing fully modern behavior and it can thus be argued that when evaluating the Aurignacian, we are looking at anatomically and behaviorally modern humans.

Scenarios explaining Neanderthal demise and modern human dispersal are the focus of current discussions. Some argue that Neanderthals were replaced/outcompeted by modern humans due to inherent biological and behavioral differences between the two species (1–3). Others consider climatic change the major cause of Neanderthal extinction, either as a consequence of one particularly severe cold event (20, 21), or a number of cold events resulting in population attrition and finally a terminal decline during a severe cold event (22). Evaluating these scenarios of the Neanderthal-modern human replacement requires data on Neanderthal and modern human technology, subsistence, and settlement patterns but also high-resolution environmental data, chronostratigraphic background, and precise age estimations.

Here, we provide high-resolution environmental and chronological data for modern human occupation in the form of an Early Aurignacian archaeological horizon at Willendorf II, Austria. The site of Willendorf II (48° 19’ 23.50” N, 15° 24’ 15.20” E), an open-air locality in the Danube Valley, preserves a long loess-paleosol sequence with abundant archaeological remains (23, 24). The site was excavated several times between 1908 and 1955 (SI Appendix, SI Text). Since 2006, new excavations have been undertaken (25). The chronological framework of the site rests on over 50 radiocarbon dates produced on charcoal samples dated by the Groningen and Oxford radiocarbon laboratories, placing the sequence between 48,000 and 25,000 radiocarbon years before present (BP) (~55,000 to 29,000 cal BP) (Figure 1, SI Appendix, SI Text, Table S1).

Key to current debates of early modern human settlement in Europe is archaeological horizon (AH) 3. In the past, AH 3 has been attributed to the Early Aurignacian (17, 28–30) based on typical stone tool types (carinated endscraper, nosed endscraper, Aurignacian blade) and the blank production modes (disassociation of blade and bladelet production sequences) (SI

Appendix, Table S2). This classification has been criticized and the possibility that AH 3 represents a transitional assemblage has been raised (31). The old collection (n=48) on which this previous discussion was based has recently been enlarged by the discovery of a box of lithic artifacts from the old excavations. This expanded old collection (n=490) can be securely attributed to the Early Aurignacian (17, 29) (SI Appendix, Table S2 and S3). Our new excavations have reopened the old excavations' trenches, correlated our new main section with the old western section (25), and produced a new lithic assemblage from AH 3. The location of AH 3 in our lithological layer C8-3 is in agreement with descriptions in the old excavations' reports. Importantly, the correlation of new and old collections is proven by several refits (Figure 2, SI Appendix, SI Text) of lithic artifacts from our new assemblage with specimens in the old collections. We also attribute the new collection to the Early Aurignacian based on its lithic technology, as described below.

The archaeological collection

The AH 3 assemblage from the 2006 to 2011 excavations consists of 32 lithic artifacts and 23 faunal remains. The latter comprise fragments smaller than 20 mm and most are burned. The bones are not identifiable to species and their surface preservation hinders an assessment of anthropogenic modifications. It is unclear whether or not the burning is anthropogenic.

All lithic artifacts are made of different varieties of hornstones/cherts that occur in the local Danube gravels. The majority of lithic artifacts is flakes (SI Appendix, Table S4); there are also bladelets, chips, one core tablet, and shattered pieces. In total, five lithic artifacts show exposure to heat in the form of color change, craquelation, and/or irregular breakage surfaces. Unfortunately, these five heated specimens were too small for thermoluminescence dating. All lithic objects have fresh edges, i.e., they are unabraded, and show no traces of rounding or

similar damage typical of post-depositionally reworked assemblages. While 20 specimens show no edge damage, 12 exhibit unifacial damage probably deriving from use. Furthermore, the lithic artifacts vary in size and weight and include small and larger items suggesting no redeposition reflected in typical differential movement of objects of different size (i.e., no size-sorting). This corresponds well with the pedosedimentary data (SI Appendix, SI Text) showing that AH 3 was not affected by large-scale, post-depositional reworking.

The new collection is attributed to the Early Aurignacian based on the bladelet technology. Refitted artifacts between the new and old collection confirm this classification. These refitted artifacts directly connect our new small collection of 32 lithics with the larger collection from the 1908 to 1955 excavations (n=490).

Bladelet technology: AH 3's bladelets demonstrate the presence of two bladelet production schemes both suggesting a disassociation of blade and bladelet technology (for definitions see SI Appendix, SI Text). The bladelet WII-L20-2492 (Figure 2a, SI Appendix, SI Text) is 8.60 mm long, 3.25 mm wide, and 1.16 mm thick, and shows skewing to the right but no twisting. Such morphology is characteristic of a reduction sequence using carinated/nosed endscrapers as cores. This is well documented for the Early and Late Aurignacian in western Europe (32). Interesting in this context is that the length of bladelet WII-L20-2492 is in the lower range of length of the last removals of carinated endscraper-cores from the old collection. This indicates that WII-L20-2492 originated from a carinated endscraper-core of similar size like those represented in the old collection. A second bladelet (WII-M20-640, Figure 2b, SI Appendix, SI Text) is an 8.12 mm long, 4.48 mm wide, and 0.89 mm-thick medial fragment. Its dorsal face demonstrates unidirectional core exploitation. The bladelet fragment shows no skewing or twisting and could belong to a bladelet production utilizing carinated/nosed endscraper-cores, but since it is fragmented and hence lacking some diagnostic landmarks, it

could also belong to other types of bladelet production. A third bladelet (WII-M20-647, Figure 2c, SI Appendix, SI Text) is a medial fragment that is 18.60 mm long, 9.80 mm wide, and 2.31 mm thick. The direction of the dorsal scar, an absence of twisting or skewing, and a rather wide width (9.80 mm) suggest that this bladelet was produced from a unidirectional, prismatic core. Moreover, during systematic refitting studies conducted on the AH 3 lithic collection, WII-M20-647 could be refitted onto the flake WII-M20-623. This is a sequence refit and shows that in addition to WII-M20-647, at least one more bladelet of the same morphology was removed. These are large, straight bladelets without torsion or skewing obtained from a unidirectional, prismatic core. This type of bladelet production is described for early phases of the Aurignacian in western Europe, the Proto-Aurignacian, and Early Aurignacian (32). Taken together, the cooccurrence of these two bladelet production schemes demonstrated by WII-L20-2492 and WII-M20-647 strongly suggests an Early Aurignacian attribution of the small new assemblage. Such a classification is supported by the old collection that also shows the cooccurrence of these two bladelet production schemes (17).

Refitted artifacts: During systematic refitting studies, four lithic artifacts from the 2006 to 2011 collection and three from the 1908 to 1909 collection could be refitted (Figure 2e, SI Appendix, SI Text). From the new collection, bladelet WII-M20-647, flakes WII-M20-623 and WII-M20-641, and core tablet WII-M18-25 (Figure 2d, SI Appendix, SI Text) refit onto a core (WII-95782) and two pieces of shatter (WII-95783 and WII-95784) from the old collection. This refit group supports our classification of the 2006–2011 assemblage as Early Aurignacian for two reasons. First, it demonstrates that the above-mentioned special reduction sequence for producing large bladelets (e.g., WII-M20-647) does not result from the reduction of a larger blade core, and hence shows a disassociation of blade and bladelet production typical of Early Aurignacian (32). This is based on the size of the original nodule (estimated to only ~80 mm) and the amount of cortex on the refitted artifacts, as well as the convexity of

cortical areas. Second, this refit group directly connects our small collection of 32 lithics with the larger collection from the 1908 to 1955 excavations comprising 490 lithics including typical stone tool types (carinated endscraper, nosed endscraper, Aurignacian blade), two specific bladelet production schemes (one using carinated/nosed endscraper-cores, the other small prismatic cores), and a clear disassociation of the blade and bladelet production typical of the Early Aurignacian material culture tradtion (17, 29). Material culture traditions, described by variation in the way tools are made, are learned behaviors that are passed on between generations (14). The Early Aurignacian material culture tradition as defined above differs significantly from that of the Proto-Aurignacian, which is characterized by a bladelet production from reduced larger blade cores resulting in larger bladelets than in the Early Aurignacian.

Age, environmental context, and chronostratigraphic position of the archaeology

The age and chronostratigraphic position of AH 3's Early Aurignacian in lithological layer C8-3 is constrained by a combination of climatostratigraphy and radiocarbon dating. The upper five meters of the sequence show evidence of seven interstadial paleosols separated from each other by loess deposits and tundra gley paleosols, indicative of stadial conditions. Here, we concentrate on the part of the sequence most important for the context of AH 3 (units D3 to C7, Figure 3, SI Appendix, SI Text, Figure S3). A first paleosol is recorded in D2–D1 resting on top of the D3 loess. It is developed in ~1 meter of colluvial deposits with a strong polyhedral structure and biogenic activity (burrows) pointing to a brown boreal soil. This correlates with the boreal mollusc assemblages (SI Appendix, SI Text, Table S5) ascribed to the Willendorf D1 Interstadial (24). A major break occurs on top of D1; the overlying lithological complex C records conditions characterized as cold steppe to medium cold steppe with some boreal trees. Unit C9 demonstrates aeolian input of sandy silt and

development of a tundra gley soil suggesting deep frost or permafrost conditions (34), i.e., periglacial steppe conditions. Later, parts of C9 were eroded prior to the deposition of loamy sediment (C8-3, contains AH 3). C8-3's pedosedimentary and malacological data suggest a slight improvement in climatic conditions (Figure 3, SI Appendix, SI Text, Table S5). Immediately after the deposition of C8-3, a humic horizon of para-rendzina type (C8-2) developed under a medium cold steppe environment with boreal trees in river valleys. No evidence of aeolian sedimentary input (suggesting stadial conditions) or an erosional event (removing such input) was observed between C8-3 and C8-2. This suggests that both units belong to the same interstadial (Schwallenbach Ia Interstadial). After localized erosion and solifluction, a new input of aeolian material (C7) preceded the development of a second weak humic horizon (C7-1), ascribed to the Schwallenbach Ib Interstadial (Figures 1 and 2, SI Appendix, SI Text, Figure S3, Table S5).

Maximum and minimum ages for AH 3 are provided by radiocarbon dates of charcoal from below and above C8-3; the horizon itself contains only scattered small charcoal fragments unsuitable for radiocarbon dating. The directly underlying unit C9 lacks any charcoal; therefore, AH 3's maximum age is provided by radiocarbon dates obtained on charcoal from D1, between 45,000 and 43,000 BP (~48,000 to 46,000 cal BP) (Figure 3, SI Appendix, SI Text, Table S1). AH 3's younger age limit is constrained by dating of *Picea/Larix* charcoal from the overlying C8-2 paleosol to ~39,000 BP (~43,000 cal BP). Based on environmental and radiometric data, the Willendorf D1 Interstadial in D2–D1 can be correlated with Greenland Interstadial (GIS) 12 (35) of the Greenland ice record GRIP ss09sea (36) that shows the best agreement with calibrated ages of radiocarbon dates obtained for D1 (Figure 3, SI Appendix, SI Text, Table S1). Similarly, we correlate the Schwallenbach Ia Interstadial (C8-3 and C8-2) with GIS 11 (SI Appendix, SI Text). This places AH 3 at the onset of GIS 11 at ~43,500 cal BP.

Discussion and Implications

The chronostratigraphic position of AH 3's lithic and faunal assemblages at the onset of GIS 11 (~43,500 cal BP), its cultural attribution to the Early Aurignacian, and its presence in a medium cold steppe environment raise a number of discussion points.

Age and chronostratigraphy. The chronostratigraphic position of AH 3 shows that modern humans were present in Central Europe at least slightly before 43,300 cal BP, at the onset of the cool Schwallenbach Ia Interstadial. This is in strong contrast to "late appearance" models (based on radiocarbon chronology) according to which the Early Aurignacian occurs within an extremely cold event synchronous with the North Atlantic Heinrich Event 4 (19, 37), dated ~40,200 to 38,300 cal BP (SI Appendix, Figure S16). Similarly, models arguing for a first appearance of the Aurignacian after ~41,500 cal BP (31) have to be questioned based on AH 3's age. Comparison with other Aurignacian sites in Central Europe shows that most other sites are younger and technologically different (e.g., Stránská skála, Stratzing and Alberndorf), or chronostratigraphic information is not available due to their excavation decades ago (e.g., Krems-Hundssteig and Senftenberg) (17). Although significantly younger than AH 3, the Early Aurignacian assemblage of Geißenklösterle-AH III (Germany), modelled to between 42,940 and 39,910 cal BP (38), and the Aurignacian bone point of Peskő (Hungary), dated to between 41,730 and 40,265 cal BP (39) (SI Appendix, Figure S16, Table S11), also pre-date the North Atlantic Heinrich Event 4 and, hence, support our "early appearance" model (17).

Environmental conditions. The high paleoenvironmental resolution of the Willendorf II sequence, combined with high-quality radiocarbon dating, provides a unique opportunity to discuss the environmental context of the first anatomically and behaviorally modern humans in Central Europe. Considering the mollusc and charcoal records at Willendorf II, the first

evidence of modern human presence in AH 3 appears in a medium cold steppe with some boreal trees along the Danube. In fact, when trying to compare our datasets with those of other sites, the scarcity of high-resolution environmental datasets for the time period of modern human dispersal into Europe becomes evident. The vast majority of currently available information on environmental or climatic context of this dispersal is inferred from calibrated radiocarbon dates and their correlation with the Greenland Ice records (10, 19, 38), rather than from independent environmental datasets. The problem with such an approach is that ages provided by radiocarbon dating (even when modeled [38]) often overlap with more than one climatic event, i.e., at least one warm interstadial and one cold stadial. Therefore, such an approach can only provide very low-resolution environmental data. Additionally, the resulting environmental context only provides information about temperature ($\delta^{18}O$ data of the ice record). Key factors for changes in the environment include moisture and nutrient availability rather than temperature alone (40). Moisture and nutrient availability are of crucial importance for animal abundance and diversity, especially for large herbivores (41). Similarly, one can argue that late Neanderthal and modern human settlement and survival were constrained by such factors (42).

Our environmental data indicating a medium cold steppe with boreal trees are in contrast with the few other available studies. For Western and Central Europe, two conflicting scenarios have been proposed. One assumes that the Aurignacian first appeared under very cold conditions, i.e., the Heinrich 4 (H4) event (19, 37, 43). Such a scenario for Central Europe is quite unlikely based on both AH 3's chronostratigraphic position and the environmental data. The second scenario proposes that Aurignacian modern humans in Western Europe first appeared during a period of climatic warming, e.g., GIS 10 or 11 (2), under at least partially wooded conditions as opposed to colder, open tundra, or steppe conditions (44). It has also been argued that these environmental conditions were similar to those of the warmer, more

forested regions of southeastern Europe and, hence, that Early Aurignacian modern humans might have come from southeastern Europe tracking these environments as they expanded further north and west (2, 45). This is in stark contrast to our central European data showing modern human presence in a medium cold steppe environment. If the pattern for Western and Southern Europe holds true, this would suggest that the first modern humans in Europe were well-adapted to a variety of environments (i.e., both warm forest [Western and Southern Europe], and cold steppe [Central Europe]). Their occurrence in such different environmental settings suggests flexibility and resilience rather than specialization or focus on a single type of environment.

Implications. The attribution of AH 3 to the Early Aurignacian and its chronostratigraphic position have implications for the taxonomic and chronological relationship of the two early phases of the Aurignacian (Proto-Aurignacian and Early Aurignacian). Until now, it has been argued the Proto-Aurignacian is older than the Early Aurignacian, i.e., that differences between the two phases are solely a factor of time (19, 30, 32). AH 3 shows that, at least for Central Europe, this is not valid. The AH 3 Early Aurignacian overlaps with the first Proto-Aurignacian assemblages (46, 47) elsewhere in Europe (SI Appendix, Figure S17). This suggests that the Proto- and Early Aurignacian might represent different developmental trajectories of modern humans foraging within Europe. A cultural interpretation of this distinction might be that the Proto-Aurignacian and Early Aurignacian represent the southern and northern dispersal routes, respectively, of modern humans within Europe (2). Alternatively, the differences between the Proto- and Early Aurignacian could relate to the exploitation of specific foraging niches requiring different food acquisition technologies. One should in the future also consider factors like site function, occupation density, and adaptation to particular environments, e.g., seasonally different mobility of populations in the Mediterranean eco-zone and in the cold steppe-type conditions at Willendorf II, when

explaining the differences between Proto- and Early Aurignacian (7, 13, 17, 46).

The ~43,500 cal BP age of AH 3 has significant implications for the appearance of behaviorally modern humans in Europe and their potential contact with Neanderthals. AH 3 predates the oldest directly dated modern human remains in Europe (SI Appendix, Figure S18) and all other Early Aurignacian assemblages (SI Appendix, Figure S9). Thus, it pushes back the presence of modern humans in Central Europe to at least ~43,500 cal BP. Based on the correlation of the Bohunice soil in southern Moravia with GIS 12 (35, 48), the Bohunician of the Middle Danube region is interpreted as evidence of modern human presence there in GIS 12 (3, 14–16, 20) or predating GIS 12 (17). Until now, no modern human remains have been discovered in association with this industry. In addition, the Bohunician, in contrast to the Aurignacian (38), has not yet yielded clear evidence of a fully "modern" material culture including evidence of symbolic artifacts, although this may in part be related to taphonomic factors. Currently, behaviorally modern humans are first documented with the Central European Aurignacian and potentially with the Italian Uluzzian (18), although the association between the modern human teeth and Uluzzian artifacts has been questioned (19). However, the age of AH 3 overlaps or pre-dates the latest directly dated Neanderthal remains (49, 50) (SI Appendix, Figure S19), and thus suggests direct or indirect contact between the two species on a European scale, potentially leading to interbreeding and acculturation. The evidence presented here shows that behaviorally modern humans occupied Central Europe in an environment characterized as medium cold steppe with some boreal trees. This offers the first, high-resolution environmental record for early modern human settlement of Europe and when compared with other available data, suggests that modern humans occupying Europe ~43,500 cal BP were well adapted to a variety of environmental conditions.

Methods

The fieldwork methodology at Willendorf II involved excavation of loessic deposits and the recording of the stratigraphic context as well as the three-dimensional position of all objects ≥5 mm. Charcoal for dating was sampled according to a special protocol, including sampling from freshly cleaned vertical sections to control the microstratigraphic position of each sample precisely. A full description of our fieldwork and sampling methodology is provided in the SI Appendix.

For the analysis of lithic artifacts, attribute analysis was applied and reduction sequences were reconstructed. Faunal analysis included specimen identification, examination of bone surfaces for anthropogenic and natural modifications, and classification of burning stages. Charcoal was dried, cleaned and identified; only *Pinus cembra*-type, *Picea, Picea/Larix* or *Larix*-type charcoal was used for radiocarbon dating with ABA and ABOx-SC pretreatment in the Groningen and Oxford AMS laboratories. Site formation processes were assessed by a combination of geological, geoarchaeological (including micromorphology), and microstratigraphic analyses. GIS analysis of three-dimensionally recorded objects was carried out, as well as fabric analysis on archaeological objects. Paleoenvironmental reconstruction is based on the pedosedimentary signature of the deposits and the rich charcoal material and mollusc fauna. Our approach to chronostratigraphy combines litho- and climatostratigraphic work with a robust chronological framework based on reliable radiocarbon dates. A detailed explanation of our laboratory methodology is provided in the SI Appendix.

Acknowledgements

We thank the Austrian Antiquity Authority (Bundesdenkmalamt, Abteilung für Bodendenkmale) and the site's landowner (2006–2007: ÖBB Infrastruktur AG, Liegenschaftsverwaltung, H. Scheibner; 2008–2011: Marktgemeinde Aggsbach, H. Gerstbauer) for the fieldwork permit. We also thank the Leakey Foundation (2006–2012),

Max Planck Society (2006–2012), University of Vienna (2006–2011), Hugo Obermaier Society (2006), Federal Office for Scientific Affairs of the State of Belgium (projects Sc-004, Sc-09, MO/36/021), and the Hochschuljubiläumsfonds of the City of Vienna (2007) for funding our research. Until 2009 B.V. has been funded by the Rat für Forschung und Technologieentwicklung (project GZ 200.093/3-VI/1/04, PI Prof H. Seidler). We further acknowledge the support of the Department of Prehistory (Natural History Museum, Vienna, Austria; W. Antl-Weiser), Marktgemeinde Aggsbach (H. Gerstbauer), Museumsverein Willendorf (K. Kappelmüller), and the Satzl and Perzl families. Many thanks to D. M. Bosch, E. Dermience, R. Farbstein, C.N. Moore, V. Schmid, A. Sonnberger, A. Stadlmayr, S. Stelzer, L. Viola, and our student excavators for field/laboratory assistance. We thank W. Antl-Weiser, D.M. Bosch, P.A. Mellars, S.P. McPherron, L. Moreau, D. Richter, M. Roussel, H. Seidler, M. Soressi, C. Stimpson, and N. Zwyns for discussions of the archaeological evidence and J. van der Plicht, T. Higham, and S. Talamo for discussion of the radiocarbon dates.

Author contributions

P.R.N. and B.V. designed research and analyzed data; P.H. collected and analyzed lithostratigraphic and pedo-sedimentary data; F.D. analyzed charcoal; C.F.F. performed malacological analysis; C.M. analysed micromorphological data; P.R.N. collected and analyzed lithic data; P.R.N., M.G. and G.T. performed lithic raw material analysis; L.N. collected and analyzed faunal data; P.R.N., P.H. and F.D. wrote the initial draft of this paper; All authors contributed to and helped to edit the final manuscript.

References

1. Klein RG (2008) Out of Africa and the evolution of human behavior. *Evolutionary Anthropology* 17(6):267–281.
2. Mellars P (2006) Archeology and the dispersal of modern humans in Europe: Deconstructing the "Aurignacian". *Evolutionary Anthropology* 15:167–182.
3. Hublin JJ (2012) The earliest modern human colonization of Europe. *Proc Natl Acad Sci USA* 109:13471–13472.
4. Trinkaus E, et al. (2003) An early modern human from the Peştera cu Oase, Romania. *Proc Natl Acad Sci USA* 100(20):11231–11236.
5. Reyes-Centeno H, et al. (2014) Genomic and cranial phenotype data support multiple modern human dispersals from Africa and a southern route into Asia. *Proc Natl Acad Sci USA* 111(20):7248–7253.
6. Prüfer K, et al (2013) The complete genome sequence of a Neanderthal from the Altai Mountains. *Nature* 505:43–49.
7. Davies W (2001) A Very Model of a Modern Human Industry: New Perspectives on the Origins and Spread of the Aurignacian in Europe. *Proceedings of the Prehistoric Society* 67:195–217.
8. Zilhão J, d'Errico F (2003) *The Chronology of the Aurignacian and of the Transitional Technocomplexes: Dating, Stratigraphies, Cultural Implications* (Instituto Portueguês de Arqueologia, Lisbon).
9. Conard NJ (2006) *When Neanderthals and Modern Humans Met* (Kerns Verlag, Tübingen).
10. Higham T, et al. (2011) The earliest evidence for anatomically modern humans in northwestern Europe. *Nature* 479:521–524.

11. White M, Pettitt P (2012) Ancient Digs and Modern Myths: The Age and Context of the Kent's Cavern 4 Maxilla and the Earliest Homo sapiens Specimens in Europe. *European Journal of Archaeology* 15:392–420.

12. Hublin JJ (2013) The Makers of the Early Upper Palaeolithic in Western Eurasia. *The Origins of Modern Humans: Biology Reconsidered*, eds Smith FH, Ahern JCM (Wiley-Blackwell, Hoboken, New Jersey), pp 223–252.

13. Davies W (2007) Re-evaluating the Aurignacian as an Expression of Modern Human Mobility and Dispersal. *Rethinking the human revolution: new behavioural and biological perspectives on the origin and dispersal of modern humans*, eds Mellars P, Boyle K, Bar-Yosef O, Stringer C (McDonald Institute for Archaeological Research, University of Cambridge, Cambridge), pp 263–274.

14. Tostevin GB (2012) *Seeing Lithics: A Middle-Range Theory for Testing for Cultural Transmission in the Pleistocene* (Oxbow Books, Oxford).

15. Bar-Yosef O (2006) Neanderthals and Modern Humans: A Different Interpretation. *When Neanderthals and Modern Humans Met*, ed Conard NJ (Kerns Verlag, Tübingen), pp 467–482.

16. Hoffecker JF (2009) The spread of modern humans in Europe. *Proc Natl Acad Sci USA* 106:16040–16045.

17. Nigst PR (2012) *The Early Upper Palaeolithic of the Middle Danube Region* (Leiden University Press, Leiden).

18. Benazzi S, et al. (2011) Early dispersal of modern humans in Europe and implications for Neanderthal behaviour. *Nature* 479:525–528.

19. Banks WE, d'Errico F, Zilhão J (2012) Human–climate interaction during the Early Upper Paleolithic: testing the hypothesis of an adaptive shift between the Proto-Aurignacian and the Early Aurignacian. *Journal of Human Evolution* 64:39–55.

20. Müller UC, et al. (2011) The role of climate in the spread of modern humans into Europe. *Quaternary Science Reviews* 30:273–279.

21. Zilhão J (2006) Genes, Fossils, and Culture. An Overview of the Evidence for Neandertal-Modern Human Interaction and Admixture. *Proceedings of the Prehistoric Society* 72:1–20.

22. Tzedakis PC, Hughen KA, Cacho I, Harvati K (2007) Placing late Neanderthals in a climatic context. *Nature* 449:206–208.

23. Felgenhauer F (1959) *Willendorf in der Wachau. Monographie der Paläolith-Fundstellen I–VII* (Rohrer, Vienna).

24. Haesaerts P, Damblon F, Bachner M, Trnka G (1996) Revised stratigraphy and chronology of the Willendorf II sequence, Lower Austria. *Archaeologia Austriaca* 80:25–42.

25. Nigst PR, et al. (2008) New research on the Aurignacian of Central Europe: A first note on the 2006 fieldwork at Willendorf II. *Quartär* 55:9–15.

26. Reimer P, et al. (2013) IntCal13 and Marine13 radiocarbon age calibration curves 0-50,000 years cal BP. *Radiocarbon* 55:1869–1887.

27. Bronk Ramsey C (2009) Bayesian analysis of radiocarbon dates. *Radiocarbon* 51:337–360.

28. Hahn J (1977) *Aurignacien: Das ältere Jungpaläolithikum in Mittel- und Osteuropa* (Böhlau Verlag, Köln).

29. Nigst PR (2006) The first modern humans in the Middle Danube Area? New Evidence from Willendorf II (Eastern Austria). *When Neanderthals and Modern Humans Met,* ed Conard NJ (Kerns Verlag, Tübingen), pp 269–304.

30. Teyssandier N (2007) *En route vers l'Ouest: Les débuts de l'Aurignacien en Europe* (John and Erica Hedges Ltd., Oxford).

31. Zilhão J, d'Errico F (1999) The Chronology and Taphonomy of the Earliest Aurignacian and Its Implications for the Understanding of Neandertal Extinction. *Journal of World Prehistory* 13:1–68

32. Le Brun-Ricalens F, Bordes JG, Bon F (2005) *Productions lamellaires attribuées à l'Aurignacien: chaînes opératoires et perspectives technoculturelles* (Musée national d'histoire et d'art, Luxembourg).

33. Haesaerts P, Damblon F, Nigst P, Hublin JJ (2013) ABA and ABOx Radiocarbon Cross-Dating on Charcoal from Middle Pleniglacial Loess Deposits in Austria, Moravia, and Western Ukraine. *Radiocarbon* 55:641–647.

34. Haesaerts P (1983) Stratigraphic distribution of periglacial features indicative of permafrost in the Upper Pleistocene loesses of Belgium. *Permafrost. Fourth International Conference: Proceedings* (National Academy Press, Washington D.C.), pp 421–426.

35. Haesaerts P, et al. (2009) Climatic signature and radiocarbon chronology of Middle and Late Pleniglacial loess from Eurasia: comparison with the marine and Greenland records. *Radiocarbon* 51:301–318.

36. Johnsen SJ, et al. (2001) Oxygen isotope and palaeotemperature records from six Greenland ice-core stations: Camp Century, Dye-3, GRIP, GISP2, Renland and NorthGRIP. *Journal of Quaternary Science* 16:299–307.

37. Jöris O, Street M (2008) At the end of the 14C time scale—the Middle to Upper Paleolithic record of western Eurasia. *Journal of Human Evolution* 55:782–802.

38. Higham T, et al. (2012) Testing models for the beginnings of the Aurignacian and the advent of figurative art and music: The radiocarbon chronology of Geißenklösterle. *Journal of Human Evolution* 62:664–676.

39. Davies W, Hedges R (2008) Dating a type site: Fitting Szeleta cave into its regional chronometric context. *Praehistoria 9–10*:35–45.

40. Guthrie RD, Kolfschoten TV (2000) Neither warm and moist, nor cold and arid: the ecology of the Mid Upper Palaeolithic. *Hunters of the Golden Age. The Mid Upper Palaeolithic of Eurasia 30,000 - 20,000 bp*, ed Roebroeks W, Mussi M, Svoboda J, Fennema K (Leiden University, Leiden), pp 13–20.

41. Olff H, Ritchie ME, Prins HHT (2002) Global environmental controls of diversity in large herbivores. *Nature* 415:901–904.

42. Verpoorte A (2009) Limiting factors on early modern human dispersals: The human biogeography of late Pleniglacial Europe. *Quaternary International* 201:77–85.

43. Conard NJ, Bolus M, Goldberg P, Münzel SC (2006) The Last Neanderthals and First Modern Humans in the Swabian Jura. *When Neanderthals and Modern Humans Met*, ed Conard NJ (Kerns Verlag, Tübingen), pp 305–341.

44. van Andel TH, Davies W (2003) *Neanderthals and modern humans in the European landscape during the last glaciation: archaeological results of the Stage 3 Project* (McDonald Institute for Archaeological Research, University of Cambridge, Cambridge).

45. Mellars P (1998) The impact of climatic changes on the demography of late Neandertal and early anatomically modern populations in Europe. *Neandertals and Modern Humans in Western Asia*, eds Akazawa T, Aoki K, Bar-Yosef O (Plenum Press, New York), pp 493–507.

46. Szmidt CC, Normand C, Burr GS, Hodgins GW, LaMotta S (2010) AMS 14C dating the Protoaurignacian/Early Aurignacian of Isturitz, France. Implications for Neanderthal-modern human interaction and the timing of technical and cultural innovations in Europe. *Journal of Archaeological Science* 37:758–768.

47. Douka K, Grimaldi S, Boschian G, Lucchese AD, Higham TF (2012) A new chronostratigraphic framework for the Upper Palaeolithic of Riparo Mochi (Italy). *Journal of Human Evolution* 62:286–299.

48. Valoch K (2008) Brno-Bohunice, eponymous Bohunician site: new data, new ideas. *Man - Millennia - Environment. Studies in Honour of Romuald Schild*, eds Sulgotowska Z, Tomaszewski J (Polish Academy of Sciences, Warsaw), pp 225–236.

49. Semal P, et al (2009) New data on the late Neandertals: Direct dating of the Belgian Spy fossils. *American Journal of Physical Anthropology* 138:421–428.

50. Hublin JJ, et al. (2012) Radiocarbon dates from the Grotte du Renne and Saint-Césaire support a Neandertal origin for the Châtelperronian. *Proc Natl Acad Sci USA* 109:18743–18748.

Figure Legends

Figure 1: Stratigraphic column of the Willendorf II sequence showing the position of archaeological horizons (AH) 3 to 9, pedological features (A1=humic horizon, Bw=incipient B horizon, TGl=tundra gley), stratigraphic position of radiocarbon dates obtained on charcoal (shown in ka BP; SI Appendix, Table S1), paleoenvironmental reconstruction (PS=periglacial steppe, CS=cold steppe, CS[B]=medium cold steppe with some boreal trees along valleys, B=boreal), and the interstadials (brown font) documented at Willendorf II. Calibration of radiocarbon ages using IntCal13 calibration curve (26) and OxCal 4.2.3 software (27). Key to graphic symbols: SI Appendix, Figure S20.

Figure 2: Lithic artifacts of archaeological horizon 3 (AH 3) at Willendorf II. a) Bladelet WII-L20-2492. b) Bladelet fragment WII-M20-640. c) Bladelet fragment WII-M20-647. d) Core tablet WII-M18-25. e) Refitted lithic artifacts of the new collection (yellow outline; WII-M18-25, WII-M20-623, WII-M20-647) and the old collection (no outline). Scale bar in all images: 10.00 mm. Images a–d were created from three-dimensional models of the lithics (SI Appendix, SI Text). Key to graphic symbols: SI Appendix, Figure S21.

Figure 3: Correlation of the lower part of the Willendorf II sequence and the Greenland ice-core climatic data showing the chronostratigraphic position of archaeological horizon 3 (AH3) at the onset of GIS 11. Shown are the lithostratigraphy, the position of AH3 and AH3ab, malacological data (SI Appendix, Tables S5 and S6; numbers right of the bars: sample IDs in Tables S5 and S6), paleoenvironment (PS=periglacial steppe, CS=cold steppe, CS[B]=medium cold steppe with some boreal trees along valleys, B=boreal), radiocarbon dates (in uncal ka BP; grouped by radiocarbon laboratory and sample pre-treatment;

GrA=Groningen radiocarbon laboratory, OxA=Oxford radiocarbon laboratory; cross-dating: radiocarbon dates on the same, homogenized sample (33)), interstadials defined at Willendorf II, correlation with the GRIP ss09sea data (H5 = Heinrich event 5), and calibrated radiocarbon ages (in ka cal BP; SI Appendix, Table S1) for the samples with ABOx-SC pre-treatment. Calibration of radiocarbon ages using IntCal13 calibration curve (26) and OxCal 4.2.3 software (27). Key to graphic symbols: SI Appendix, Figure S20.

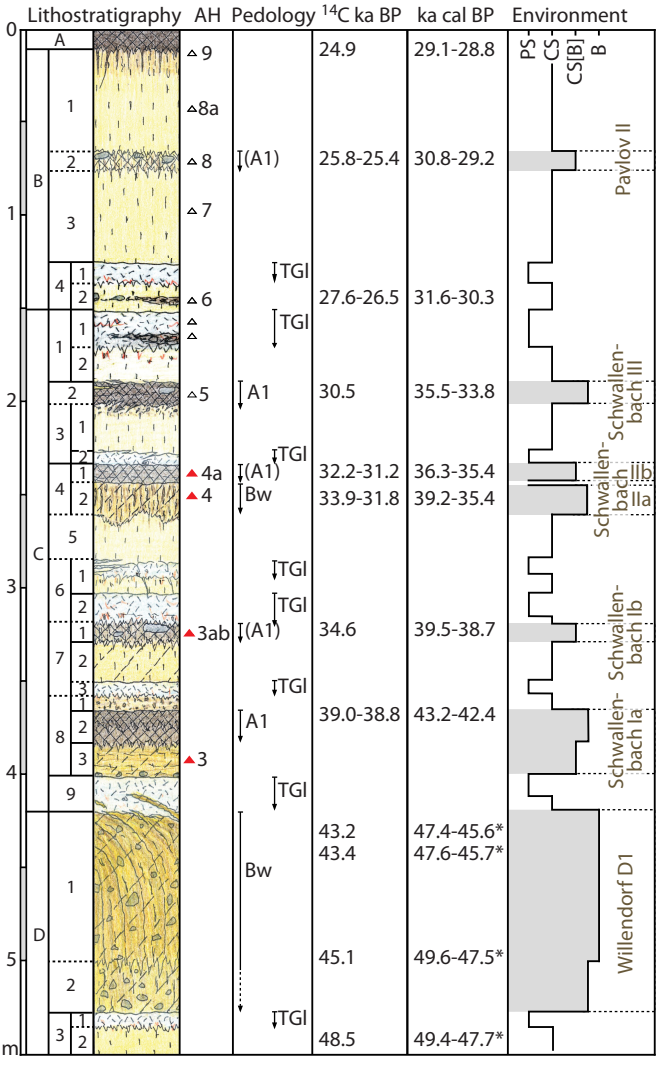
Lithostratigraphy
AH
Pedology
14C ka BP
ka cal BP
Environment
PS
CS
CS[B]
B
0
1
2
3
4
5
m
A
B
C
D
9
8a
8
7
6
5
4a
4
3ab
3
TGI
A1
(A1)
Bw
24.9
25.8-25.4
27.6-26.5
30.5
32.2-31.2
33.9-31.8
34.6
39.0-38.8
43.2
43.4
45.1
48.5
29.1-28.8
30.8-29.2
31.6-30.3
35.5-33.8
36.3-35.4
39.2-35.4
39.5-38.7
43.2-42.4
47.4-45.6*
47.6-45.7*
49.6-47.5*
49.4-47.7*
Pavlov II
Schwallen-bach III
Schwallen-bach IIb
Schwallen-bach IIa
Schwallen-bach Ib
Schwallen-bach Ia
Willendorf D1

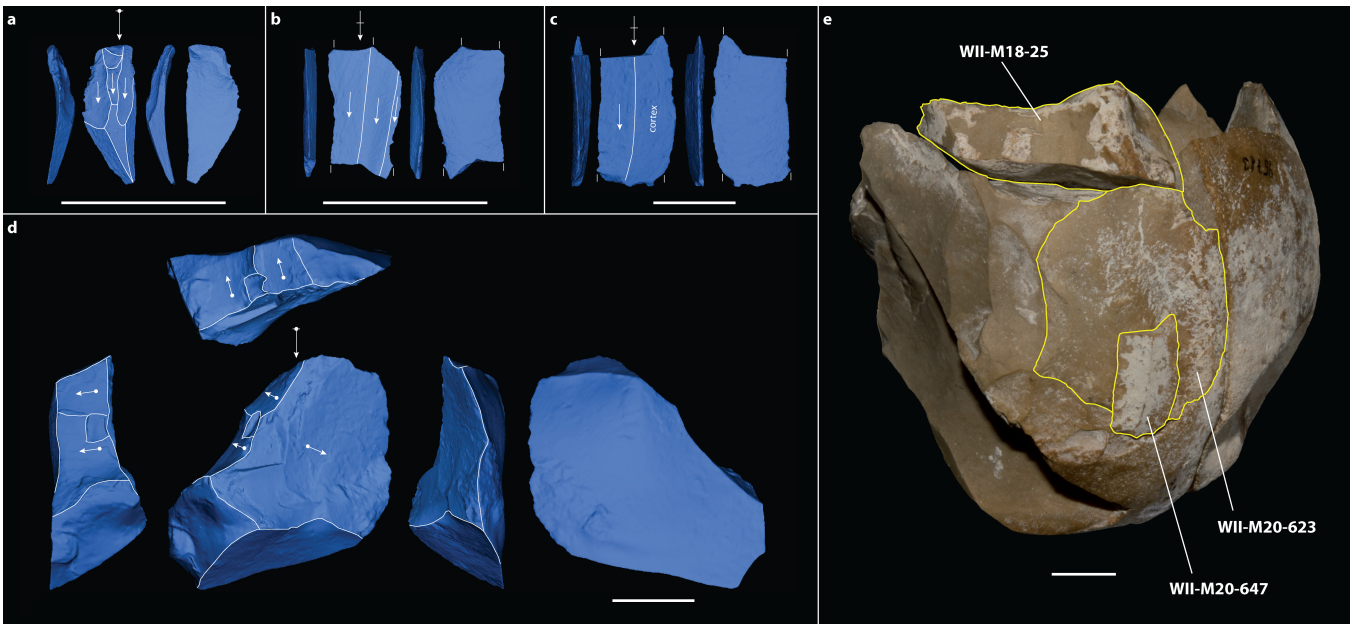
a
b
c
cortex
d
e
WII-M18-25
WII-M20-623
WII-M20-647

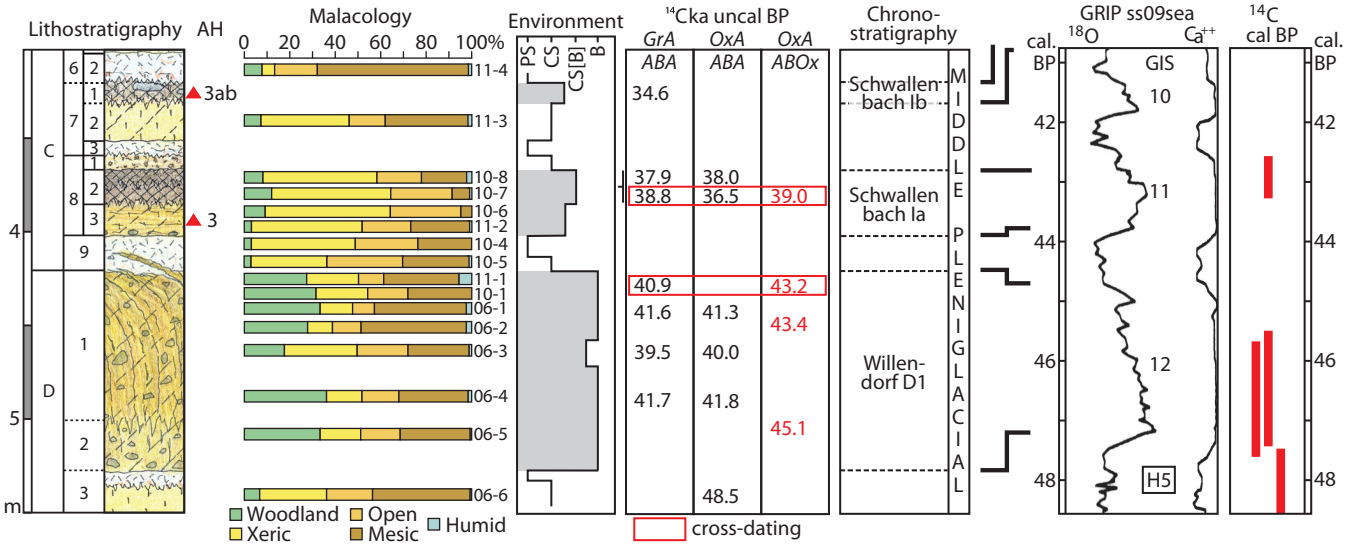
Lithostratigraphy
AH
Malacology
Environment
14Cka uncal BP
Chrono-stratigraphy
GRIP ss09sea
14C cal BP
cal. BP
18O
Ca++
GIS
10
11
12
H5
3ab
3
C
D
4
5
m
6
7
8
9
1
2
3
0 20 40 60 80 100%
11-4
11-3
10-8
10-7
10-6
11-2
10-4
10-5
11-1
10-1
06-1
06-2
06-3
06-4
06-5
06-6
PS
CS
CS[B]
B
GrA
OxA
OxA
ABA
ABA
ABOx
34.6
37.9
38.8
38.0
36.5
39.0
40.9
43.2
41.6
41.3
43.4
39.5
40.0
41.7
41.8
45.1
48.5
Schwallen-bach Ib
Schwallen-bach Ia
Willen-dorf D1
MIDDLE PLENIGLACIAL
42
44
46
48
Woodland
Xeric
Open
Mesic
Humid
cross-dating

Supporting Information

Early modern human settlement of Europe north of the Alps occurred 43,500 years ago in a cold steppe-type environment

Philip R. Nigst[1,2*], Paul Haesaerts[3], Freddy Damblon[3], Christa Frank-Fellner[4], Carolina Mallol[5,6], Bence Viola[1,4,7], Michael Götzinger[8], Laura Niven[1], Gerhard Trnka[9], Jean-Jacques Hublin[1]

Affiliations:

[1]Department of Human Evolution, Max-Planck-Institute for Evolutionary Anthropology, Leipzig, Germany.

[2]Division of Archaeology, Department of Archaeology and Anthropology, University of Cambridge, Cambridge, UK.

[3]Department of Paleontology, Royal Belgian Institute of Natural Science, Brussels, Belgium.

[4]Department of Anthropology, University of Vienna, Vienna, Austria.

[5]Departmento de Geografia e Historia, Universidad de La Laguna, Tenerife, Spain.

[6]Instituto Universitario de Bio-Orgánica Antonio Gonzáles, Tenerife, Spain.

[7]Department of Evolutionary Genetics, Max-Planck-Institute for Evolutionary Anthropology, Leipzig, Germany.

[8]Institute of Mineralogy and Crystallography, University of Vienna, Vienna, Austria.

[9]Department of Prehistoric and Historic Archaeology, University of Vienna, Vienna, Austria.

*Corresponding author: prn25@cam.ac.uk

Table of Contents

SI Text

1 Site background

The site of Willendorf II is situated in the Danube valley, about 80 km west of Vienna (Austria), at a place where the river cuts a narrow and deep valley into the Paleozoic Bohemian Massif. Willendorf II, on the left bank of the Danube, belongs to a cluster of eight Paleolithic sites (Willendorf I, Willendorf I-Nord, and Willendorf II to VII) (1-4). The loess deposits of Willendorf II lie on top of a lower terrace of the Danube. The archeological horizons (AH) are found in the upper half of the about 20 m thick loess deposits.

Willendorf II was first mentioned as a Paleolithic site in the second half of the 19th century (1, 4). The first scientific excavation at Willendorf II was conducted in the summer of 1908 (J. Szombathy, H. Obermaier, and J. Bayer); during this work, the Venus I figurine was discovered. More excavations followed in 1909, 1912/13, 1926/27, and 1955 (1, 4). In 1981 and then again in 1993, geological fieldwork was conducted (P. Haesaerts, G. Trnka) (2, 5, 6). Since 2006, our team has been removing large volumes of backdirt from these old excavations. We have been exposing the entire sequence, including the lower part up to now only excavated in 1909 (3, 4). Our excavation strategy involves excavating back the old excavation's western section (the only remaining part of the site) and by moving it further into the slope. We excavated six trenches (excavation zones 01 to 06; Figure S1) of which all directly connect to previous fieldwork, which makes correlation of the geological deposits and archeological horizons straightforward (3).

2 Methods

2.1 Fieldwork methodology

During our fieldwork, we apply the highest standard methods for Paleolithic excavations. We employ an excavation methodology and documentation process based on piece-plotting all objects and detailed recording of their stratigraphic context[3]. Our excavation methodology involves excavating in stratigraphic units, which are also geological units, sub-units and horizons. Geological units (e.g. Unit C) are subdivided in sub-units (e.g. C8) and these further into horizons (e.g. C8-2). Archeological horizons (AH) are labeled separately and one AH cannot span over more than one geological horizon, while one geological unit, sub-unit or horizon can contain several AHs. Within each stratigraphic unit, we are using the documentation unit concept (7) for exposing finds: all objects ≥ 5 mm are left in place and recorded individually by a total station. We measure one point in the center of each object after it is removed. Two points are recorded on elongated objects: one point at each end of the long axis. This information is later used for fabric analysis (8-12). Larger objects are drawn from rectified photographs (7). All finds are assigned a unique ID number. Within stratigraphic units, sediment is collected per quarter-square meter in arbitrary spits, i.e. the documentation units mentioned above. Normally, these are less than 1cm thick; the maximum thickness is defined as 2.5 cm. The sediment collected is wet-sieved (1.2 mm mesh) for recovering the smallest fractions. In difficult stratigraphic situations, we employ vertical excavation to have maximum control over the micro-stratigraphic position of each find object or sample. Analysis of stratigraphy, lithological record and pedosedimentary description of the excavated deposits is done in the field by the quaternary geologist together with the archeologists.

Large parts of the documentation process are digital (3, 7), supplemented by diaries, situational sketches and field drawings. All measured points (find locations, ground control points for rectifying digital photographs, surface and outline points of features, sample locations, etc.) are coded and stored in a handheld computer running EDM Mobile software (www.oldstoneage.com/technology) (13). All additional information (point type, find category, stratigraphic unit, archeological horizon, etc.) is recorded in that device as well. These data are synchronized with a Microsoft Access database.

Charcoal used for dating is collected in the field in two ways. All charcoal fragments >5 mm encountered during the excavation are three-dimensionally recorded using the above described system, assigned a unique ID number and packed separately. Additionally, charcoal is collected from freshly cleaned vertical sections by the quaternary geologist ensuring tight control over the microstratigraphic position of each sample and to observe each sample's location in relation to the lithology and geometry of the deposits. This is of primary importance to ensure a reliable connection between the pedosedimentary event and the material for dating. All charcoal samples are collected with their surrounding sediment in order to protect the sample during transport.

Soil micromorphology samples are described sedimentologically, and their stratigraphic context recorded by drawing and photographs; then, the samples are cut out from the stratigraphic profile, mapped using a total station and carefully removed as blocks of undisturbed, oriented sediment. Samples are cut out of the section using a knife (Opinel n°12) and the top is marked on the sample. Each sample receives a unique ID and is wrapped in newspaper and aluminum foil.

2.2 Laboratory methodology

Lithic artifacts are described using standard metric and technological attributes (14-16) as well as standard tool types (17). Lithic technology is analyzed using a reduction sequence and attribute analysis approach (14, 16, 18). Raw material analysis includes macroscopic description (and microscopic analysis where necessary) and a detailed raw material comparison collection (Vienna Lithotheque, Institute of Prehistoric and Historic Archaeology, University of Vienna). Nodule analysis (refitting and attribution of lithics to hypothetical nodules) (18-20) is used to assess raw material economy, technology, and settlement dynamics.

Lithic blank types follow standard definitions (see [18] for a summary); “blades” and “bladelets” are defined here because of their importance in our argumentation regarding the cultural classification of the AH 3 assemblage. “Blades” are defined as blanks with a length/width-ratio of >2.0, a morphological axis of the blank parallel to the knapping direction, and more or less parallel edges. “Bladelets” are blades with a maximum width ≤ 10.00 mm. This definition includes microblades as used by many colleagues working in Eastern Europe and Asia, as well as microblades as used in Paleoindian contexts in North America.

Analysis of faunal remains follows standard zooarcheological methodologies. In particular, each bone specimen is documented employing the tripartite “element, portion, segment” coding format (21). This system is beneficial in that each tier records information at an increasingly detailed level. Quantification of remains involves the Number of Identified Specimens (NISP), which includes finds identified to taxon (22). Indeterminate specimens are quantified by Number (N). Bone surfaces are examined under a powerful light source with the aid of 10x magnification in order to identify natural traces such as sediment scratches, root etching, and carnivore tooth

marks; and anthropogenic modifications like stone tool cut marks, hammerstone impacts, chopping, or scraping. Weathering stages (following (23)) are recorded on cortical bone surfaces whenever possible.

Charcoal samples collected in the field are dried and then dispersed in water, sieved at 1.0 mm, 0.5 mm and 0.25 mm, chemically treated with HF and HCl, and subsequently rinsed in distilled water following the methodology by Damblon (24-26). This also involves potential supplementary treatment with aqua regia (HNO_3 + 3 HCl) to remove iron oxides and hydroxides, and the removal of contaminants like rootlets under the binocular and microscope. In the next step, charcoal is identified to at least genus level; only well preserved and identifiable conifer charcoal fragments are used for radiocarbon dating. Charcoal identification also allows assessment of the homogeneity and coherence of the samples. Willendorf II samples consist of *Picea*, *Picea/Larix, Larix*-type or *Pinus cembra*-type only, demonstrating the homogeneity and coherence of the charcoal samples. Here, the charcoal samples selected for radiocarbon dating contain the same taxa. While some samples are made of only one piece of charcoal, the majority of our samples consist of several charcoal fragments. They originate from the same small area and never from more than 10 cm distance to the nearest section that has been documented by a quaternary geologist. When dealing with several large charcoal fragments in one sample, we homogenize (27) the sample, i.e. breaking larger pieces into a size of approximately 2-3 mm and mix the sample well. This guarantees that the radiocarbon laboratory cannot preferentially select larger pieces from our submitted sample and consequently biasing the results towards better-preserved or less-fragmented pieces.

For two samples older than 34 ka BP, cross-dating between the Groningen and Oxford laboratories is applied in order to compare results from ABA and ABOx-SC pre-

treatments (27). For this purpose, we sub-sampled homogenized charcoal material for acid-base-acid (ABA) pretreatment in Groningen and acid-base-oxidation stepped combustion (ABOx-SC) pre-treatment in Oxford.

Sample pretreatment for radiocarbon dating was executed by the radiocarbon laboratories of University of Groningen (Centrum voor Isotopen Onderzoek) and University of Oxford (Oxford Radiocarbon Accelerator Unit). Pretreatment followed ABA and ABOx-SC protocols (27-30). All measurements were done using AMS at the two laboratories in Groningen and Oxford. The radiocarbon ages were calibrated using the IntCal13 (31) calibration curve and OxCal 4.2.3 software (32).

Assessment of site formation processes includes detailed GIS analysis of three-dimensionally piece-plotted objects, fabric analysis applied to archeological objects (as the loess deposits do not contain sufficient numbers of natural elongated objects), detailed analysis of the pedosedimentary signature of the deposits, and soil micromorphological analysis. Additionally, taphonomic analysis including refitting, edge damage and surface weathering of faunal remains and lithic artifacts is considered.

Blocks recovered for micromorphological/geoarcheological analysis are hardened using an unpromoted resin mix and thin section manufacture is performed by the CNRS-UMR 5198 Sedimentology Laboratory, Tautavel, France (140 x 65 mm thin sections), Spectrum Petrographics Inc, Vancouver, USA (75 x 50 mm thin sections) and Thomas Beckmann, Germany (90 x 60 mm thin sections). All slides are trimmed to 30 μm in thickness. Microscopic observation of the thin sections is carried out using a polarizing microscope under plane polarized (PPL) and crossed polarized light (XPL) with magnifications ranging from 20X to 400X, using the descriptive guidelines in (33).

Reconstruction of paleoenvironment and climatic conditions is based on a combination of soil micromorphology and analysis of pedosedimentary signatures with special attention to frost processes and mollusk fauna.

Malacological analysis comprises determination of species and coenological analysis. Samples of 250-300 g are wet sieved (0.25 mm mesh). After drying, the shells and fragments are sorted and identified. For evaluation of the individual numbers in each sample, the apices, apertures and fragments of whorls are counted. The calculation of the total specimens number is according to the proposal in (34). The species are included into ecological groups, conforming to their requirements, and the percentage rates of species and individuals within each group are calculated. These groups refer to woodland, xeric, open, mesic and humid habitats (35). Their distribution contributes to the definition of various environments ranging from permafrost steppe to boreal types.

Selected lithics (see Figure 2, main paper) were µCT-scanned using the Skyscan 1172 micro-CT of the Department of Human Evolution (Max-Planck-Institute for Evolutionary Anthropology, Leipzig, Germany). We used the following scan parameters: 100 kV source voltage, 0.1 mA source current, 0.5 mm Al and 0.04 mm Cu filter. We reconstructed the dataset with a resolution of 0.013 mm (isovoxel). To facilitate segmenting and increase contrast, we used a filtering protocol developed at the Max-Planck-Institute for Evolutionary Anthropology for working with dental µCT scans, consisting of a Kiwahara and 3D median filter. The filtered image stacks were interactively segmented using Avizo 7.0 (VSG3d, Burlington MA, USA). Threshold values for the segmenting were determined using the half maximum height (36). We generated surface models from the segmented dataset, and exported them as .stl files to Rapidform 2006 (Inus Technology Inc., Seoul, Korea) for postprocessing. For

visualization we downsampled the surface meshes in Rapidform to about 100 000 triangles (thus the resolution depends on the size of the object). The resulting smaller surfaces were then loaded into Meshlab 1.3.2. (Visual Computing Lab, ISTI, CNR, http://meshlab.sourceforge.net) and manually oriented in the standard views used in lithic studies.

3 Stratigraphy, site formation, radiocarbon dating and chronostratigraphy

Here, we first provide an overview of the stratigraphic sequence, then present the pedosedimentary processes and radiocarbon chronology of sub-units D3 to C1 more thoroughly. The third part deals in more detail with dating and the chronostratigrapic position of AH 3.

Radiocarbon dates are listed here in radiocarbon years before present (BP) or thousand radiocarbon years before present (ka BP). Calibrated ages (calibration curve: IntCal13 (31) and software OxCal 4.2.3 (32) for all radiocarbon dates can be found in Table S1. In section 3.3, we use calendar years before present (cal BP) or thousand calendar years before present (ka cal BP)

3.1 Stratigraphy overview

The sequence of Willendorf II represents a succession of loess and pedological horizons deposited throughout the Middle Pleniglacial and the beginning of the Late Pleniglacial (1-6, 18). The fieldwork between 2006 and 2011 exposed a more than seven meters-thick sequence encompassing the four basic units D, C, B and A (Figure 1). Unit D consists of three bodies of bioturbated sandy loam with two loess layers in between. Unit C records a complete set of greyish to yellowish loesses and pedological horizons, while units B and A fit with the late Pleniglacial upper dusty loess cover and the current Holocene soil, respectively (2, 5, 6).

We focus here on the lower part of the sequence from sub-unit D3 at the bottom to sub-unit C1 at the top (Figure 1), because our field and laboratory research resulted in a new interpretation of this part, while the overlying units B and A are still valid as published (2, 6).

The base of the sequence is formed by the loess D3 capped by the upper sandy loam body D2-D1, ca. 1.0 m thick and characterized by heterogeneous and ochre aspects. Microscopically, the presence of root channels with hypercoatings was documented (see section 6 below). The upper 0.3 m of D1 is stretched along a gentle slope to the south, with a much stronger component to the east. The entire unit C is about 2.70 m thick (Figure 1) and can be summarized as a complex set of loess layers and pedological horizons, subdivided into nine sub-units. These consist of light grey silt (C9, C7-3, C6-2, C3-2, and C1-1), yellowish grey silt and sandy silt (C7-2, C6-1, C5, C3-1, and C1-2), olive-grey sandy loam (C8-3), and grey brownish to dark grey silty humic horizons (C8-2, C8-1, C7-1, C4-2, C4-1, and C2). Geological field observations show different degrees of bioturbation and cryogenic processes at certain positions in the sequence. There is also a large lateral variablity in the preservation of the deposits. Soil micromorphological analysis supports these observations and shows that the pedological horizons are affected by bioturbation and frost processes (see section 6 below).

3.2 Pedosedimentary processes and radiocarbon chronology (sub-units D3 to C1)

Sub-units D2 and D1, overlying the lower loess layer (D3) dated around 48 ka BP, are colluvial deposits with increasing bioactivity and boreal mollusk assemblages (Figure 3). Radiocarbon dates on *Picea* and *Larix*-type charcoal (Figure S2), related to natural fires uphill during the sedimentation, provided ages between 45 and 43 ka BP for D2-D1 (Table S1).

Faint erosion of D1 together with development of thin frost wedges precede the input of aeolian sandy silt (C9) with an cold steppe mollusk assemblage, followed by the

development of a tundra gley under deep frost or permafrost conditions, with cryo-injection of lenses of D1 into C9.

In the southern part of the site, the top of C9 is eroded by a shallow gully with scattered gravel at the base, filled by the sandy loam of C8-3 under rather moist and cool conditions (N 118 - N 120, Figure S3). The sedimentation also coincides with human occupation of the site, as documented by lithic artifacts and bone fragments of AH 3. Afterwards, bioturbated para-rendzina C8-2 developed on top of the sandy loam, together with a mollusk assemblage pointing to medium cold steppe with some boreal trees conditions. Numerous *Picea/Larix* and *Picea* charcoal concentrations in the upper part of the humic horizon, linked to natural fires, provided radiocarbon dates 39.0 and 38.9 ka BP for this pedogenesis (Table S1 and Figure S3). Locally, faint erosion of the humic horizon C8-2 leads to redeposition of humic pellets in layer C8-1 (N 124 – 125).

The base of C7 indicates again cold steppe conditions and deep frost with the thin tundra-gley of C7-3 related to solifluction processes which affect sub-unit C8 in the northern part of the site (N 127-129). The sandy silt of C7-2 records the restart of aeolian sedimentation; it is capped by an incipient bioturbated para-rendzina (C7-1) that coincided with another human occupation (AH 3ab) of the site in medium cold steppe with some boreal trees along valleys conditions around 34.6 ka BP. The overlying sub-units C6 and C5 represent again aeolian input and cold steppe conditions with in part the development of tundra gleys (C6-2 and C6-1).

This is followed by the development of a yellow-brown bioturbated horizon with dark brown root casts and a wavy lower boundary (C4-2). This horizon - radiocarbon dated on *Pinus cembra*-type charcoal (Figure S2) to between 33.9 and 31.8 ka BP (Table S1) - is associated with a human occupation (AH 4, pre-2006 excavations' AH 4 *pro*

parte). After cryogenic disturbance developing a stripped soil pattern and faint erosion of the top of C4-2 (Figure S3), humic silt was deposited (C4-1). It contains abundant *Picea/Larix* charcoal (radiocarbon dated to between 32.2 and 31.2 ka BP, Table S1, Figure S3) and lithic artefacts (AH 4a, pre-2006 excavations' AH 4 *pro parte*).

The following sub-unit C3 is indicator of another cold steppe phase with loess sedimentation and at the base, a thin tundra-gley horizon developed under deep frost conditions (C3-2). This loess bears a well-developed para-redzina (C2) with charcoal, dated to 30.5 ka BP (Table S1), as well as lithic artifacts and numerous bone fragments indicating human occupation (AH 5, pre-2006 excavations' AH 5 *pro parte*). A final aeolian input results in the deposition of sandy silt (C1) with the development of a thick tundra-gley under permafrost conditions (C1-1) on top, which is overlain by the thick loess cover of unit B related to the Late Pleniglacial.

In sum, we see evidence of six "interstadial events" documented by D2-D1, C8-2, C7-1, C4-2, C4-1, and C2 in the lower part of the sequence (Units D and C). They were labelled in the local chronostratigraphic system as Willendorf D1, Schwallenbach Ia and Ib, Schwallenbach IIa and IIb, and Schwallenbach III Interstadials, respectively (Figure 1). By proxy-correlation (26, 37) with the ice-core data from Greenland (38, 39) we correlate them to the Greenland Interstadials (GIS) 12 (Willendorf D1), 11 (Schwallenbach Ia), 9 (Schwallenbach Ib), 8 (Schwallenbach IIa and IIb), and 7 (Schwallenbach III).

3.3 Dating and chronostratigraphic position of AH 3

The age and chronostratigraphic position of the lithic artifacts and faunal remains of AH 3 were established using a combination of stratigraphic, paleoenvironmental and

chronological data. Stratigraphically, AH 3 is located in C8-3 while the dated charcoal comes from under- and overlying deposits. Radiocarbon dates on charcoal materials from the overlying C8-2 provide a minimum age for AH 3, while dates on charcoal from underlying D1 provide a maximum age.

In total, we used five charcoal samples from C8-2 and its lateral extension, resulting in 10 radiocarbon dates (Table S1). One is related to the humic horizon preserved *in situ* and four from stretched charcoal lenses. While the humic horizon is preserved *in situ* at two spots, from N 117 to N 121 and from N 124 to N 126, respectively, with a sharp upper limit and a strongly bioturbated lower boundary, in other spots, especially from N 127 to N 130, it is passing into semi-continuous lenses, often duplicated (Figure S3). Charcoal related to wildfire is abundant in both the *in situ* and stretched parts of C8-2. Our charcoal samples come from different locations, including the material collected at the site in 1981 (5) and 1993 (2)

First, two samples were taken from stretched charcoal lenses at ca. N 129 in 1981 and further at the same spot in 1993 (2, 5, 6) (Table S1). The 1981 raw uncleaned material provided an age of 34,100 +1,200/-1,000 BP (GrN-11192), while the 1993 cleaned and selected sample was dated to 38,880 +1,560/-1,280 BP (GrN-17805) and to 37,930 ±750 BP (GrA-896).

The second set of two samples (A-1933 and A-2039) come from the 2006 and 2007 excavations. They originate from the stretched charcoal lenses between N 126 and N 127 in a similar context as the 1981 and 1993 samples. They provided ages of 37,980 ±300 BP (OxA-17397) and 37,320 +390/-350 BP (GrA-35411) (Table S1 and Figure S3).

Finally, sample A-1935 was taken from the *in situ* undisturbed horizon C8-2 between N 124 and N 124.5 (Table S1 and Figure S3). In a first step, two sub-samples (a and

b) of non-homogenized materials were dated 37,910 +440/-380 BP (GrA-35409) and 37,420 +300/-270 BP (GrA-44894). In a second step, a third sub-sample (c) was homogenized and divided into three parts (c1, c2, c3) for cross-dating following the above-mentioned methodology (see section 2). The first part was dated in Groningen using ABA pre-treatment to 38,790 +400/-350 BP (GrA-45012), another one in Oxford with ABA pre-treatment to 36,500 ±450 BP (OxA-22295), and the last one in Oxford with ABOx-SC pre-treatment to 39,000 ±500 BP (OxA-23520), respectively. All together, the dates GrA-45012 and OxA-23520 around 39 ka BP obtained by cross-dating on homogenized material are considered as the most reliable, as they show good agreement with the other dates obtained for C8-2 with the exception of the under-estimated Oxford ABA date 36,500 ±450 BP (Figures S3 and S4) and the date 34,100 +1,200/-1,000 BP on uncleaned material. These dates around 39 ka BP (c. 43.0 ka cal BP) serve as minimum ages, as they give an age for C8-2 directly overlying C8-3 that contains AH 3.

Maximum ages are provided by 10 charcoal dates of unit D1-D2 that is underlying C8-3 but separated from it by the sterile sandy loess C9. We dated nine charcoal samples using ABA and ABOx-SC pre-treatment (Table S1 and Figures S3 and S4).

Similar to C8-2, we tested cross-dating on the homogenized sample A-2541 from the top of D1 at N 120. The results give an older age for the ABOx-SC pre-treated sample in Oxford than for the ABA pre-treated sample in Groningen, 43,200 ±900 BP (OxA-25836) and 40,870 +480/-400 BP (GrA-52417), respectively. Moreover, the age of the ABOx-SC pre-treated sample fits well with the ages of two other ABOx-SC pre-treated samples obtained separately at N 121 for the upper part of D1 (43,400 ±900 BP: OxA-25838) and for the D1/D2 transition (45,100 ±1,100 BP: OxA-25837). These dates are also in good agreement with the date 48,500 ±800 BP (OxA-17401)

for the ABA pre-treated *Larix* type charcoal from the underlying loess of D3. Consequently, the youngest Groningen ABA date of the cross-dating (GrA-52417) clearly underestimates the sample's age.

Actually, this underestimated ABA date may be compared with the set of three Oxford ABA dates distributed through D1 between 40.0 and 41.8 ka BP (OxA-17399, OxA-17398, and OxA-17400) at N 127 as well as with the former Groningen decay-counting dates from the 1981 and 1993 fieldwork, which range from 39.5 to 41.7 ka BP (GrN-11190, GrN-11195, and GrN-17806) (Table S1 and Figures S3 and S4).

We therefore conclude that the age of D1-D2 is roughly between 45 and 43 ka BP (48 and 46 ka cal BP). This provides us with a maximum age of 43 ka BP (46 ka cal BP) for AH 3. Furthermore, the dating results of the D1-D2 samples pre-treated with ABA vs. the ones pre-treated with ABOx-SC seem to confirm the need for the latter pre-treatment of samples older than 40 ka BP (27, 28). Taking minimum and maximum ages together, this leaves us with a time-window between roughly 43 and 39 ka BP (46 and 43.0 ka cal BP) for the age of AH 3.

We can further constrain the chronostratigraphic background of the Willendorf II sequence by taking into account the environmental data based on pedosedimentary signatures and mollusk fauna. Both lines of evidence suggest that sub-units D1-D2 belong to a well-expressed boreal interstadial (Figure 3), based on a pronounced interstadial mollusc fauna (see section 5 below). We correlate this climatic event with GIS 12 using the proxy correlation scheme of the Greenland ice-core (38) and loess paleosol sequence of Eurasia (26, 37) as well as taking into account the environmental signature of D1-D2.

Above D1, the aeolian sandy silt input and tundra gley of C9 clearly point to cold steppe conditions with deep frost or permafrost (40, 41). This is clear evidence of a

stadial event that we correlate with Greenland Stadial (GS) 12. Directly above, the sandy loam of C8-3 with AH 3 is overlain by a humic horizon of para-rendzina type (C8-2) associated with radiocarbon dates of around 39 ka BP (43.0 ka cal BP) (see above and Table S1 and Figures 3, S3 and S4) and a mollusc fauna typical of medium cold steppe with some boreal trees (see section 5 below and Table S5 and S6); this allows correlation with GIS 11 in good agreement with the calibrated ages produced using the IntCal13 calibration curve (31) and OxCal 4.2.3 software (32) for the accepted ages of D1-D2 and C8-2 (Figure 3).

Based on its mollusc fauna (Figure 3 and Tables S5 and S6), C8-3 points to less cold steppe conditions than C9 and is capped by the medium cold steppe with some boreal trees-type humic horizon of C8-2. Therefore, we conclude that C8-3 and the embedded AH 3 have to be positioned after the cold event GS 12, but before the soil development of C8-2, hence at the onset of GIS 11.

An alternative approach to the approximation of AH 3's age would be using Bayesian modeling of calibrated radiocarbon dates and utilizing their stratigraphic position as constraints. Such an approach is currently widely used (42-46) for age estimations of archeological occupations of a site and for the correlation of studied sequences with climatic events. While in some contexts such an approach is useful, we argue that our approach combining climatostratigraphy with radiocarbon dating is more suited to Willendorf II and long sequences of similar paleoenvironmental resolution. Our approach allows a detailed understanding of the sedimentary dynamics and site formation processes as well as environmental conditions (as shown above); we consider these as prerequisites for approximating the chronostratigraphic position of any archeological or geological horizon.

Nevertheless, we provide here a Bayesian model for comparative purposes shown in Figure S5 (calibrated and modeled ages are shown in Table S7). It covers the lower part of the Willendorf II sequence (D2-D1 to C7-1). The Bayesian model (software: OxCal 4.2.3 (32), calibration curve: IntCal13 (31)) was constructed using the reliable radiocarbon ages and their stratigraphic position. To obtain an age for AH 3, we used the "Date" command in OxCal 4.2.3. The age modeled for AH 3 is 45,800 to 43,835 cal BP (68.2% probability) and 46,721 to 43,133 cal BP (95.4% probability) (Table S7) suggesting that AH 3's humans might have been present at the site somewhere in a time slice of about three millennia, from GIS 12 to the onset of GIS 11. However, our pedosedimentary and environmental data point to a more restricted chronological frame for AH 3, at the beginning of GIS 11.

4 Archeological horizon 3

AH 3 is located in SU C8-3 and has been excavated during the old and the new fieldwork. Our new fieldwork identified SU C8-3 only in zones 03 and 04. The excavated area of SU C8-3 (8.66 m^2) is shown in Figure S6. The thickness of SU C8-3 varies between 5 and 15 cm. The new excavation produced an AH 3 assemblage of 32 lithic artifacts and 23 faunal remains. Their spatial distribution shows a low-density scatter (Figure S7). For average density calculations we used a volume of 0.65 m^3 for C8-3 (using average thickness of 7.5 cm). The density is 49.3 lithic per m^3 and 35.4 faunal remains per m^3.

The 2006 to 2011 excavations' AH 3 assemblage consists of 32 lithic artifacts and 23 faunal remains. The faunal assemblage consists of fragments smaller than 20 mm and most of them are burned. None of the specimens is identifiable to species and their surface preservation does not allow an assessment of anthropogenic modifications like cutmarks, etc. It is unclear whether or not the burning is anthropogenic.

The 32 lithic artifacts all have fresh edges, i.e. are unabraded, and do not show any traces of rounding or similar damage that would be typical for postdepositionally reworked objects. In total, 20 lithics do not show any kind of edge damage, while 12 show such damage that probably derives from use (scars/edge damage on only one face). Many lithic artifacts show on parts of their surface a thin whitish calcareous deposit, something that is also observed on the old collections and has been observed on artifacts from all AHs at Willendorf II.

The lithic artifacts are made of different varieties of hornstones/cherts. All of these occur in the local Danube gravels. In total, five lithic artifacts show exposure to heat in the form of colour change, craquellation, and/or irregular breakage surfaces.

The majority of the lithic artifacts are flakes (Table S4); there are also shattered pieces, bladelets, chips, one core tablet, and one thermal shatter (categories defined in (18)). They vary in size and weight and include small items, which suggests no re-deposition with its typical differential movement of objects of different size (i.e. no size-sorting). This is in good agreement with the other observations (Section 2) that AH 3 is not affected by large-scale, post-depositional reworking.

4.1 Description of selected lithic artifacts of the new collection of AH 3

The entire assemblage of AH 3 is listed in Table S8; here we are presenting only selected artifacts in detail. These mainly include those important for the attribution of the assemblage to the Early Aurignacian. The classification as Early Aurignacian is mainly based on the bladelets of the collection. Below, we first describe some selected lithics and then discuss their cultural classification.

WII-L20-2492

WII-L20-2492 (Figure 2a) is an 8.60 mm long, 3.25 mm wide and 1.16 mm thick bladelet made from reddish fossiliferous hornstone. There is no cortex on the dorsal/exterior face. It is not fragmented and shows skewing to the right but no twisting. The platform is linear and there is evidence of dorsal thinning/reduction on the exterior platform edge; the interior platform edge exhibits a lip. The dorsal scars are unidirectional and demonstrate that the previous bladelets were removed from the core in the same direction as WII-L20-2492. Bladelets of these technological features and shape are characteristic of a reduction sequence using carinated/nosed

endscrapers as cores.

WII-M20-640

WII-M20-640 (Figure 2b) is an 8.12 mm long, 4.48 mm wide and 0.89 mm thick medial fragment of a bladelet. A fossiliferous hornstone was utilized as raw material. There is no cortex on the dorsal/exterior face; in fact, the dorsal face shows three scars that demonstrate a unidirectional core exploitation. The bladelet fragment does not show skewing or twisting. It can belong to a bladelet production utilizing carinated/nosed endscraper-cores, but since it is fragmented and hence lacking some diagnostic landmarks, it could also belong to other types of bladelet production.

WII-M20-647

For the production of bladelet WII-M20-647 (Figure 2c) greyish-beige coloured fossiliferous hornstone was used. It is a 18.60 mm long, 9.80 mm wide and 2.31 mm thick medial bladelet fragment. About 50% of the dorsal/exterior face is covered by cortex and the dorsal scar demonstrates unidirectional core exploitation. The fact that it does not show any twisting or skewing and the rather wide width of 9.80 mm suggests that this bladelet was produced from a unidirectional, prismatic core. This is a different core reduction schematic than the one employed to produce WII-L20-2492.

WII-M18-25

WII-M18-25 (Figure 2d) is a core tablet made from greyish-beige coloured fossiliferous hornstone. The piece exhibits left-lateral remnants of cortex. The non-fragmented core-tablet is 29.10 mm long, 32.29 mm wide and 14.19 mm thick. It shows on its proximal and sinistrolateral edge the core's platform edge with traces of at least three unidirectional removals.

WII-M20-623

WII-M20-623 is a flake with a length of 34.04 mm, width of 29.64 mm and thickness

of 5.30 mm. It is made from the same greyish-beige coloured fossiliferous hornstone as WII-M18-25 and WII-M20-647. Remnants of cortex are present along the right edge. The platform is plain and the exterior platform edge shows evidence of dorsal thinning. The interior platform edge has a lip. The dorsal face shows evidence of four unidirectional removals of which at least two can be attributed to bladelets.

WII-M20-641

WII-M20-641 is also made from the same greyish-beige coloured fossiliferous hornstone. This flake has a length of 29.82 mm, width of 24.20 mm and a thickness of 12.45 mm. Nearly the entire dorsal face is cortical.

During systematic refitting studies conducted on the AH 3 lithic collection, WII-M20-647 could be refitted onto WII-M20-623. This is a sequence refit and shows that prior to WII-M20-647, at least one more bladelet was removed. These are large, straight bladelets without torsion or skewing from unidirectional, prismatic cores. This type of bladelet production is described for both early phases of the Aurignacian, the Proto-Aurignacian and the Early Aurignacian in Western Europe (47).

4.2 Attribution of the 2006-2011 excavations' lithic artifacts of AH 3 to the Early Aurignacian

The majority of the lithic assemblage is not diagnostic of any specific technocomplex, but a small number of lithics strongly point to Aurignacian. These are the bladelets WII-L20-2492 and WII-M20-647. WII-L20-2492 is typical for a reduction sequence using carinated/nosed endscrapers as cores; this is well documented for the Early and Late Aurignacian in Western Europe (48). The bladelet WII-M20-647 originates from a unidirectional, prismatic core; such a core reduction strategy is rather different and

is documented in both early phases of the Aurignacian in Western Europe (Proto-Aurignacian and Early Aurignacian (47, 49). Finally, WII-M20-640 falls in the variability of the frontal, unskewed small bladelets of reduction sequences that utilize carinated/nosed endscrapers as cores, but could also originate from other core reduction sequences, e.g. utilizing burin cores. Taking this evidence together, we argue that since both the carinated/nosed endscraper-cores and the unidirectional, prismatic bladelet cores are known from the Early Aurignacian, an attribution of AH 3's lithic assemblage to this period is the most parsimonious classification with the current data at hand.

This attribution to the Early Aurignacian is further supported through a refit group that connects our new AH 3 assemblage with the old excavation's assemblage attributed to AH 3. During refitting studies, we were able to refit four lithic artifacts of our excavation with a refit group from the 1908 excavation. This 1908 excavation refit group consists of three lithics. From our new collection, the bladelet WII-M20-647, the flakes WII-M20-623 and WII-M20-641, and the core tablet WII-M18-25 refit onto a core (WII-95782) and two pieces of shatter (WII-95783 and WII-95784) from the old collection (Figure 2e). This refit group is interesting for several reasons. First, it demonstrated the validity of the old excavation's attribution of the lithics to AH 3. Second, it connects our small collection with the larger collection from the 1908 to 1955 excavations consisting of 490 lithics, among them carinated/nosed endscraper-cores. The old collection has also been attributed to the Early Aurignacian (6, 15, 18, 50). This agrees with our interpretation of the 32 lithics of the new excavation's AH 3. Third, the refit group demonstrates that a special reduction sequence existed for the production of large bladelets, which did not result from the reduction of a larger blade core. This is based on the size of the original nodule (estimated to ca. 80 mm) and the

amount of cortex on the refitted artifacts. Reduction of larger blade cores has been described as typical for the Proto-Aurignacian, while the dissociation of blade and bladelet reduction is said to be typical for the Early Aurignacian in Western Europe (47, 48). In sum, this again is an argument for AH 3's attribution to the Early Aurignacian.

4.3 Overview of the 1908 to 1955 collection of AH 3

The old collection of AH 3 consists of lithic artefacts and faunal remains (1, 18). Here we focus on the lithics as they are important for the attribution to a technocomplex. In total there are 500 lithic objects, of which 490 are knapped lithics. The rest are hammerstones etc. (18). Below we present a brief summary of the main characteristics of the assemblage (a more detailed description and analysis can be found in (18), but see also (6, 15, 50, 51)).

The raw material composition is very variable and the assemblage is dominated by locally available of silicic limestone and hornstones/cherts. The assemblage also includes some exogenous and intermediate raw materials (18). The direction of the cortex removal is clearly unidirectional. Core preparation is evident from crested blades, bladelets and flakes as well as core tablets. The blank production shows the production of blades, flakes, and bladelets.

Bladelet production is documented in two different reduction sequences, one utilizing carinated/nosed endscrapers as cores for the production of small bladelets (Fig. S8) and one using small volumetric cores for the production of large bladelets (Fig. S9). Both bladelet reduction sequences are disassociated from the blade production (18). The carinated/nosed endscraper cores were produced on thick flakes, and it is possible that there existed a special reduction sequence to produce these, but currently this

cannot be demonstrated. Blade production is well documented by blades and refitted blade sequences. Some of these show that raw material blocks were sometimes utilized without decortification or ridge/crest preparation. Flake production is well documented by various cores and flakes. Platforms are predominantly unprepared (plain) and the dorsal scar patterns of both, flakes and blades, are dominated by unidirectional patterns. This demonstrates unidirectional core exploitation.

Tool production is characterized by Upper Palaeolithic tool types, dominated by endscrapers. Endscrapers include carinated and nosed endscrapers (Fig. S8) as well a simple endscrapers (Fig. S10). Further, there is one fragment of an Aurignacian blade, burins, retouched blades and flakes, etc. (Table S2 and Fig. S11 and S12) (18, 50, 51). The old collection has been attributed to the Early Aurignacian (1, 15, 50) based on the tool types, the bladelet production and the overall knapping behavior preserved in the assemblage (detailed analysis in (18)). Specifically when comparing bladelet production with blade production, the disassociation of bladelet and blade production is obvious and is in line with the classification of AH 3 as Early Aurignacian.

5 Malacological data

The malacological analysis reported here supplements results of previous studies (35, 52, 53). The samples of the 1993 fieldwork were all collected from the section in the approximate location of N 129 in our fieldwork grid. Due to the lateral variability in the preservation of the stratigraphic units, we collected 43 new samples covering the whole exposed sequence during the 2006-2011 excavations. The results of 16 samples are presented below, covering the sub-units D3 to C6-2 (Table S5).

Sub-unit D3: sample 06-6

For sub-unit D3, one sample (sample 06-6, see Table S6) has been analysed consisting of 1399 specimens and 29 species. *Trochulus hispidus* (31.88%) and *Pupilla triplicata* (29.24%) predominate; percentage rate of forest species is 48.28%, but of their individuals only 6.43%. Cold-tolerant species are represented to a small degree. The peculiar species is the hygrophile *Perforatella bidentata*, pointing to wet microhabitats. In this respect, the shells of three *Deroceras* species are also worth mentioning. With regard to habitat, mesic to humid, herbaceous habitats with interweaving dry and open zones are prevailing. Wooded areas seem to be reduced, although niche-habitats and a favorable structure of the remaining woods are persisting. Compared to overlying sub-units D1-D2 (see below), a lower temperature is evident, while the climate is moderated and of average humidity. This evidence corresponds to the character of the sediment, a homogeneous loess (Section 3).

Sub-unit D2: sample 06-5

Sample 06-5 from sub-unit D2 consisted of 299 individuals distributed over 35 species (Table S6). The woodland species show high diversity (19 species, 54.29% of species), the percentage of individuals is 33.44%. Xeric habitat species are

represented by 11.43% (species) and 17.73% (individuals). Open habitat species (20% species, 17.06% individuals) are dominated by *Vallonia costata*. Mesic habitat species (11.43% species, 31.10% individuals) are represented by mainly *Trochulus hispidus* and *Succinella oblonga*. This points towards warm and humid conditions and the sample shows great similarity to sample 06-4 of sub-unit D1 (see below).

Sub-unit D1: samples 06-1, 06-2, 06-3, 06-4, 10-1, and 11-1

Within sub-unit D1, six samples were collected and yielded specimens (samples 06-1 to 06-4, 10-1, and 11-1). A seventh sample (sample 10-2) provided only one shell fragment of *Trochlus hispidus*, so this sample is not further considered here. Numbers of species and individuals for each sample are listed in Table S6.

In sample 06-4, woodland species show high diversity (20 species, 57.14%), similar to sample 06-2 (18 species, 66.67%). The percentages of their individuals are between 17.22% (sample 06-3) and 36.15% (sample 06-4) and reflect wooded parcels of different expansion, but with a favorable structure. In sample 11-1, the appearance of more demanding species like *Ena montana*, a slug (*Limax* sp.), *Helicigona lapicida*, and *Euomphalia strigella* would suggest a diversified vegetation due to a mild and humid climate.

The percentage of drought-tolerant species is the highest in sample 06-3 (31.94%), due to *Pupilla triplicata* (29.10%). The open-ground species are also represented here more than in the other samples (22.24%). In samples 06-1 and 06-2 the group “mesic habitats” predominates due to high amounts of *Trochulus hispidus* (35.31% and 35.96%); together with the other species, the percentages of this ecological group are 40.76% and 46.23%, respectively. In sample 06-4, this group is also strongly represented (30.51%), mainly with *Trochulus hispidus* and *Succinella oblonga*. This

points to areas with low, dense, herbaceous vegetation. Species inhabiting wet biotopes are absent or their percentages are insignificant.

Open-dry habitats seem to have been most extensive in the middle part of D1 (sample 06-3). Moreover, the cold-tolerant species, which are scarce in samples 06-1 and 06-2, are a little more numerous here.

Thus, a slight oscillation with more dry and unfavorable conditions is marked in unit D1 at the level of sample 06-3, visible also in the low percentage of closed-forest species. The upper part of D1 (sample 06-1) is of warm and humid character, comparable to the horizons with samples 06-2 and 06-4.

Peculiarities include the shell of a Milacidae species in sample 06-4 and of *Vitrinobrachium* sp. in sample 06-3. A shell of Milacidae, cf. *Tandonia* sp., was found during the 1993 fieldwork (unit D: sample nr. 20; depth 6.0m – 6.2m (*75*)). Shells found in deep layers, together with a lot of demanding species, are presumably autochthonous. Since most of the Milacidae are subterranean animals, shells could have been replaced into deeper layers and misinterpreted. Some members of this gastropod family, spread at present across the whole Mediterranean region, seem to have been more widespread during warm Pleistocene periods and in the Holocene (Atlantic or Epiatlantic phase (35)) compared to today.

Vitrinobrachium sp. (sample 06-3) was never observed in the Willendorf II samples (53). Pleistocene and Holocene records of this genus are very scarce because the shells are very similar to those of *Semilimax*; furthermore, they are very fragile. *Vitrinobrachium breve* (A. FÉRUSSAC 1821), spread across the western parts of Central Europe, is very expansive today in more or less open anthropogenic habitats (54). The few finds in Austrian Quaternary deposits evidently originate from warm intervals (35).

Sub-unit C9: samples 10-4 and 10-5

Two samples (10-4 and 10-5) from sub-unit C9 are presented here, consisting of 267 individuals (9 species) and 142 individuals (13 species), respectively (Table S6). Very unfavorable conditions are expressed in both samples, reflecting a dry climate. This compares favorably with the geological observations suggesting input of aeolian sandy silt and the development of a tundra gley (Section 3).

Sub-unit C8-3: samples 10-6 and 11-2

Samples 10-6 (23 individuals, 7 species) and 11-2 (467 individuals, 13 species) cover sub-unit C8-3 (with AH 3). In the larger sample 11-2, individuals of woodland (3.43%) and humic (0.10%) species are poorly represented, while those of xeric habitat species (48.39%) dominate. Additionally, there are specimens of mesic (25.70%) and open (21.84%) habitat species documented. The climate indicated in samples 10-6 and 11-2 is dry, more cool than moderate (but not cold), with open to semi-open habitats predominating.

Sub-unit C8-2: samples 10-7 and 10-8

The samples 10-7 (496 individuals, 22 species) and 10-8 (181 individuals, 18 species) are both dominated by individuals of xeric (53.83% and 49.72%) and open (25.60% and 19.89%) habitat species pointing to medium cold steppe with some boreal trees in river valleys conditions (Table S6). Sample 10-7 points to a relatively mild but dry climate.

Sub-unit C7-2: Sample 11-3

917 individuals (16 species) were documented in sample 11-3, covering sub-unit C7-2. The cold-tolerant elements are distinct (*Vertigo parcedentata, Columella columella* and *Vallonia tenuilabris, Pupilla sterrii,* appearance of forma *elongata* of *Succinella oblonga*). Individuals of xeric (39.26%), open (16.03%) and mesic (35.99%) habitat

species are predominant. The climate appears more humid and cooler than in sub-unit C8-3.

Sub-unit C6-2: sample 11-4

Sample 11-4 from sub-unit C6-2 consists of 715 individuals (18 species). Numbers of woodland species are very low (7.97%), with *Clausilia dubia* as the most numerous. From this point of view, the evidence is similar to that from sample 11-3. Among the xeric habitat species, *Pupilla triplicata* is more numerous than *Pupilla sterrii*, like in other samples of Willendorf II. The *Pupilla triplicata – Pupilla sterrii* percentage is only 5.03%. The share of the open habitats group, with cold-tolerant species, is 18.32% and similar to that of the underlying sample 11-3. *Columella columella* is clearly dominant and the insignificant number of *Vallonia costata* points to cool climate as well. The representatives of mesic habitats are quite numerous with 66.99%. The most frequent species is *Succinella oblonga* with 34.55% of all individuals; *Trochulus hispidus* (31.47% of all individuals) is predominant. Species restricted to very humid and wet habitats are represented by only 1.68%. In summary, this points to cool and humid conditions, especially in regard to the percentage of *Columella columella*, occurrence of *Vertigo modesta arctica*, relatively low percentage of *Vallonia costata,* and the quite numerous *Succinella oblonga (+forma elongata*). This evidence corresponds well to the soil type (tundra gley) (Section 3).

6 Micromorphological data regarding environmental conditions

In total, 94 undisturbed, oriented sediment samples were collected during the 2006 - 2011 field seasons at Willendorf II. The current analysis includes 14 samples (20 thin sections), listed in Table S9. Here we present the analytical results concerning paleoenvironmental aspects, concentrating on sub-units D2 to C7 (Table S10).

6.1 The Paleosol Units

Sub-unit D1 comprises decalcified clay showing speckled or granostriated b-fabrics indicative of postdepositional clay translocation (Figure S13) to a larger extent than any of the other samples studied. However, as in the rest of the samples, there is no evidence of clay illuviation or blocky pedogenic microstructures documented in the thin sections. The sedimentary mass is strongly bioturbated and exhibits iron-manganese mottling and secondary calcite derived from root activity. Towards the base of D1 and in D2, iron manganese mottling and recalcification features, particularly extensive hypocoatings (Figure S14), are more prominent than in the rest of the samples. Thus, these two units represent a high fluctuating moisture regime under a stable surface.

Sub-unit C8-2 comprises an accumulation of charcoal-rich humic aggregates, fragments of lignified and melanized plant tissue and citomorphic calcite mixed with loessic sand in a complex vermicular and granular microstructure resulting from earthworm activity. In addition, it locally exhibits relict undisturbed micro-frost lensing (<1mm thick lenses) indicative of seasonal freezing throughout the life of the soil. There is no evidence of clay illuviation or any blocky pedogenic microstructures, which is in agreement with classification of this paleosol as the A horizon of a para-

rendzina or mollisol (Section 3). It consists of basal humic layer residues of a forest soil formed on loess. The topsoil was eroded by cryogenic processes, possibly at the onset of a cooling climate (represented by the C7-3 and C7-2 deposits), i.e. a shift from medium cold steppe with some boreal trees along valleys to cold steppe environmental conditions as suggested in Section 3. This is in agreement with macroscopic periglacial deformation as documented in the field at N 127 and N 129.

Sub-unit C7-1 does not exhibit humic aggregates. It comprises strongly bioturbated (as evidenced by vermicular and granular microstructures) sandy loess with iron manganese mottling indicative of seasonal waterlogging. Although primary calcite was observed (Figure S13), this loess is partly decalcified, as indicated by locally speckled b-fabrics. As in C8-2, there is no evidence of clay illuviation or pedogenic microstructures, but biogenic recalcification in the form of calcareous root hypo-coatings, infillings and needle-fiber calcite fillings are present throughout the C7-1 samples. These features are suggestive of the A horizon of an incipient para-rendzina formed under a colder climate than in C8-2. Although seasonally waterlogged, the weak stage of development of this soil suggests a low moisture regime. A similar suite of micromorphological features (i.e. speckled b-fabric, lack of clay illuviation, recalcification features and few iron manganese pedofeatures) on Pleistocene loessic paleosols have been ascribed to a xeric (500-700 mm) climate (55). The unit C paleosols (e.g., C8-2 and C7-1) represent lower moisture regimes and shorter lasting stable surfaces than the subunit D2-D1 paleosol.

6.2 The loess deposits

Sub-units C7-2 and C9 are calcareous (now partly decalcified), micaceous sandy loess deposits (Figure S13). Although they have been strongly affected by earthworm activity, some of the C7-2 samples exhibit a massive microstructure reminiscent of the original loessic deposit. Some samples also exhibit relict micro-frost lensing (Figure S15), but this is very weakly expressed and quartz grains are not frost-shattered. Iron manganese mottling is a recurring feature, indicating seasonal high moisture. Secondary carbonate infillings and hypocoatings are common and possibly derive from bioturbation linked to overlying soils. Both loessic deposits (C7-2 and C9) exhibit moderately good sorting and no grain clustering was observed, suggesting aeolian deposition. Both the C7-2 and C9 loessic deposits represent a cold, arid climate and a landscape devoid of woody vegetation.

7 References

1. Felgenhauer F (1959) *Willendorf in der Wachau. Monographie der Paläolith-Fundstellen I-VII* (Rohrer, Vienna).
2. Haesaerts P, Damblon F, Bachner M, Trnka G (1996) Revised stratigraphy and chronology of the Willendorf II sequence, Lower Austria. *Archaeologia Austriaca* 80:25-42.
3. Nigst PR, et al. (2008) New research on the Aurignacian of Central Europe: A first note on the 2006 fieldwork at Willendorf II. *Quartär* 55:9-15.
4. Nigst PR, Viola TB, Haesaerts P, Trnka G (2008) Willendorf II. *Wissenschaftliche Mitteilungen aus dem Niederösterreichischen Landesmuseum* 19:31-58.
5. Haesaerts P (1990) Nouvelles recherches au gisement de Willendorf (Basse Autriche). *Bulletin de l'Institut Royal des Sciences Naturelles de Belgique, Sciences de la Terre* 60:203-218.
6. Nigst PR, Haesaerts P (2012) L'Aurignacien en Basse Autriche : résultats préliminaires de l'analyse technologique de la couche culturelle 3 de Willendorf II et ses implications pour la chronologie du Paléolithique supérieur ancien en Europe centrale. *L'Anthropologie* 116:575-608
7. Nigst PR, Viola BT, Antl-Weiser W (2010) Digital Documentation of Palaeolithic Excavations: A Case Study. *New Aspects of the Central and Eastern European Upper Palaeolithic - methods, chronology, technology and subsistence*, eds Neugebauer-Maresch C, Owen LR (Verlag der Österreichischen Akademie der Wissenschaften, Vienna), pp 311-317.
8. Mark DM (1973) Analysis of Axial Orientation Data, Including Till Fabrics. *Geological Society of America Bulletin* 84:1369-1374.

9. Mark DM (1974) On the Interpretation of Till Fabrics. *Geology* 2:101-104.

10. Bertran P, Texier J-P (1995) Fabric Analysis: Application to Paleolithic Sites. *Journal of Archaeological Science* 22:521-535.

11. Lenoble A, Bertran P (2004) Fabric of Palaeolithic levels: methods and implications for site formation processes. *Journal of Archaeological Science* 31:457-469.

12. McPherron SP (2005) Artifact orientations and site formation processes from total station proveniences. *Journal of Archaeological Science* 32:1003-1014.

13. McPherron SP, Dibble HL (2002) *Using Computers in Archaeology: A Practical Guide* (McGraw-Hill, Boston).

14. Tostevin GB (2012) *Seeing Lithics: A Middle-Range Theory for Testing for Cultural Transmission in the Pleistocene* (Oxbow Books, Oxford).

15. Hahn J (1977) *Aurignacien: Das ältere Jungpaläolithikum in Mittel- und Osteuropa* (Böhlau Verlag, Köln).

16. Adler DS (2002) *Late Middle Palaeolithic Patterns of Lithic Reduction, Mobility, and Land Use in the Southern Caucasus.* PhD thesis, Havard University.

17. Demars PY, Laurent P (1992) *Types d'outils lithiques du Paléolithique supérieur en Europe* (Presses du CNRS, Paris).

18. Nigst PR (2012) *The Early Upper Palaeolithic of the Middle Danube Region* (Leiden University Press, Leiden).

19. Conard NJ, Adler DS (1997) Lithic reduction and hominid behavior in the Middle Paleolithic of the Rhineland. *Journal of Anthropological Research* 53:147-175.

20. Larson ML, Kornfeld M (1997) Chipped Stone Nodules: Theory, Method, and Examples. *Lithic Technology* 22:4-17.

21. Gifford DP, Crader DC (1977) A Computer Coding System for Archaeological Faunal Remains. *American Antiquity* 42:225.

22. Lyman RL (1994) *Vertebrate Taphonomy* (Cambridge University Press, Cambridge).

23. Behrensmeyer AK (1978) Taphonomic and Ecologic Information from Bone Weathering. *Paleobiology* 4:150-162.

24. Damblon F, Haesaerts P, van der Plicht J (1996) New Datings and Considerations on the Chronology of Upper Palaeolithic Sites in the Great Eurasiatic Plain. *Préhistoire Européenne* 9:177-231.

25. Damblon F, Haesaerts P (2002) Anthracology and radiochronology of the Upper Pleistocene in the loessic areas of Eurasia. *Charcoal Analysis. Methodological Approaches, Palaeoecological Results and Wood Uses*, ed Thiébault S (Archaeopress, Oxford).

26. Haesaerts P, et al. (2010) Charcoal and wood remains for radiocarbon dating Upper Pleistocene loess sequences in Eastern Europe and Central Siberia. *Palaeogeography, Palaeoclimatology, Palaeoecology* 291:106-127.

27. Haesaerts P, Damblon F, Nigst P, Hublin JJ (2013) ABA and ABOx Radiocarbon Cross-Dating on Charcoal from Middle Pleniglacial Loess Deposits in Austria, Moravia, and Western Ukraine. *Radiocarbon* 55:641-647.

28. Bird MI, et al. (1999) Radiocarbon Dating of "Old" Charcoal Using a Wet Oxidation, Stepped-Combustion Procedure. *Radiocarbon* 41:127-140.

29. Bird MI, et al. (2003) Radiocarbon dating from 40 to 60 ka BP at Border Cave, South Africa. *Quaternary Science Reviews* 22:943–947.

30. Brock F, Higham T, Ditchfield P, Bronk Ramsey C (2010) Current Pretreatment Methods for AMS Radiocarbon Dating at the Oxford Radiocarbon Accelerator Unit (ORAU). *Radiocarbon* 52:103-112.

31. Reimer P, et al. (2013) IntCal13 and Marine13 radiocarbon age calibration curves 0-50,000 years cal BP. *Radiocarbon* 55:1869-1887.

32. Bronk Ramsey C (2009) Bayesian analysis of radiocarbon dates. *Radiocarbon* 51:337-360.

33. Stroops G (2003) *Guidelines for analysis and description of soil and regolith thin sections* (Soil Science Society of America Inc., Madison).

34. Ložek V (1964) *Quartärmollusken der Tschechoslowakei* (Nakladatelství ČSAV, Prague).

35. Frank C (2006) *Plio-pleistozäne und holozäne Mollusken Österreichs* (Verlag der Österreichischen Akademie der Wissenschaften, Vienna).

36. Spoor CF, Zonneveld FW, Macho GA (1993) Linear measurements of cortical bone and dental enamel by computed tomography: applications and problems. *American Journal of Physical Anthropology* 91:469-484.

37. Haesaerts P, et al. (2009) Climatic signature and radiocarbon chronology of Middle and Late Pleniglacial loess from Eurasia: comparison with the marine and Greenland records. *Radiocarbon* 51:301-318.

38. Johnsen SJ, et al. (2001) Oxygen isotope and palaeotemperature records from six Greenland ice-core stations: Camp Century, Dye-3, GRIP, GISP2, Renland and NorthGRIP. *Journal of Quaternary Science* 16:299-307.

39. Svensson A, et al. (2008) A 60 000 year Greenland stratigraphic ice core chronology. *Climate of the Past* 4:47-57.

40. Haesaerts P (1983) Stratigraphic distribution of periglacial features indicative of permafrost in the Upper Pleistocene loesses of Belgium. *Permafrost. Fourth International Conference: Proceedings* (National Academy Press, Washington D.C.), pp 421-426.

41. Van Vliet-Lanoë B (1985) Frost effects in soils. *Soils and Quaternary landscape evolution*, ed Boardman J (J Wiley & Sons, New York), pp 117-158.

42. Higham T, et al. (2012) Testing models for the beginnings of the Aurignacian and the advent of figurative art and music: The radiocarbon chronology of Geißenklösterle. *Journal of Human Evolution* 62:664-676.

43. Douka K, Grimaldi S, Boschian G, Lucchese AD, Higham TF (2012) A new chronostratigraphic framework for the Upper Palaeolithic of Riparo Mochi (Italy). *Journal of Human Evolution* 62:286-299.

44. Hublin JJ, et al. (2012) Radiocarbon dates from the Grotte du Renne and Saint-Césaire support a Neandertal origin for the Châtelperronian. *Proc Natl Acad Sci USA* 109:18743-18748.

45. Higham T, et al. (2011) The earliest evidence for anatomically modern humans in northwestern Europe. *Nature* 479:521-524.

46. Pinhasi R, Higham TFG, Golovanova LV, Doronichev VB (2011) Revised age of late Neanderthal occupation and the end of the Middle Paleolithic in the northern Caucasus. *Proc Natl Acad Sci USA* 108:8611-8616.

47. Bon F (2006) A brief overview of Aurignacian cultures in the context of the industries of the transition from Middle to the Upper Paleolithic. *Towards a definition of the Aurignacian,* eds Bar-Yosef O, Zilhão J (Instituto Portueguês de Arqueologia, Lisbon), pp 133-144.

48. Le Brun-Ricalens F, Bordes JG, Bon F (2005) *Productions lamellaires attribuées à l'Aurignacien: chaînes opératoires et perspectives technoculturelles* (Musée national d'histoire et d'art, Luxembourg).

49. Blades BS (2001) *Aurignacian Lithic Economy. Ecological Perspectives from Southwestern France* (Kluwer Academic/Plenum Publishers, New York).

50. Teyssandier N (2007) *En route vers l'Ouest: Les débuts de l'Aurignacien en Europe* (John and Erica Hedges Ltd., Oxford).

51. Nigst PR (2006) The first modern humans in the Middle Danube Area? New Evidence from Willendorf II (Eastern Austria). *When Neanderthals and Modern Humans Met,* ed Conard NJ (Kerns Verlag, Tübingen), pp 269-304.

52. Frank C, Rabeder G (1994) Neue ökologische Daten aus dem Lößprofil von Willendorf in der Wachau. *Archäologie Österreichs* 5:59-65.

53. Frank C, Rabeder G (1997) Willendorf in der Wachau. *Pliozäne und pleistozäne Faunen Österreichs – Ein Katalog der wichtigsten Fossilfundstellen und ihrer Faunen*, eds Döppes D, Rabeder G (Verlag der Österreichischen Akademie der Wissenschaften, Vienna), pp 68-74.

54. Beckmann KH, Lill K (2001) Die Kurze Glasschnecke *Vitrinobrachium breve* (A. Férussac 1821) im Hönnetal/Sauerland – zur zoogeographischen und taxonomischen Bedeutung der nordwestdeutschen Vorkommen dieser Art (Gastropoda: Stylommatophora, Vitrinidae). *Heldia* 3:59-66.

55. Khormali F, Kehl M (2011) Micromorphology and development of loess-derived surface and buried soils along a precipitation gradient in Northern Iran. *Quaternary International* 234:109-123.

56. Zilhão J, d'Errico F (1999) The Chronology and Taphonomy of the Earliest Aurignacian and Its Implications for the Understanding of Neandertal Extinction. *Journal of World Prehistory* 13:1-68

57. Zilhão J (2006) Neandertals and moderns mixed, and it matters. *Evolutionary Anthropology* 15:183-195.

58. Teyssandier N (2008) Revolution or evolution: the emergence of the Upper Paleolithic in Europe. *World Archaeology* 40:493-519

59. Jöris O, Street M (2008) At the end of the 14C time scale—the Middle to Upper Paleolithic record of western Eurasia. *Journal of Human Evolution* 55:782-802.

60. Richter D, Waiblinger J, Rink WJ, Wagner GA (2000) Thermoluminescence, Electron Spin Resonance and 14C-dating of the Late Middle and Early Upper Palaeolithic Site of Geißenklösterle Cave in Southern Germany. *Journal of Archaeological Science* 27:71-89

61. Davies W, Hedges R (2008) Dating a type site: Fitting Szeleta cave into its regional chronometric context. *Praehistoria 9-10*:35-45.

62. Higham T, et al. (2009) Problems with radiocarbon dating the Middle to Upper Palaeolithic transition in Italy. *Quaternary Science Reviews* 28:1257-1267.

63. Camps M, Higham T (2012) Chronology of the Middle to Upper Palaeolithic transition at Abric Romaní, Catalunya. *Journal of Human Evolution* 62:89-103.

64. Talamo S, Soressi M, Roussel M, Richards M, Hublin JJ (2012) A radiocarbon chronology for the complete Middle to Upper Palaeolithic transitional sequence of Les Cottés (France). *Journal of Archaeological Science* 39:175-183.

65. Schmidt C, et al. (2013) First chronometric dates (TL and OSL) for the Aurignacian open-air site of Românești-Dumbrăviţa I, Romania. *Journal of Archaeological Science* 40:3740-3753.

66. Szmidt CC, Normand C, Burr GS, Hodgins GW, LaMotta S (2010) AMS 14C dating the Protoaurignacian/Early Aurignacian of Isturitz, France. Implications for Neanderthal-modern human interaction and the timing of technical and cultural innovations in Europe. *Journal of Archaeological Science* 37:758-768.

67. Trinkaus E, et al. (2003) An early modern human from the Peştera cu Oase, Romania. *Proc Natl Acad Sci USA* 100(20):11231-11236.

68. Higham TFG, Bronk Ramsey C, Brock F, Baker D, Ditchfield P (2007) Radiocarbon dates from the Oxford AMS system: Archaeometry Datelist 32. *Archaeometry* 49:S1-S60.

69. Prat S, et al. (2011) The Oldest Anatomically Modern Humans from Far Southeast Europe: Direct Dating, Culture and Behavior. *PLoS ONE* 6:e2083.

70. Higham TFG, Jacobi RM, Ramsey CB (2006) AMS radiocarbon dating of ancient bone using ultrafiltration. *Radiocarbon* 48:179.

71. Marom A, McCullagh JSO, Higham TFG, Sinitsyn AA, Hedges REM (2012) Single amino acid radiocarbon dating of Upper Paleolithic modern humans. *Proc Natl Acad Sci USA* 109:6878-6881.

72. Crevecoeur I, et al. (2010) The Spy VI child: A newly discovered Neandertal infant. *Journal of Human Evolution* 59:641-656.

73. Toussaint M, Pirson S (2006) Neandertal studies in Belgium: 2000–2005. *Period Biol* 108:373-387.

74. Semal P, et al (2009) New data on the late Neandertals: Direct dating of the Belgian Spy fossils. *American Journal of Physical Anthropology* 138:421-428.

75. Schmitz RW, et al. (2002) The Neandertal type site revisited: interdisciplinary investigations of skeletal remains from the Neander Valley, Germany. *Proc Natl Acad Sci USA* 99:13342-13347.

76. Higham T, Ramsey CB, Karavanić I, Smith FH, Trinkaus E (2006) Revised Direct Radiocarbon Dating of the Vindija G_1 Upper Paleolithic Neandertals. *Proc Natl Acad Sci USA* 103:553-557.

77. Krause J, et al. (2007) Neanderthals in central Asia and Siberia. *Nature* 449:902-904.

78. Beauval C, Lacrampe-Cuyaubère F, Maureille B, Trinkaus E (2006) Direct Radiocarbon Dating and Stable Isotopes of the Neandertal femur from Les Rochers-de-Villeneuve (Lussac-les-Chiteaux, Vienne). *Bulletins et Memoires de la Societe d'Anthropologie de Paris* 18:35-42.

79. Lalueza-Fox C, et al. (2005) Neandertal evolutionary genetics: mitochondrial DNA data from the Iberian Peninsula. *Molecular Biology and Evolution* 22:1077-1081.

80. 1. De Torres T, et al. (2010) Dating of the hominid (Homo neanderthalensis) remains accumulation from El Sidrón cave (Piloña, Asturias, North Spain): an example of a multi-methodological approach to the dating of upper Pleistocene sites. *Archaeometry* 52:680-705.

Acknowledgements

We thank the Austrian Antiquity Authority (Bundesdenkmalamt, Abteilung für Bodendenkmale) and the site's landowner (2006-2007: ÖBB Infrastruktur AG, Liegenschaftsverwaltung, H. Scheibner; 2008-2011: Marktgemeinde Aggsbach, H. Gerstbauer) for the fieldwork permit. We also thank the Leakey Foundation (2006–2012), Max Planck Society (2006–2012), University of Vienna (2006–2011), Hugo Obermaier Society (2006), Federal Office for Scientific Affairs of the State of Belgium (projects Sc-004, Sc-09, MO/36/021), and the Hochschuljubiläumsfonds of the City of Vienna (2007) for funding our research. We further acknowledge the support of the Department of Prehistory (Natural History Museum, Vienna, Austria; W. Antl-Weiser), Marktgemeinde Aggsbach (H. Gerstbauer), Museumsverein Willendorf (K. Kappelmüller), and the Satzl and Perzl families. Many thanks to D. M. Bosch, E. Dermience, R. Farbstein, C.N. Moore, V. Schmid, A. Sonnberger, A. Stadlmayr, S. Stelzer, L. Viola, and our student excavators for field/laboratory assistance. We thank W. Antl-Weiser, D.M. Bosch, P.A. Mellars, S.P. McPherron, L. Moreau, D. Richter, M. Roussel, H. Seidler, M. Soressi, C. Stimpson, and N. Zwyns for discussions of the archaeological evidence and J. van der Plicht, T. Higham, and S. Talamo for discussion of the radiocarbon dates.

SI Figures

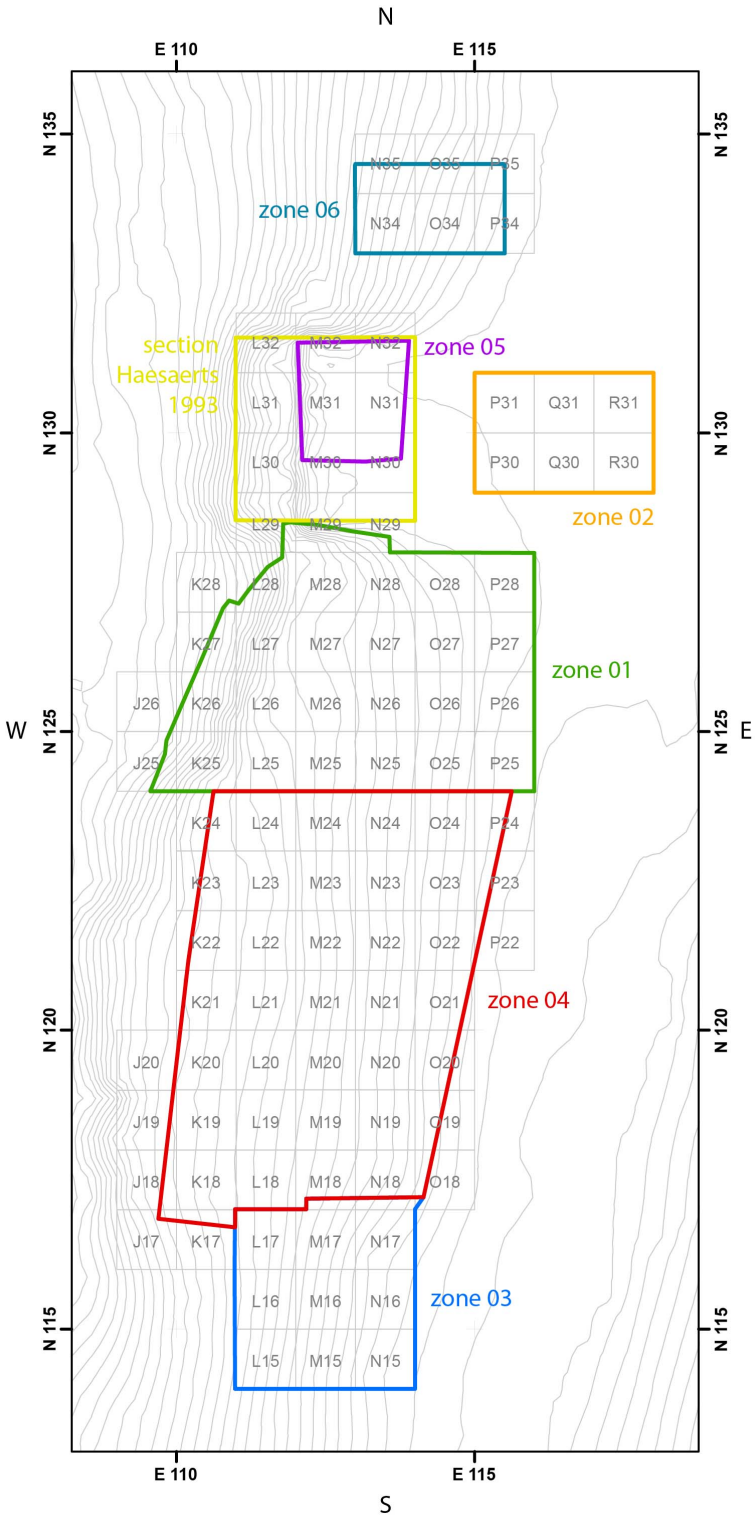

Figure S1: Willendorf II – excavation 2006-2011. Location of the 2006-2011 excavation zones 01 to 06 and the section 1993 by Haesaerts et al. (2) are shown. Scale in metres; local coordinate system of the Willendorf II excavation. Contour

lines: 0.2 m intervals. Squares are labeled in the Willendorf II excavation square system.

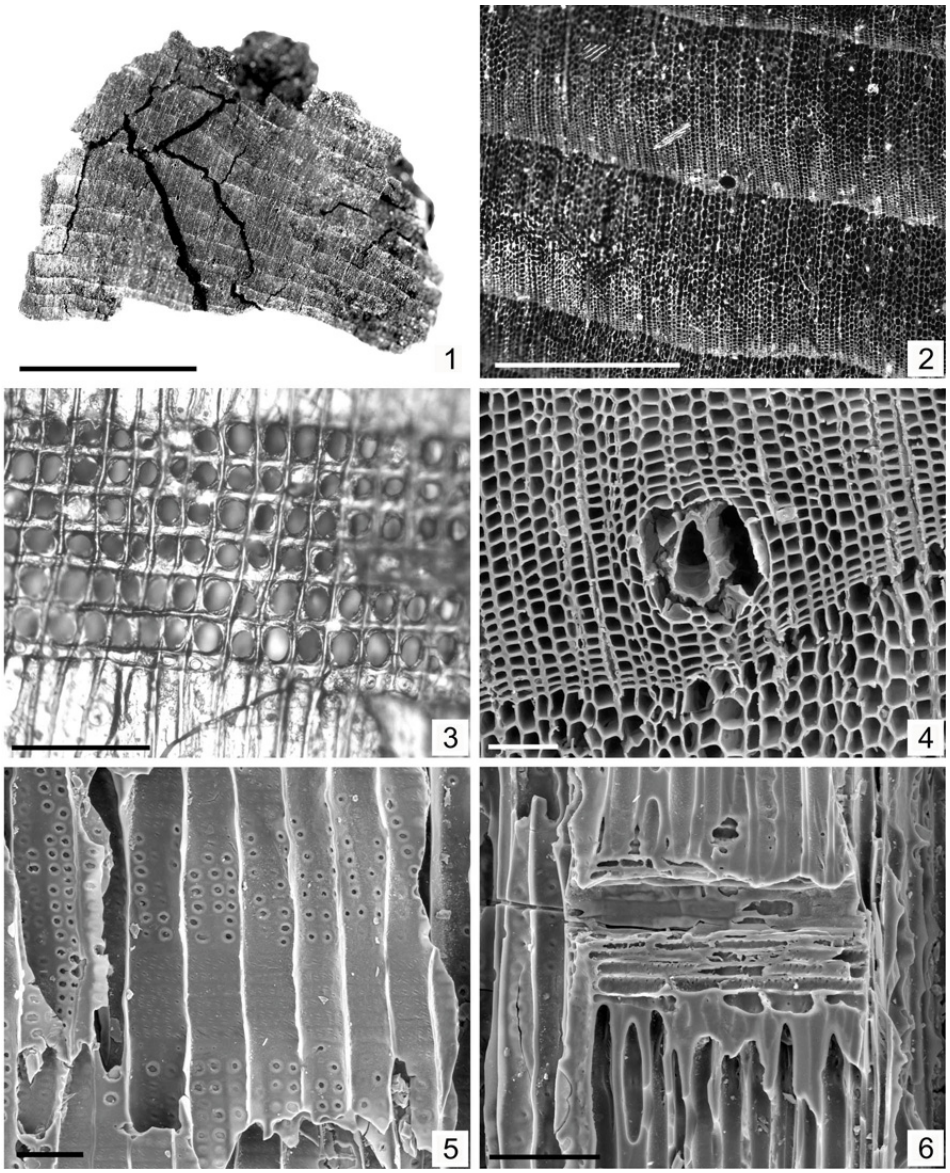

Figure S2: Wilendorf – examples of charcoal of *Pinus cembra*-type (1, 3, 4), *Picea/Larix*-type (2) and *Larix*-type (5, 6). 1) *Pinus cembra*-type. Transversal section showing the tree rings. Scale: 1 cm. Willendorf II/C4-2 (A-2421). 2) *Picea/Larix*-type. Transversal section showing the tree rings. Dark-field microscopy. Scale: 1 mm. Willendorf II/C4-1 (A-1912). 3) *Pinus cembra*-type. Radial section showing a cross-field (fenestrate pits) with one line of radial tracheids (small areolate pits) at the base of the cross-field. Dark-field microscopy. Scale: 100 µm. Willendorf II/C4-2 (A-

1915). 4) *Pinus cembra*-type. Transversal section showing the tree rings limit and one resin canal. Environmental Scanning Electron Microscope. Scale: 100 µm. Willendorf II/C4-2 (A-2421). 5) *Larix*-type. Radial section showing the contact of vertical tracheids and a ray with six lines of horizontal parenchyma cells (small pits in elongated parenchyme cells) bordered by one line of tracheids (small areolate pits) at the base of the cross-field. Environmental Scanning Electron Microscope. Scale: 100 µm. Willendorf II/ D1 top (A-2541). 6) *Larix*-type. Radial section showing vertical tracheids with files of big areolate pits and horizontal parenchyma cells bordered with one line of large tracheid cells. Environmental Scanning Electron Microscope. Scale: 100 µm. Willendorf II/ D1 top (A-2541).

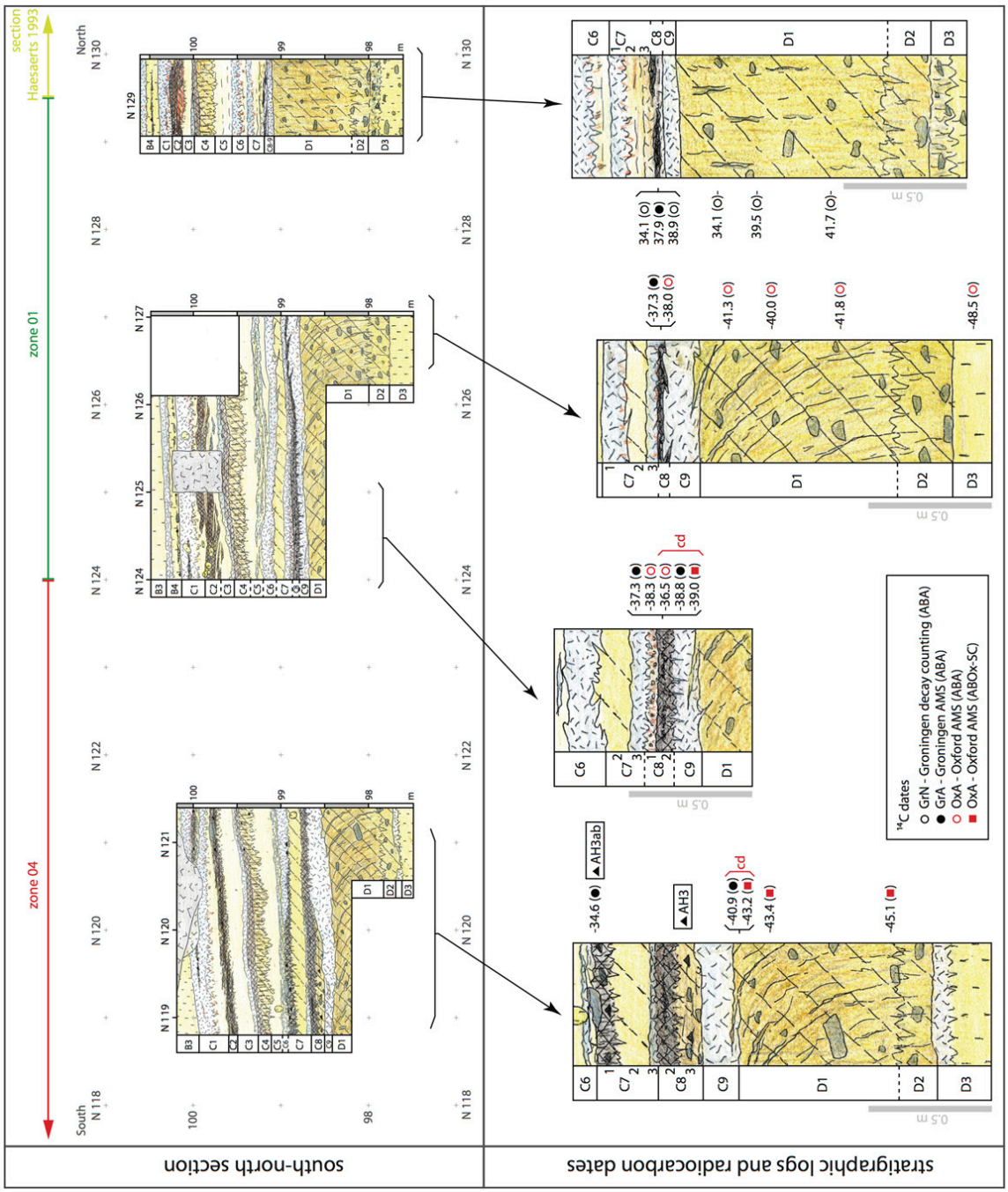

Figure S3: Willendorf II – excavation 2006-2011: Location and stratigraphic position of the radiocarbon dates. Top: north-south section. The figure shows the central excavated part of the 2006-2011 zones 01 and 04 (i.e. N 118 to N 130; see also Figure S1). The entire illustrated area was excavated, but only representative parts of the section highlighting different preservation of horizon C8-3 and under-/overlying units

are shown in detail. Bottom: Stratigraphic logs with stratigraphic position of radiocarbon dating samples. Radiocarbon ages are in ka BP. For a comparison of the radiocarbon ages, see also Figure S4. Key to graphic symbols: Figure S20.

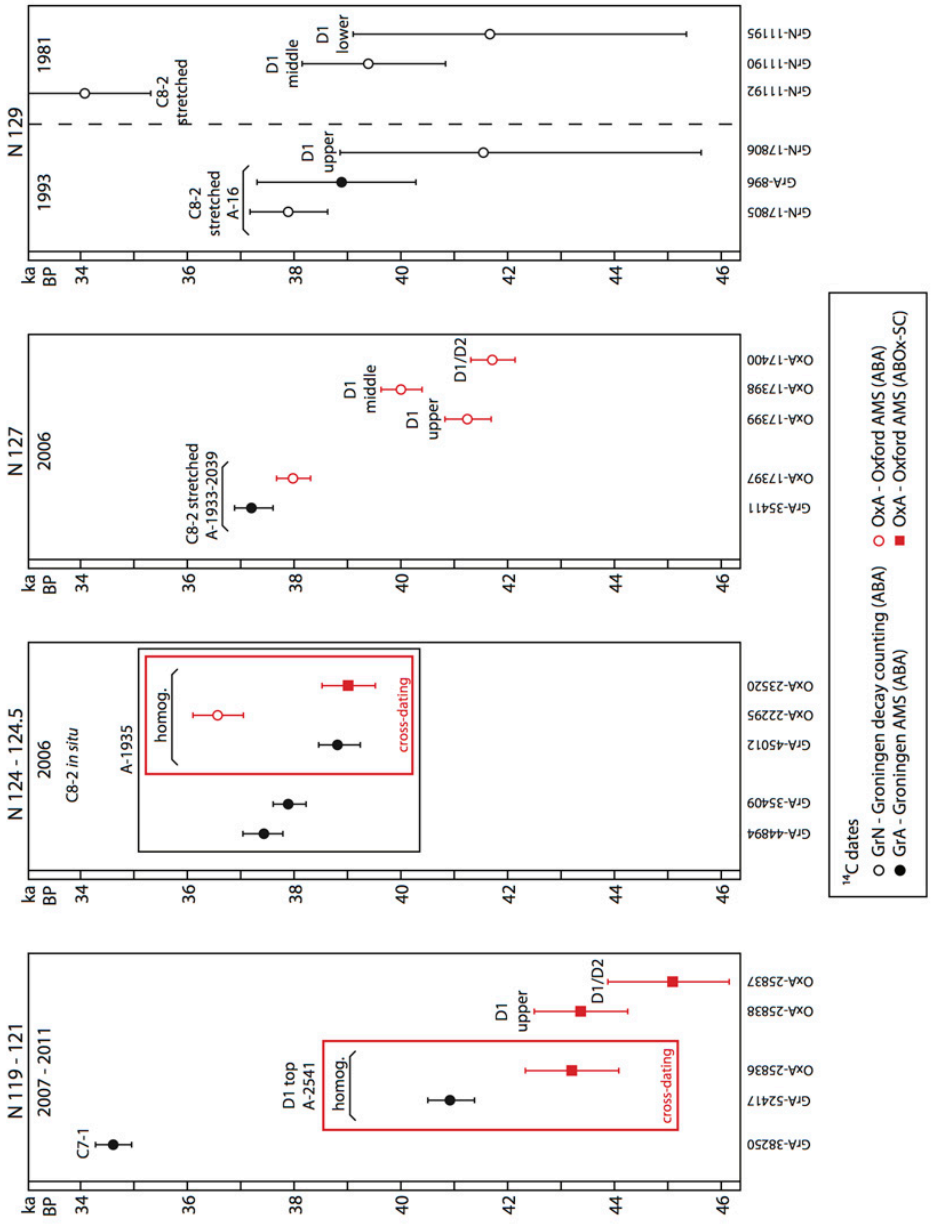

Figure S4: Willendorf II – excavation 2006-2011: Comparison of radiocarbon dates grouped in the four areas shown in Figure S3. Stratigraphic horizons (e.g. C7-1) and charcoal samples numbers (e.g. A-2541) are listed. Red boxes show radiocarbon dates produced in our cross-dating (27). Radiocarbon ages are in ka BP. Laboratory numbers of dates are shown at the bottom.

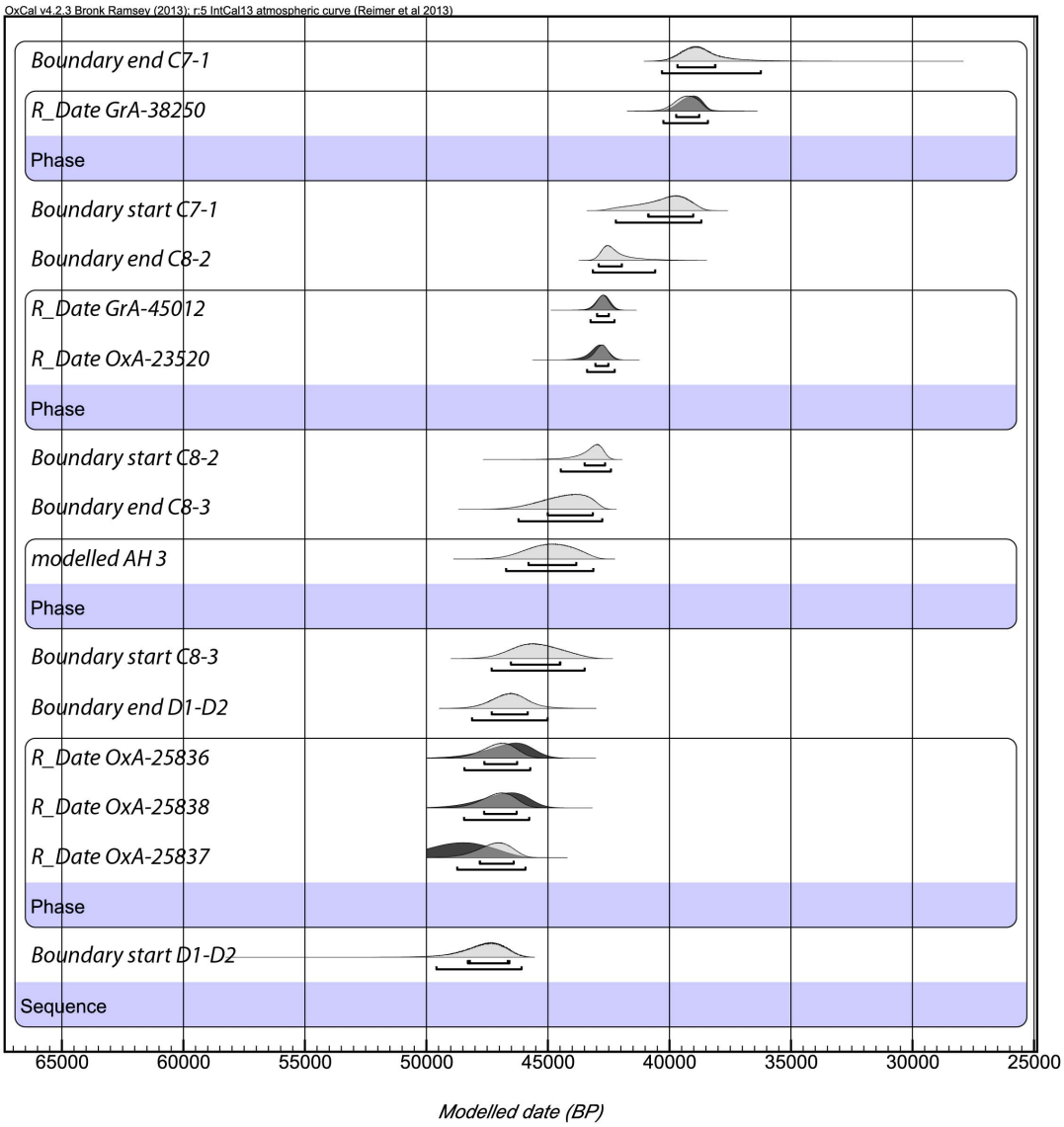

Figure S5: Willendorf II - Bayesian age model for the lower part of the sequence (D2-D1 to C7-1) produced using OxCal4.2.3 software (32). Radiocarbon ages are calibrated using the IntCal13 calibration curve (31). Radiocarbon likelihoods are illustrated by the dark grey distributions and the lighter grey distributions represent the posterior probability distributions. See also Table S7.

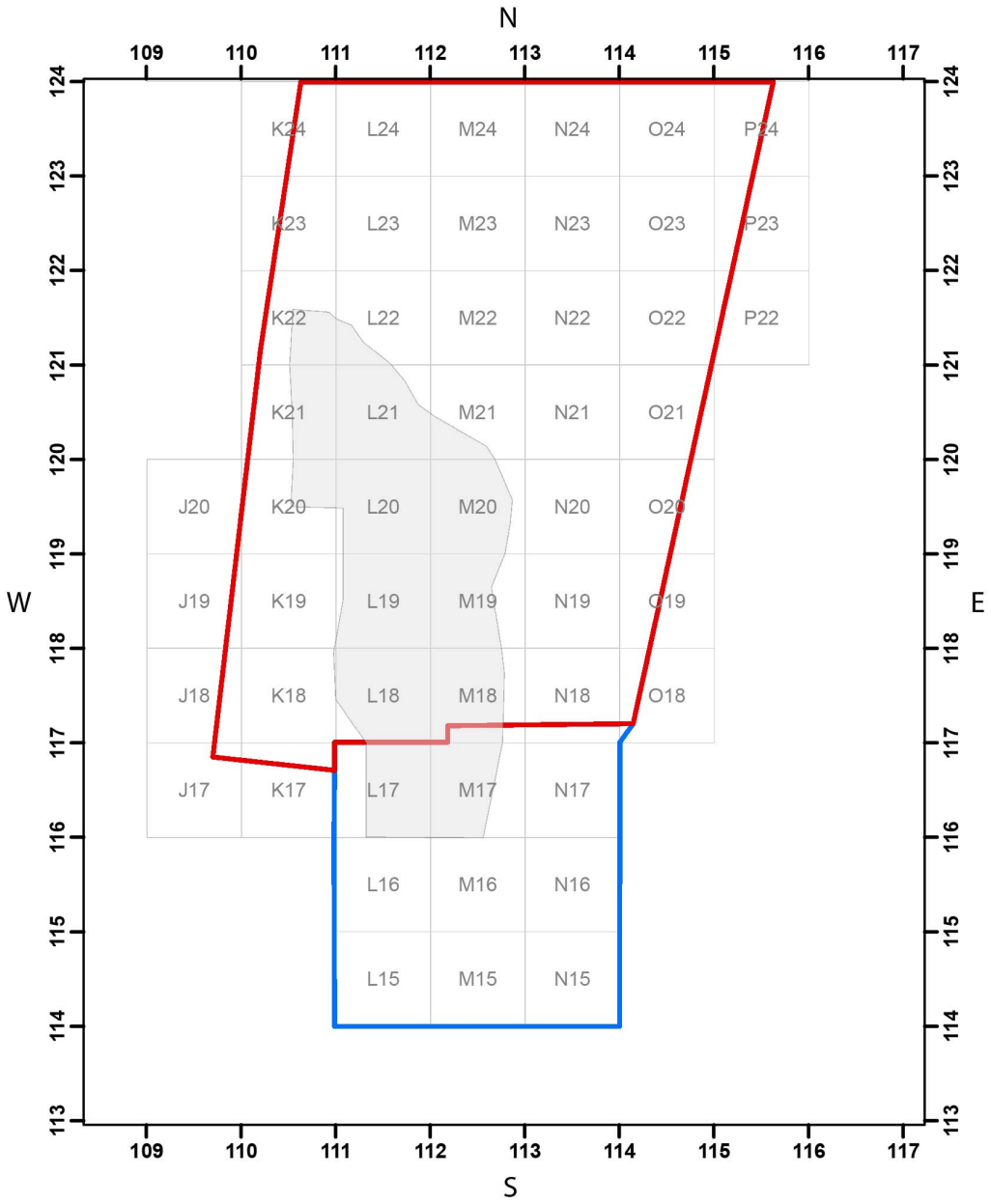

Fig. S6: Willendorf II – Excavated extent of SU C8-3 (grey) in zones 03 (blue) and 04 (red). Scale in meters.

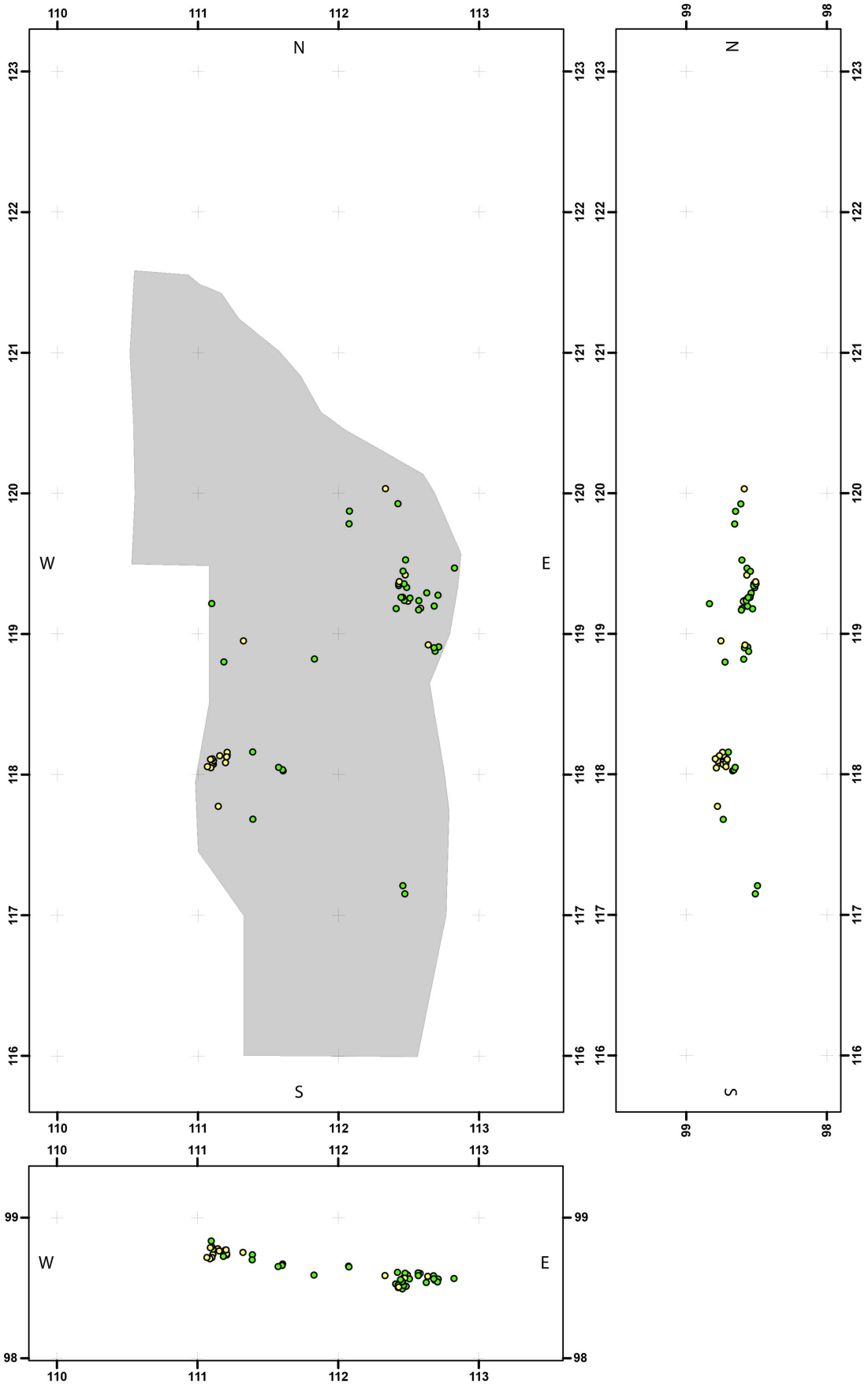
110
111
112
113
123
122
121
120
119
118
117
116
N
W
E
S
99
98

Fig. S7 (previous page): Willendorf II – AH3: Spatial distribution of lithic artifacts (green) and faunal remains (yellow). Shown are the map view and the section views (bottom: east-west-projection, right: south-north-projection). Please note that the east-west-projection and south-north-projection show the finds of the entire area. Therefore the vertical distribution appears larger than the usual 5 to 15 cm thickness of SU C8-3. This is due to the slight general northwest to southeast inclination of all sedimentary bodies. Excavated extent of SU C8-3 is shown in grey. Scale in meters.

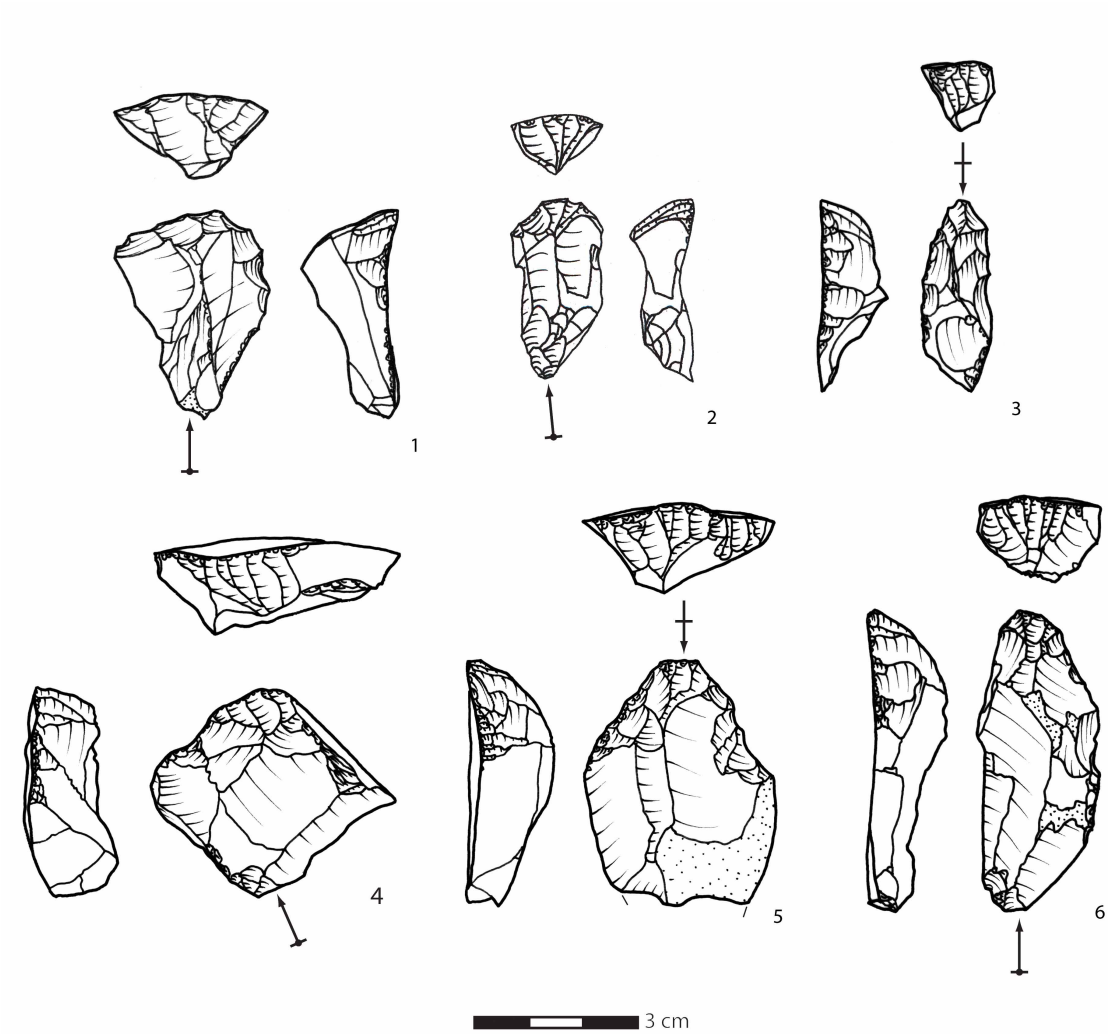

Fig. S8: Willendorf II –AH 3/old collection. 1-6: Carinated/nosed endscraper-cores for the production of small bladelets. Key to graphic symbols: Figure S21.

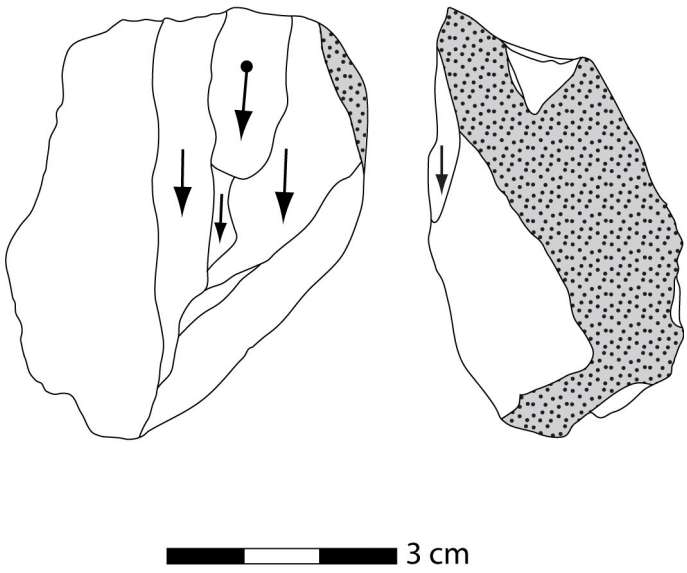

Fig. S9: Willendorf II – AH 3/old collection: Unidirectional bladelet core for the production of large bladelets. Key to graphic symbols: Figure S21.

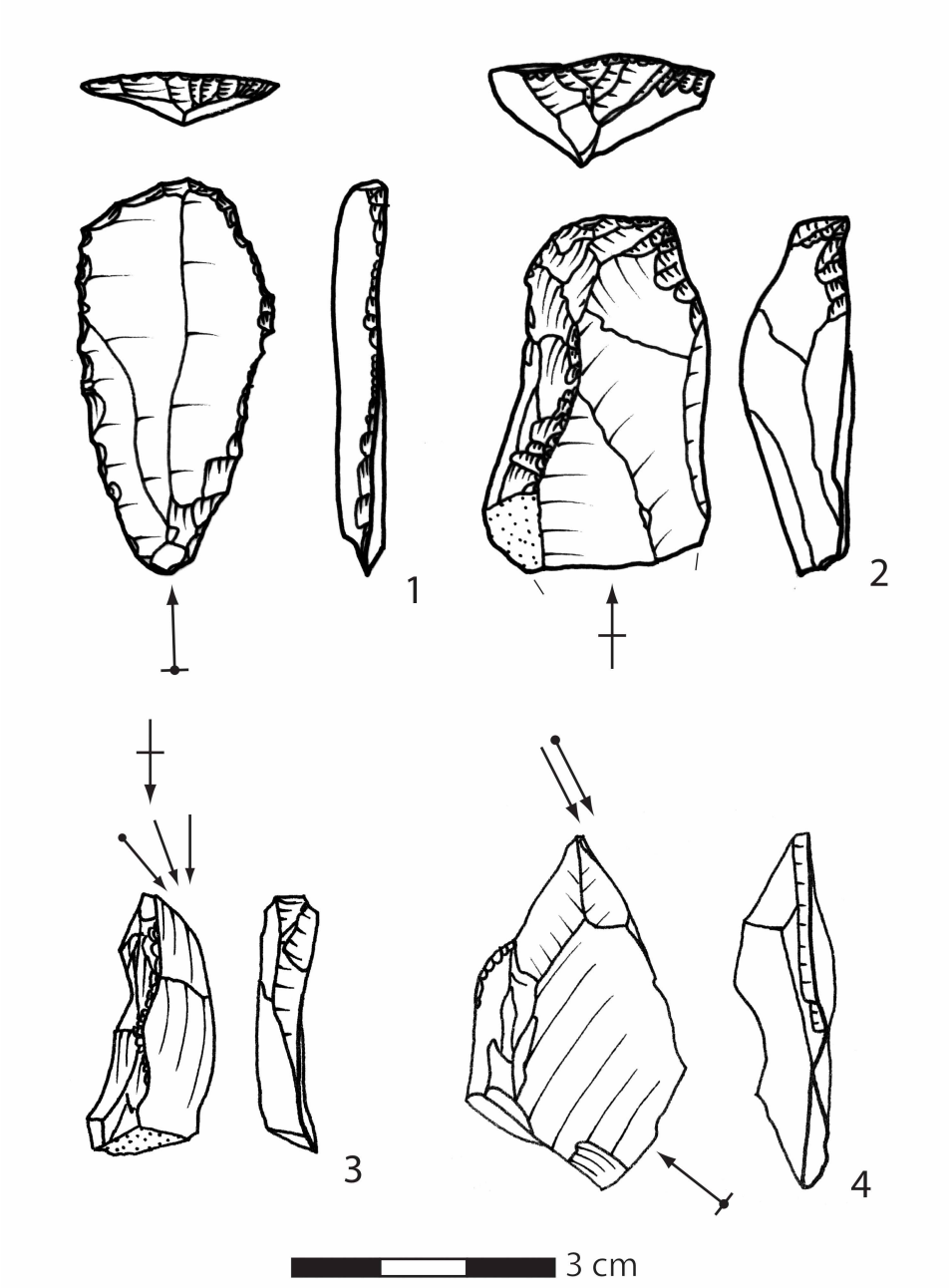

Fig. S10: Willendorf II – AH 3/old collection: 1, 2: endscraper. 3, 4: burin. Key to graphic symbols: Figure S21.

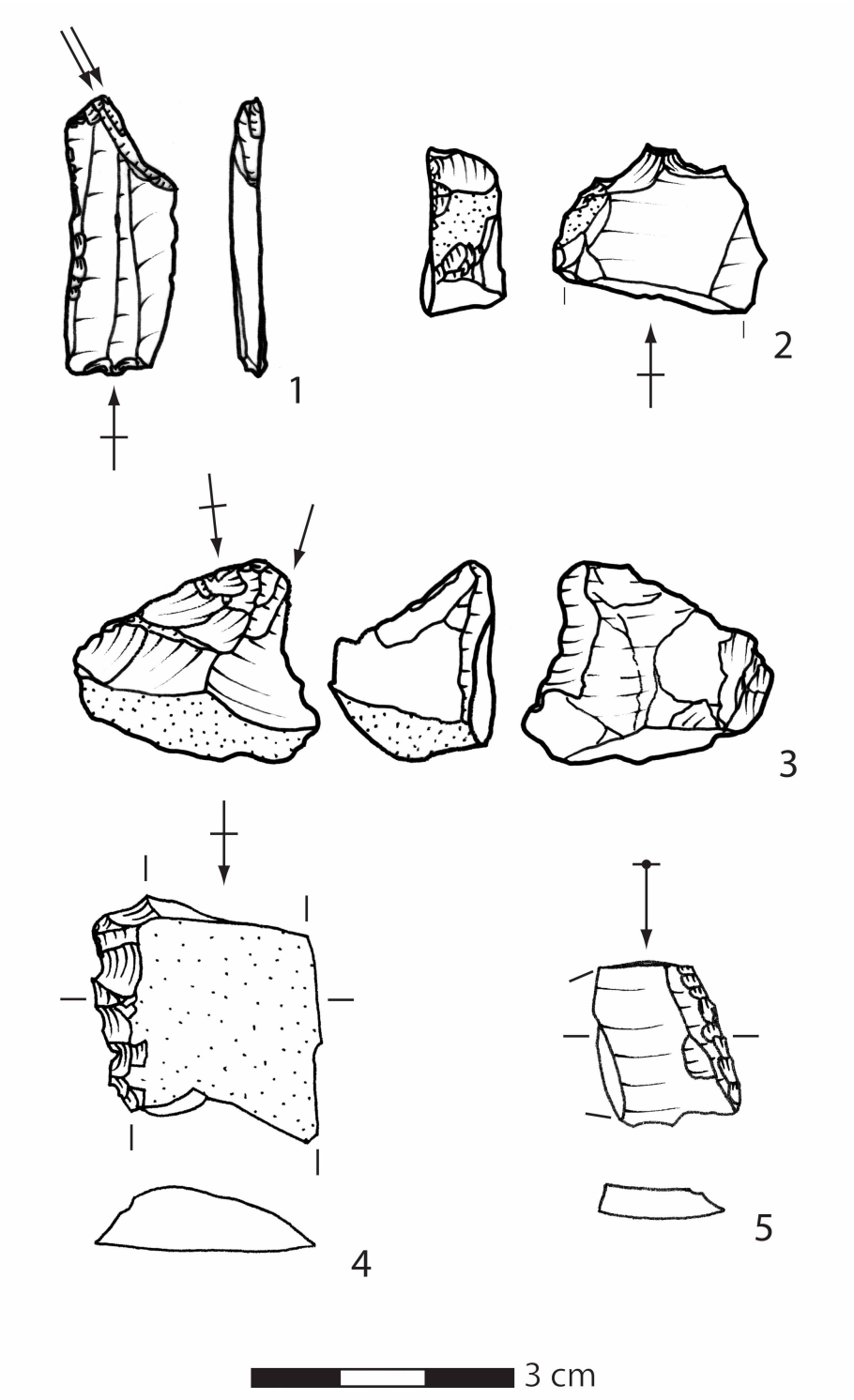

Fig. S11: Willendorf II – AH 3/old collection: Retouched lithics. 1, 3: burin. 2: borer. 4, 5: edge/lateral retouch. Key to graphic symbols: Figure S21.

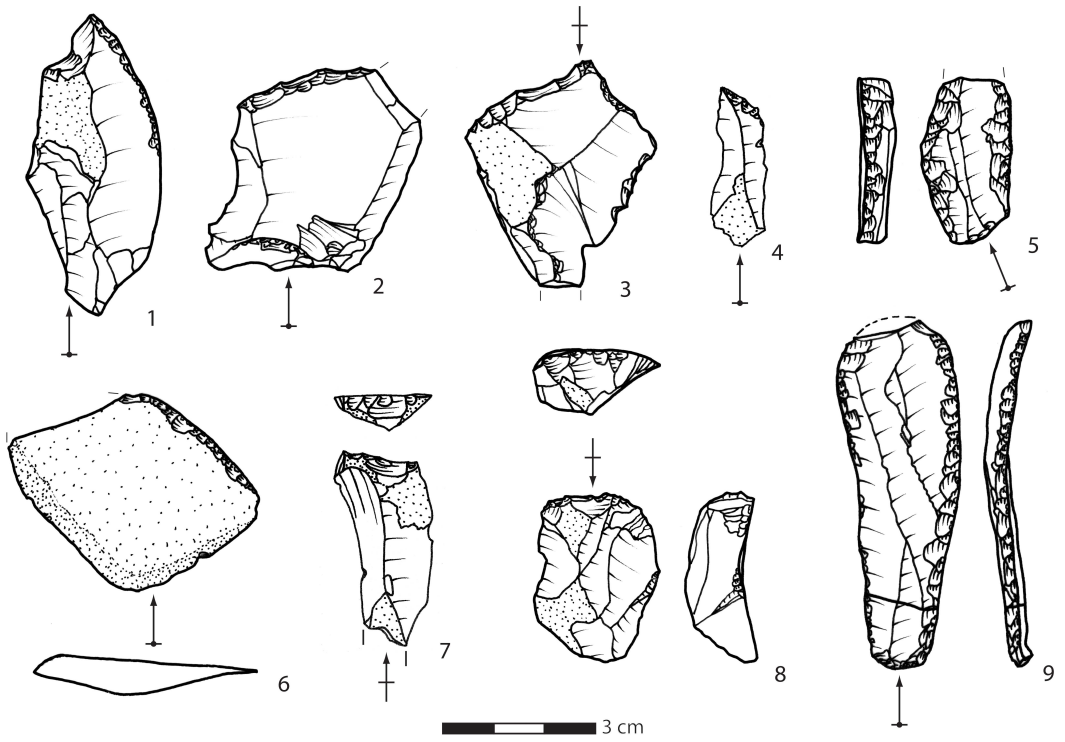

Fig. S12: Willendorf II – AH 3/old collection: Retouched lithics. 1, 9: lateral retouch. 2, 6: scraper. 3: thin nosed endscraper. 4, 7, 8: truncated piece. 5: fragment of Aurignacian blade. Key to graphic symbols: Figure S21.

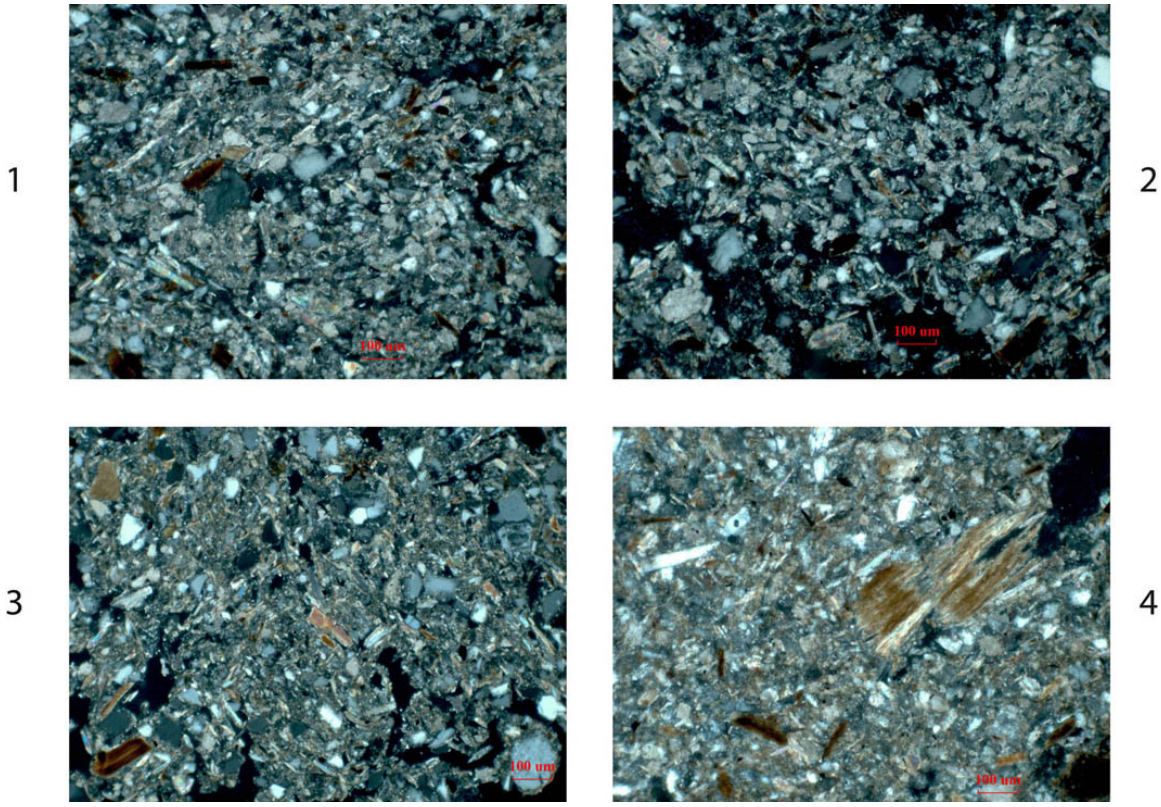

Figure S13: Willendorf II – micromorphology: Representative views of sub-units C7-2 (1), C9 (2), D1 (3) and D2 (4). Note their sandy, calcareous composition and the presence of clay and weathered mica in D1 and D2. Images in crossed polarized light (XPL).

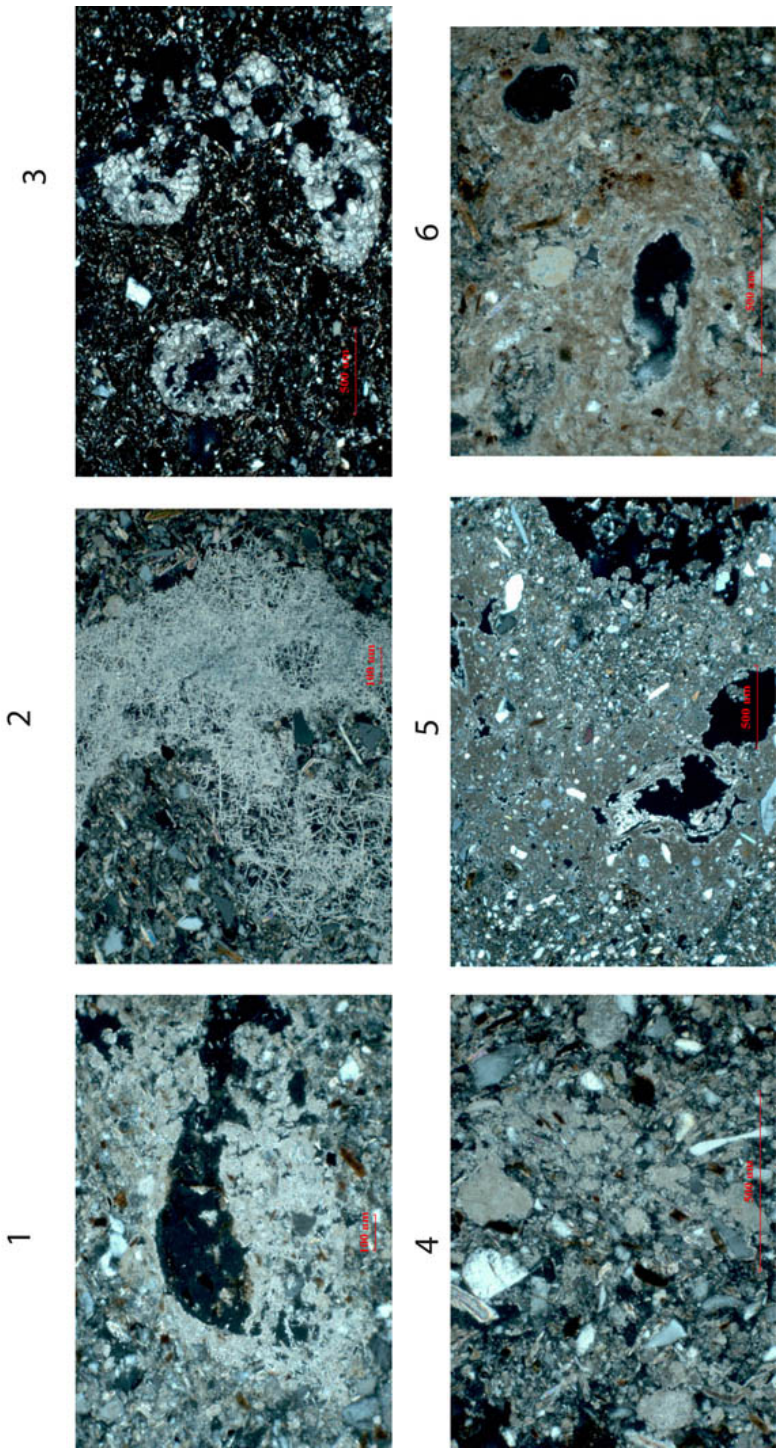

Figure S14: Willendorf II – micromorphology: Selected examples of the different kinds of calcareous biogenic pedofeatures observed in the different stratigraphic units: 1 and 2: Needle-fiber calcite infillings (C7-1 (1) and C8-2 (2)). 3: cytomorphic calcite (C8-2). 4: micritic aggregates (C9). 5 and 6: micritic hypocoatings (D1 (5) and D2 (6)). Images in XPL.

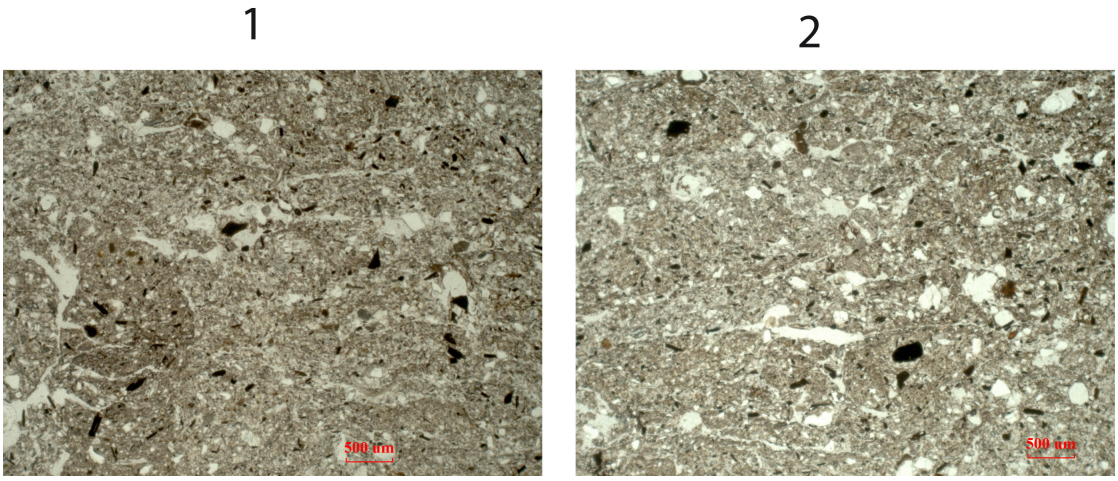

Figure S15: Willendorf II – micromorphology: Plane polarized light (PPL) images of loessic sediment from C9 (1 and 2) affected by micro-frost lensing.

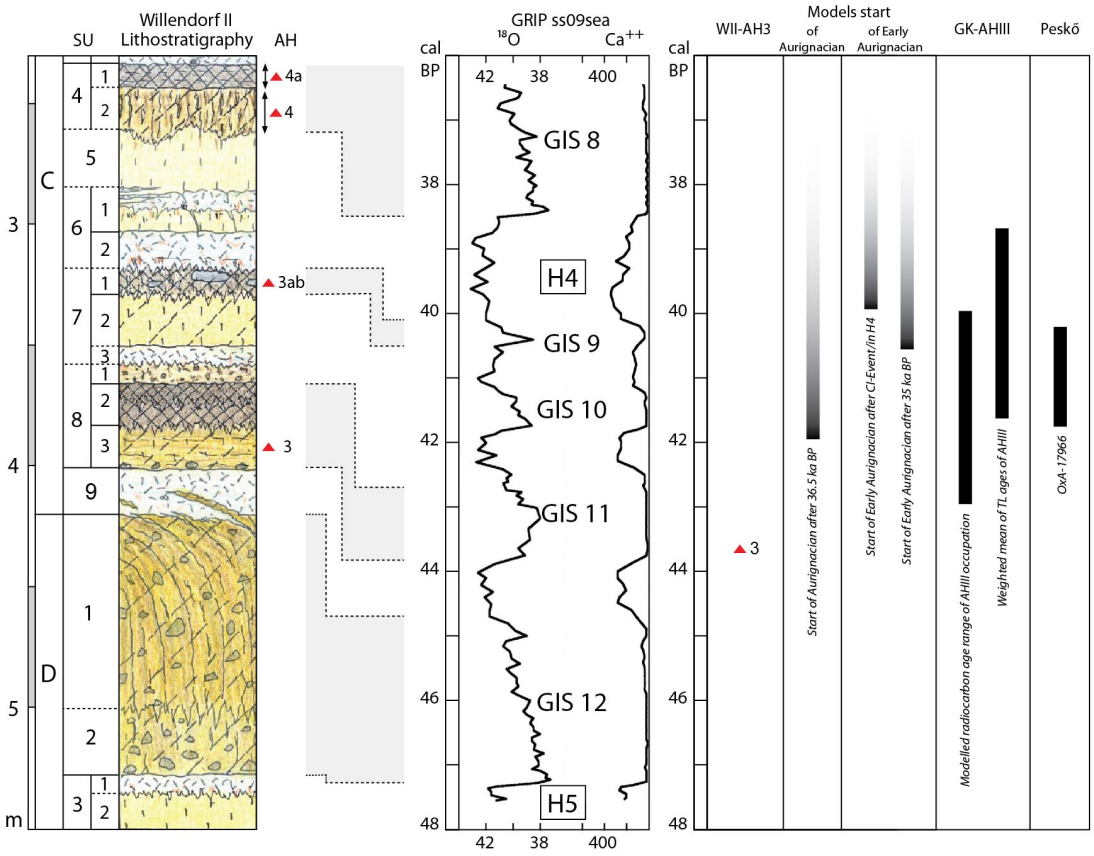

Figure S16: Comparison of the chronostratigraphic position of AH 3 at the onset of GIS 11 with late appearance models for the Aurignacian (56) and Early Aurignacian (57-59), the published ages estimations for AH III of Geißenklösterle, Germany (modelled radiocarbon ages (42) and TL ages (60)) and the calibrated radiocarbon date for an Aurigncian bone point of Peskő, Hungary (61). Modeled radiocarbon and TL ages are given at 68.2% probability. Table S11 lists the ages used in uncal BP and cal BP. Key to graphic symbols: Figure S20. H4 = Heinrich Event 4, H5 = Heinrich Event 5.

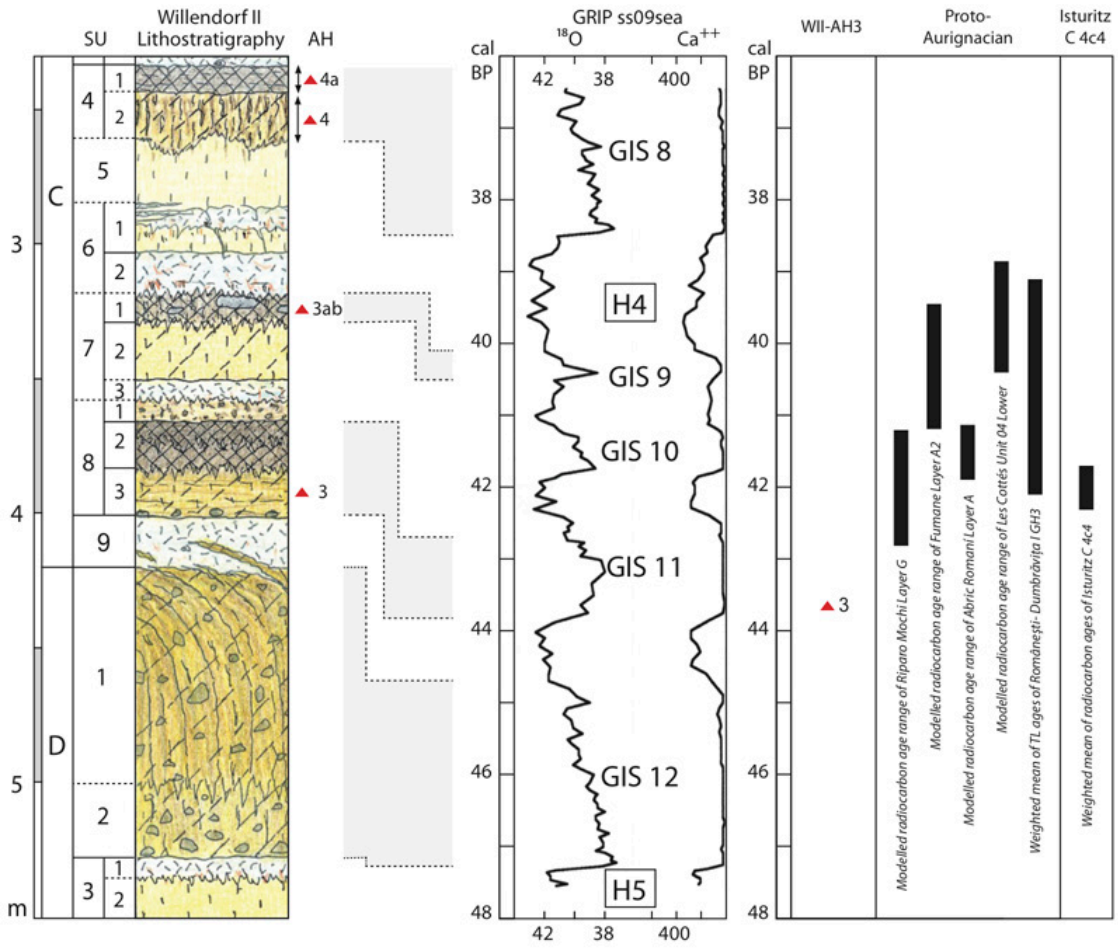

Figure S17: Comparison of the chronostratigraphic position of AH 3 at the onset of GIS 11 with modelled radiocarbon ages for the Proto-Aurignacian archeological horizons at Riparo Mochi (43), Fumane (62), Abric Romani (63) and Les Cottes (64), the weighted mean of TL dates from Romansesti-Dubravita I (65), and the calibrated age of the weighted mean of radiocarbon dates from Isturitz C 4c4 (66). Modeled radiocarbon and TL ages are given at 68.2% probability. Table S12 lists the ages in uncal BP and cal BP. Key to graphic symbols: Figure S20. H4 = Heinrich Event 4, H5 = Heinrich Event 5.

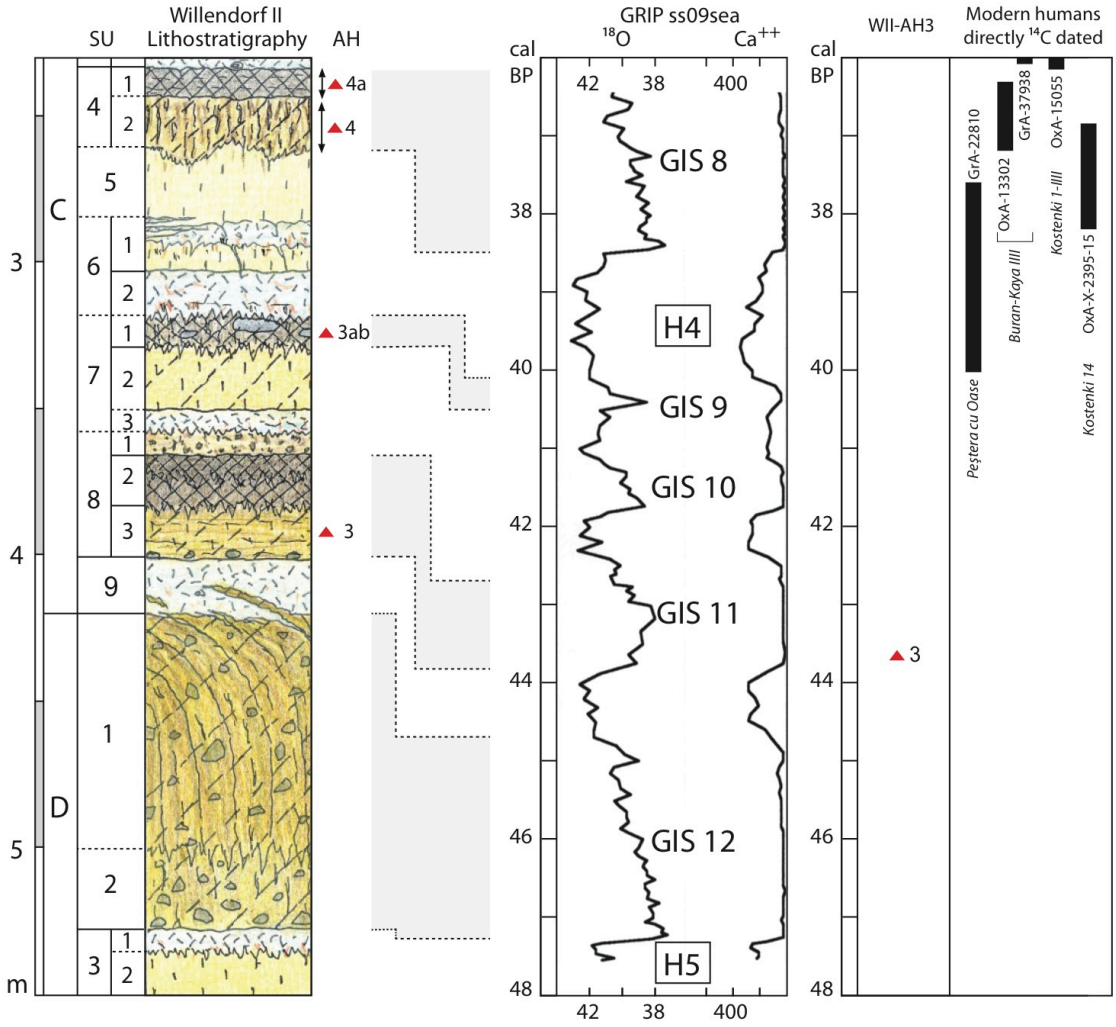

Figure S18: Comparison of the chronostratigraphic position of AH 3 at the onset of GIS 11 with calibrated radiocarbon ages of directly-dated modern human fossils. Calibrated radiocarbon ages are plotted at 68.2% probability. For references and details, see Table S13. Key to graphic symbols: Figure S20. H4 = Heinrich Event 4, H5 = Heinrich Event 5.

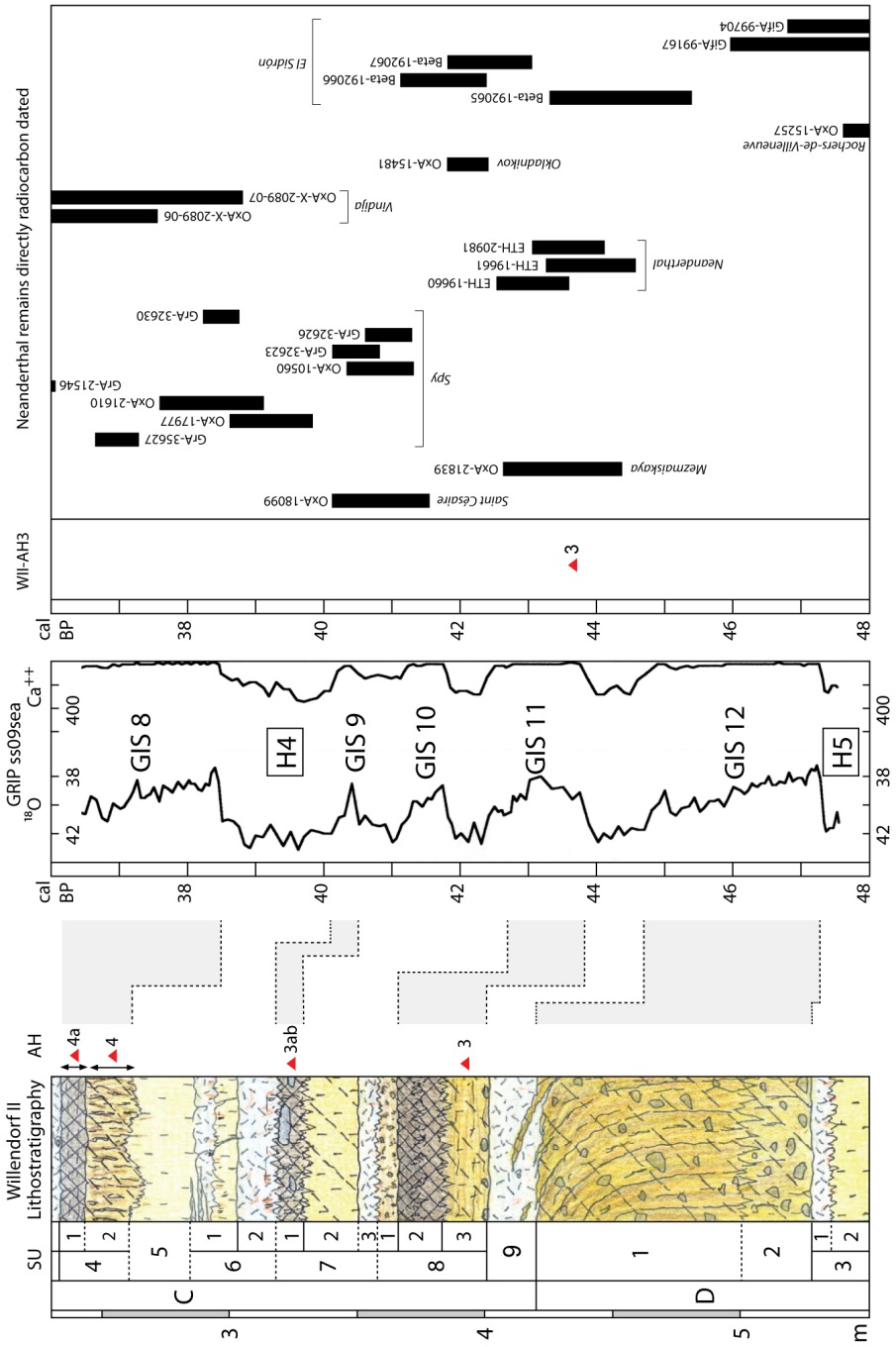

Figure S19: Comparison of the chronostratigraphic position of AH 3 at the onset of GIS 11 with calibrated radiocarbon ages of directly dated (radiocarbon) Neanderthal fossils. Calibrated radiocarbon ages are plotted at 68.2% probability. For references and details, see Table S14. Key to graphic symbols: Figure S20. H4 = Heinrich Event 4, H5 = Heinrich Event 5.

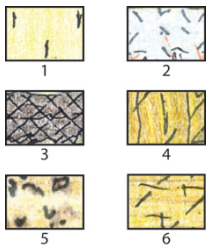

Figure S20: Key to figures with stratigraphic logs. 1: loess. 2: tundra gley. 3: humic horizon. 4: bioturbated B horizon. 5: redeposited humic pellets. 6: sandy loam.

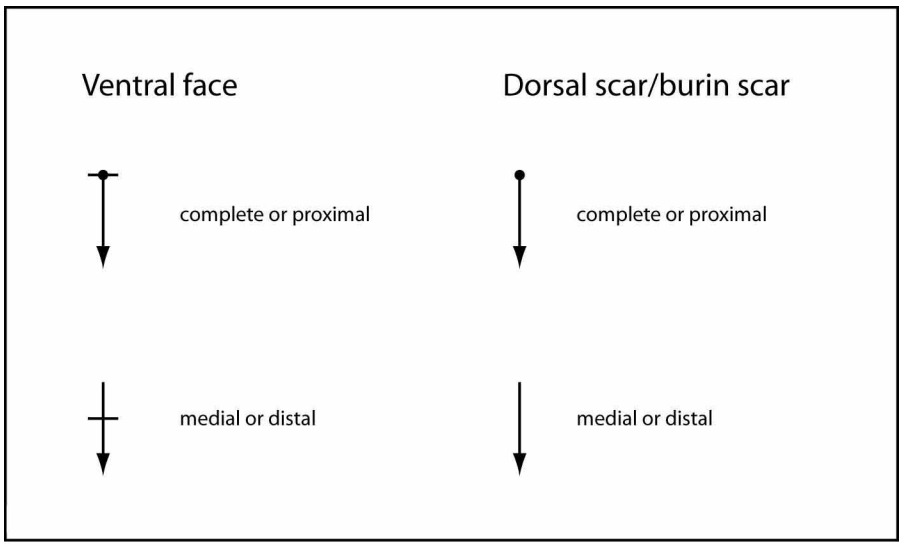

Fig. S21: Key to figures with lithic artifacts.

SI Tables

Table S1: Willendorf II – Radiocarbon dates for geological sub-units D2-D1 to C4. Dates are grouped by geological horizon (e.g. C7-1) and position along the north-south section (e.g. N 121; see Figures S3 and S4). The column "Cal age BP" shows the calibrated radiocarbon ages at 68.2% probability (calibration curve: InCal13 (31), software: OxCal4.2.3 (32)). For radiocarbon dates from sub-unit C3 to the top of sequence, see (2). Asterisks (*) mark out-of-range dates.

(next page)

n° charcoal sample	Year	Taxon	pretreatment	laboratory n°	14C age BP	Cal age BP	reference
C4-1	**N 125-126**						
Two samples, non homogenized							
A-1905	2006	*Picea/Larix*	ABA	GrA-35403	31250 +230/-210	35380 - 34870	(3)
A-1906	2006	*Picea/Larix*	ABA	GrA-35404	31770 +250/-230	35982 - 35387	(3)
One sample, non homogenized, sub-samples a and b							
A-1912 a	2006	*Picea/Larix*	ABA	GrA-35406	31170 +230/-210	35965 - 35404	(3)
A-1912 b	2006	*Picea/Larix*	ABA	OxA-17396	32230 ±190	36338 - 35919	this paper
C4-2	**N 126**						
One sample, non homogenized							
A-2421 a	2007	*Pinus t. cembra*	ABA	GrA-45804	32360 +210/-190	36483 - 36021	this paper
The same sample, homogenized (cross-dating)							
A-2421 a	2007	*Pinus t. cembra*	ABA	GrA-45011	32790 +210/-200	37042 - 36369	this paper
A-2421 b	2007	*Pinus t. cembra*	ABA	OxA-22294	31750 ±260	35969 - 35351	this paper
A-2421 c	2007	*Pinus t. cembra*	ABOx-SC	OxA-23562	33850 ±800	39160 - 37066	this paper
C7-1 (AH3ab)	**N 121**						
A-2131	2007	*Picea*	ABA	GrA-38250	34570 +410/-330	39531 - 38650	this paper
C8-2 stretched	**N 129**						
One sample, non homogenized							
PH 1990	1981	charcoal	ABA	GrN-11192	34100 +1200/-1000	39905 - 36984	(5)
One sample, non homogenized, sub-samples a and b							
A-166 a	1993	*Picea*	ABA	GrA-896	37930 ±750	42721 - 41686	(2)
A-166 b	1993	*Picea*	ABA	GrN-17805	38880 +1530/-1280	44372 - 41816	(2)
C8-2 stretched	**N 127**						
Two samples, non homogenized							
A-2039	2006	*Picea*	ABA	GrA-35411	37320 +390/-350	42086 - 41510	this paper
A-1933	2006	*Picea*	ABA	OxA-17397	37980 ±300	42437 - 42010	this paper
C8-2 in situ	**N 124-124.5**						
One sample, non homogenized, sub-samples a and b							
A-1935 a	2006	*Picea/Larix*	ABA	GrA-44894	37420 +300/-270	42094 - 41640	this paper
A-1935 b	2006	*Picea/Larix*	ABA	GrA-35409	37910 +440/-380	42484 - 41888	this paper
The same sample, homogenized, sub-sample c in three parts (cross-dating)							
A-1935 c2	2006	*Picea/Larix*	ABA	OxA-22295	36500 ±450	41575 - 40697	this paper
A-1935 c1	2006	*Picea/Larix*	ABA	GrA-45012	38790 +400/-350	43001 - 42445	this paper
A-1935 c3	2006	*Picea/Larix*	ABOx-SC	OxA-23520	39000 ±500	43226 - 42504	this paper
D1 top	**N 121**						
One sample, homogenized (cross-dating)							
A-2541 a	2011	*Larix* type	ABA	GrA-52417	40870 ±480/400	44881 - 43951	this paper
A-2541 b	2011	*Larix* type	ABOx-SC	OxA-25836	43200 ±900	47431 - 45562*	this paper
D1 upper	**N 127**						
A-1911	2006	*Larix type*	ABA	OxA-17399	41280 ±380	45124 - 44418	this paper
D1 upper	**N 121**						
A-2542	2011	*Larix/Picea*	ABOx-SC	OxA-25838	43400 ±900	47644 - 45737*	this paper
D1 upper	**N 129**						
A-17	1993	*Larix/Picea*	ABA	GrN-17806	41600 +4900/-2700	-	(2)
D1 middle	**N 127**						
A-1907	2006	*Larix type*	ABA	OxA-17398	39980 ±350	43950 - 43245	this paper
D1 middle	**N 129**						
PH 90	1981	charcoal	ABA	GrN-11190	39500 +1500/-1200	44745 - 42264	(5)
D1 lower	**N 127**						
A-1908	2006	*Picea*	ABA	OxA-17400	41800 ±400	45551 - 44829	this paper
D1 lower	**N 129**						
PH 90	1981	charcoal	ABA	GrN-11195	41700 +3700/-2500	-	(5)
D1/D2	**N 121**						
A-2537	2011	*Larix/Picea*	ABOx-SC	OxA-25837	45100 ±1100	49570 - 47500*	this paper
D3	**N 127**						
A-2017	2006	*Larix* type	ABA	OxA-17401	48500 ±800	49351 - 47731*	this paper

Tab. S2: Willendorf II – AH 3 (old and new collections): Lithics dataclasses and tool types. Cores and formal tool types both include carinated/nosed endscraper cores. Flakes, blades and bladelets include crested specimens. Data on old collections after Nigst 2012 (18).

Category	**Old collection**	**Old box collection**	**New collection (2006-2011)**	**Total**
Lithics	48	442	32	522
Debitage	39	302	21	362
Cores	8	27	0	35
Formal tool types	26	10	0	36
nosed endscraper	*4*	*0*	*0*	*4*
carinated endscraper	*3*	*0*	*0*	*3*
carinated endscraper + edge retouch	*2*	*0*	*0*	*2*
endscraper	*2*	*0*	*0*	*2*
endscraper + edge retouch	*2*	*0*	*0*	*2*
truncation	*2*	*1*	*0*	*3*
sidescraper	*2*	*0*	*0*	*2*
Aurignacian blade	*1*	*0*	*0*	*1*
burin	*1*	*1*	*0*	*2*
dihedral burin	*0*	*1*	*0*	*1*
dihedral burin + edge retouch	*0*	*1*	*0*	*1*
burin + truncation + edge retouch	*1*	*0*	*0*	*1*
borer	*1*	*0*	*0*	*1*
edge/lateral retouch	*5*	*6*	*0*	*11*
Carinated/nosed endscraper-cores	6	0	0	6
Flakes	21	255	18	294
Blades	17	42	0	59
Bladelets	1	5	3	9
Core tablet	1	0	1	2

Tab. S3: Collections of AH 3 and their classification by different researchers.

Collection	Number of lithic artifacts	Researcher(s)	Classification	Reference
old collection (1908-1955)	48	Felgenhauer	Aurignacian	(1)
		Broglio & Laplace	Aurignacian	(83)
		Hahn	Aurignacian	(15)
		Kozlowski & Otte	Typical Aurignacian	(84)
		Zilhão & d'Ericco	"Transitional"	(56)
		Teyssandier	Early Aurignacian	(50)
		Zilhão	Early Aurignacian	(57)
48 old collection and 442 old box collection (1908-1955)	490	Nigst	Early Aurignacian	(18)
new collection (2006-2011)	32	Nigst	Early Aurignacian	This paper

Table S4: Willendorf II – AH3 (2006-2011 excavations): Frequencies of basic lithic dataclasses. For definitions of terms see (18).

Dataclass	***Frequency***
Flake	20
Shatter	5
Bladelet	3
Chip	2
Core tablet	1
Thermal shatter	1
Total	**32**

Table S5: Willendorf II – Malacological samples: Number of individuals grouped by ecological groups (refering to woodland, xeric, open, mesic and humid (including wet) habitats). The column "sub-unit" lists the geological sub-unit each sample was collected in. For further details see Table S6.

sample ID	sub-unit	Woodland n	Woodland %	Xeric n	Xeric %	Open n	Open %	Mesic n	Mesic %	Humid n	Humid %	total n	total %
11-4	C6-2	57	7.97	36	5.03	131	18.32	479	66.99	12	1.68	715	100.00
11-3	C7-2	67	7.31	360	39.26	147	16.03	330	35.99	13	1.42	917	100.00
10-8	C8-2 upper	15	8.29	90	49.72	36	19.89	36	19.89	4	2.21	181	100.00
10-7	C8-2 lower	60	12.10	267	53.83	127	25.60	39	7.86	3	0.60	496	100.00
10-6	C8-3 upper	2	8.70	13	56.52	7	30.43	1	4.35	0	0.00	23	100.00
11-2	C8-3 lower	16	3.43	226	48.39	102	21.84	120	25.70	3	0.64	467	100.00
10-4	C9 upper	8	3.00	123	46.07	75	28.09	61	22.85	0	0.00	267	100.00
10-5	C9 middle	3	2.11	46	32.39	50	35.21	42	29.58	1	0.70	142	100.00
11-1	D1 top	30	27.27	25	22.73	12	10.91	37	33.64	6	5.45	110	100.00
10-1	D1 upper	4	30.77	3	23.08	1	7.69	5	38.46	0	0.00	13	100.00
06-1	D1 upper	143	33.89	59	13.98	40	9.48	172	40.76	8	1.90	422	100.00
06-2	D1 middle	82	28.08	32	10.96	37	12.67	135	46.23	6	2.05	292	100.00
06-3	D1 middle	103	17.22	194	32.44	133	22.24	162	27.09	6	1.00	598	100.00
06-4	D1 lower	141	36.15	61	15.64	63	16.15	119	30.51	6	1.54	390	100.00
06-5	D2	100	33.44	53	17.73	51	17.06	93	31.10	2	0.67	299	100.00
06-6	D3	90	6.43	419	29.95	284	20.30	600	42.89	6	0.43	1,399	100.00

Table S6: Willendorf II – malacological samples: Numbers of Species (S) and Individuals (I) for each species identified and grouped into ecological groups (refering to woodland, xeric, open, mesic and humid (including wet) habitats). Abbreviations: W = (dense) forest; Wf and W(Wf) = rocky woodland, rocks; W(Ws) = light, xeric woodland; Wh = humid woods; Ws(S) = light, xeric woodland to open, xeric habitats; Ws(Of) = light, xeric woodland to open, rocky habitats; W, Ws(M) = woodland in general, open, light woods to mesic habitats; W(M) = woodland to mesic habitats; W(H) = woodland to humid habitats; S(Sf) = xeric, open, mostly rocky habitats; SX and X= xeric to extremely dry habitats; X(Sf) = very xeric to dry, rocky habitats; O = open habitats in general; O(Of) = open, mostly rocky habitats; O(Ws) = open habitats to light, xeric woodland; O(X) = open habitats in general to xeric habitats; O(H) = open habitats in general to humid habitats; M = mesic habitats in general; Mf = mesic, rocky habitats; M(W) = mesic habitats to woodland; M(X) = mesic to xeric habitats; M(P) = mesic to wet habitats; H = humid habitats in general; H(M) = humid to mesic habitats; P = wet habitats in general.

(next 18 pages)

sample ID	11-1	11-1	11-1	11-1	11-2	11-2	11-2	11-2	11-3	11-3	11-3	11-3
	S n	S %	I n	I %	S n	S %	I n	I %	S n	S %	I n	I %
Species/Preferred Type of Habitat												
W	**3**	**15.00**	**4**	**3.64**								
Acanthinula aculeata												
Ena montana			*1*									
Discus ruderatus			*1*									
Aegopinella nitens												
Aegopis verticillus												
Limax sp.			*2*									
Ruthenica filograna												
Semilimax kotulae												
Helicodonta obvoluta												
Monachoides incarnatus												
cf. Bulgarica cana												
Causa holosericea												
Wf	**2**	**10.00**	**16**	**14.55**	**2**	**15.38**	**14**	**3.00**	**1**	**6.25**	**59**	**6.43**
Orcula dolium			*2*				*1*					
Vertigo alpestris												
Clausilia dubia			*14*				*13*				*59*	
W(Wf)	**1**	**5.00**	**1**	**0.91**								
Helicigona lapicida			*1*									
W(Ws)												
Vertigo pusilla												
Wh												
Perforatella bidentata												
Ws(S)	**1**	**5.00**	**1**	**0.91**								
Euomphalia strigella			*1*									
Ws(Of)												
Milacidae (cf., Schaelchen)												
W, Ws(M)												
Helix pomatia												
W(M)	**3**	**15.00**	**8**	**7.27**	**2**	**15.38**	**2**	**0.43**	**2**	**12.50**	**8**	**0.87**
Balea biplicata												
Discus rotundatus												
Vitrea crystallina			*2*									
Euconulus fulvus												
Nesovitrea hammonis			*2*				*1*				*7*	
Fruticicola fruticum												
Arianta arbustorum			*4*				*1*				*1*	
W(H)												
Vertigo substriata												
Semilimax semilimax												
Petasina unidentata												
Trochulus suberectus												
Woodland total	**10**	**50.00**	**30**	**27.27**	**4**	**30.77**	**16**	**3.43**	**3**	**18.75**	**67**	**7.31**
S(Sf)	**2**	**10.00**	**25**	**22.73**	**2**	**15.38**	**226**	**48.39**	**2**	**12.50**	**360**	**39.26**
Pupilla triplicata			*24*				*223*				*243*	
Pupilla sterrii			*1*				*3*				*117*	
Granaria frumentum												
SX												
Chondrula tridens												

sample ID	11-1	11-1	11-1	11-1	11-2	11-2	11-2	11-2	11-3	11-3	11-3	11-3
	S n	S %	I n	I %	S n	S %	I n	I %	S n	S %	I n	I %
X												
Monacha cartusiana												
X(Sf)												
Cochlicopa lubricella												
Cochlicopa cf. *lubricella*												
Xeric total	**2**	**10.00**	**25**	**22.73**	**2**	**15.38**	**226**	**48.39**	**2**	**12.50**	**360**	**39.26**
O	**1**	**5.00**	**2**	**1.82**	**2**	**15.38**	**2**	**0.43**	**3**	**18.75**	**60**	**6.54**
Vallonia tenuilabris							1				13	
Vertigo modesta arctica												
Vertigo parcedentata											34	
Pupilla alpicola densegyrata												
Pupilla muscorum			2				1					
Pupilla muscorum vel alpicola densegyrata											7	
Pupilla loessica												
Pupilla sp., apices												
Pupilla sp. juv.											6	
Vertigo pygmaea												
Vertiginidae indet.												
O(Of)									**1**	**6.25**	**14**	**1.53**
Columella columella											14	
O(Ws)	**1**	**5.00**	**10**	**9.09**	**1**	**7.69**	**100**	**21.41**	**1**	**6.25**	**73**	**7.96**
Vallonia costata			10				100				73	
O(X)												
Truncatellina cylindrica												
O(H)												
Vallonia pulchella												
Open total	**2**	**10.00**	**12**	**10.91**	**3**	**23.08**	**102**	**21.84**	**5**	**31.25**	**147**	**16.03**
M	**1**	**5.00**	**24**	**21.82**	**2**	**15.38**	**87**	**18.63**	**1**	**6.25**	**153**	**16.68**
Limacoidea							1					
Trochulus hispidus			*24*				*86*				*153*	
Mf												
Clausilia rugosa parvula												
M(W)									**1**	**6.25**	**1**	**0.11**
Punctum pygmaeum											*1*	
M(X)	**1**	**5.00**	**12**	**10.91**	**1**	**7.69**	**33**	**7.07**	**1**	**6.25**	**168**	**18.32**
Succinella oblonga			*12*				*33*				*168*	
Succinella oblonga >f. *elongata*												
M(P)	**1**	**5.00**	**1**	**0.91**					**1**	**6.25**	**8**	**0.87**
Deroceras sp.			*1*								*8*	
Deroceras sp. 1												
Deroceras sp. 2												
Deroceras sp. 3												
Mesic total	**3**	**15.00**	**37**	**33.64**	**3**	**23.08**	**120**	**25.70**	**4**	**25.00**	**330**	**35.99**
H									**1**	**6.25**	**1**	**0.11**

sample ID	11-1	11-1	11-1	11-1	11-2	11-2	11-2	11-2	11-3	11-3	11-3	11-3
	S n	S %	I n	I %	S n	S %	I n	I %	S n	S %	I n	I %
Nesovitrea petronella											*1*	
H(M)	**1**	**5.00**	**4**	**3.64**	**1**	**7.69**	**3**	**0.64**				
Cochlicopa lubrica			*4*				*3*					
P	**2**	**10.00**	**2**	**1.82**					**1**	**6.25**	**12**	**1.31**
Vertigo antivertigo			*1*									
Euconulus praticola			*1*								*12*	
Humid & Wet total	**3**	**15.00**	**6**	**5.45**	**1**	**7.69**	**3**	**0.64**	**2**	**12.50**	**13**	**1.42**
TOTAL	***20***	***100.00***	***110***	***100.00***	***13***	***100.00***	***467***	***100.00***	***16***	***100.00***	***917***	***100.00***

sample ID	11-4	11-4	11-4	11-4	10-1	10-1	10-1	10-1	10-4	10-4	10-4	10-4
	S n	S %	I n	I %	S n	S %	I n	I %	S n	S %	I n	I %
Species/Preferred Type of Habitat												
W	**1**	**5.56**	**4**	**0.56**								
Acanthinula aculeata												
Ena montana												
Discus ruderatus												
Aegopinella nitens												
Aegopis verticillus												
Limax sp.												
Ruthenica filograna												
Semilimax kotulae			*4*									
Helicodonta obvoluta												
Monachoides incarnatus												
cf. Bulgarica cana												
Causa holosericea												
Wf	**1**	**5.56**	**48**	**6.71**	**1**	**16.67**	**3**	**23.08**	**1**	**11.11**	**8**	**3.00**
Orcula dolium												
Vertigo alpestris												
Clausilia dubia			*48*				*3*				*8*	
W(Wf)												
Helicigona lapicida												
W(Ws)												
Vertigo pusilla												
Wh												
Perforatella bidentata												
Ws(S)												
Euomphalia strigella												
Ws(Of)												
Milacidae (cf., Schaelchen)												
W, Ws(M)												
Helix pomatia												
W(M)	**2**	**11.11**	**5**	**0.70**	**1**	**16.67**	**1**	**7.69**				
Balea biplicata												
Discus rotundatus												
Vitrea crystallina												
Euconulus fulvus												
Nesovitrea hammonis			*4*									
Fruticicola fruticum												
Arianta arbustorum			*1*				*1*					
W(H)												
Vertigo substriata												
Semilimax semilimax												
Petasina unidentata												
Trochulus suberectus												
Woodland total	**4**	**22.22**	**57**	**7.97**	**2**	**33.33**	**4**	**30.77**	**1**	**11.11**	**8**	**3.00**
S(Sf)	**2**	**11.11**	**36**	**5.03**	**1**	**16.67**	**3**	**23.08**	**2**	**22.22**	**123**	**46.07**
Pupilla triplicata			*21*				*3*				*108*	
Pupilla sterrii			*15*								*15*	
Granaria frumentum												
SX												
Chondrula tridens												

sample ID	11-4	11-4	11-4	11-4	10-1	10-1	10-1	10-1	10-4	10-4	10-4	10-4
	S n	S %	I n	I %	S n	S %	I n	I %	S n	S %	I n	I %
X												
Monacha cartusiana												
X(Sf)												
Cochlicopa lubricella												
Cochlicopa cf. *lubricella*												
Xeric total	**2**	**11.11**	**36**	**5.03**	**1**	**16.67**	**3**	**23.08**	**2**	**22.22**	**123**	**46.07**
O	**4**	**22.22**	**32**	**4.48**					**2**	**22.22**	**2**	**0.75**
Vallonia tenuilabris			5								1	
Vertigo modesta arctica			2									
Vertigo parcedentata			7									
Pupilla alpicola densegyrata			5									
Pupilla muscorum											1	
Pupilla muscorum vel alpicola densegyrata												
Pupilla loessica												
Pupilla sp., apices												
Pupilla sp. juv.			13									
Vertigo pygmaea												
Vertiginidae indet.												
O(Of)	**1**	**5.56**	**95**	**13.29**								
Columella columella			95									
O(Ws)	**1**	**5.56**	**4**	**0.56**	**1**	**16.67**	**1**	**7.69**	**1**	**11.11**	**73**	**27.34**
Vallonia costata			4				1				73	
O(X)												
Truncatellina cylindrica												
O(H)												
Vallonia pulchella												
Open total	**6**	**33.33**	**131**	**18.32**	**1**	**16.67**	**1**	**7.69**	**3**	**33.33**	**75**	**28.09**
M	**1**	**5.56**	**225**	**31.47**	**1**	**16.67**	**2**	**15.38**	**1**	**11.11**	**18**	**6.74**
Limacoidea												
Trochulus hispidus			*225*				*2*				*18*	
Mf												
Clausilia rugosa parvula												
M(W)	**1**	**5.56**	**5**	**0.70**								
Punctum pygmaeum			*5*									
M(X)	**1**	**5.56**	**247**	**34.55**	**1**	**16.67**	**3**	**23.08**	**2**	**22.22**	**43**	**16.10**
Succinella oblonga			*247*				*3*				*42*	
Succinella oblonga >f. *elongata*											*1*	
M(P)	**2**	**11.11**	**2**	**0.28**								
Deroceras sp.												
Deroceras sp. 1			*1*									
Deroceras sp. 2			*1*									
Deroceras sp. 3												
Mesic total	**5**	**27.78**	**479**	**66.99**	**2**	**33.33**	**5**	**38.46**	**3**	**33.33**	**61**	**22.85**
H												

sample ID	11-4	11-4	11-4	11-4	10-1	10-1	10-1	10-1	10-4	10-4	10-4	10-4
	S n	S %	I n	I %	S n	S %	I n	I %	S n	S %	I n	I %
Nesovitrea petronella												
H(M)												
Cochlicopa lubrica												
P	**1**	**5.56**	**12**	**1.68**								
Vertigo antivertigo												
Euconulus praticola			*12*									
Humid & Wet total	**1**	**5.56**	**12**	**1.68**	**0**	**0.00**	**0**	**0.00**	**0**	**0.00**	**0**	**0.00**
TOTAL	***18***	***100.00***	***715***	***100.00***	***6***	***100.00***	***13***	***100.00***	***9***	***100.00***	***267***	***100.00***

sample ID	10-5	10-5	10-5	10-5	10-6	10-6	10-6	10-6	10-7	10-7	10-7	10-7
	S n	S %	I n	I %	S n	S %	I n	I %	S n	S %	I n	I %
Species/Preferred Type of Habitat												
W									**2**	**9.09**	**2**	**0.40**
Acanthinula aculeata												
Ena montana											*1*	
Discus ruderatus												
Aegopinella nitens												
Aegopis verticillus												
Limax sp.												
Ruthenica filograna											*1*	
Semilimax kotulae												
Helicodonta obvoluta												
Monachoides incarnatus												
cf. Bulgarica cana												
Causa holosericea												
Wf	**1**	**7.69**	**3**	**2.11**	**1**	**14.29**	**1**	**4.35**	**1**	**4.55**	**43**	**8.67**
Orcula dolium												
Vertigo alpestris												
Clausilia dubia			*3*				*1*				*43*	
W(Wf)												
Helicigona lapicida												
W(Ws)									**1**	**4.55**	**2**	**0.40**
Vertigo pusilla											*2*	
Wh												
Perforatella bidentata												
Ws(S)												
Euomphalia strigella												
Ws(Of)												
Milacidae (cf., Schaelchen)												
W, Ws(M)												
Helix pomatia												
W(M)					**1**	**14.29**	**1**	**4.35**	**3**	**13.64**	**12**	**2.42**
Balea biplicata												
Discus rotundatus												
Vitrea crystallina											*2*	
Euconulus fulvus												
Nesovitrea hammonis							*1*				*9*	
Fruticicola fruticum												
Arianta arbustorum											*1*	
W(H)									**1**	**4.55**	**1**	**0.20**
Vertigo substriata											*1*	
Semilimax semilimax												
Petasina unidentata												
Trochulus suberectus												
Woodland total	**1**	**7.69**	**3**	**2.11**	**2**	**28.57**	**2**	**8.70**	**8**	**36.36**	**60**	**12.10**
S(Sf)	**2**	**15.38**	**46**	**32.39**	**2**	**28.57**	**13**	**56.52**	**3**	**13.64**	**267**	**53.83**
Pupilla triplicata			*37*				*12*				*224*	
Pupilla sterrii			*9*				*1*				*42*	
Granaria frumentum											*1*	
SX												
Chondrula tridens												

sample ID	10-5	10-5	10-5	10-5	10-6	10-6	10-6	10-6	10-7	10-7	10-7	10-7
	S n	S %	I n	I %	S n	S %	I n	I %	S n	S %	I n	I %
X												
Monacha cartusiana												
X(Sf)												
Cochlicopa lubricella												
Cochlicopa cf. *lubricella*												
Xeric total	**2**	**15.38**	**46**	**32.39**	**2**	**28.57**	**13**	**56.52**	**3**	**13.64**	**267**	**53.83**
O	**4**	**30.77**	**14**	**9.86**					**4**	**18.18**	**17**	**3.43**
Vallonia tenuilabris			2								2	
Vertigo modesta arctica												
Vertigo parcedentata			2								1	
Pupilla alpicola densegyrata												
Pupilla muscorum			1								3	
Pupilla muscorum vel alpicola densegyrata												
Pupilla loessica												
Pupilla sp., apices			9								11	
Pupilla sp. juv.												
Vertigo pygmaea												
Vertiginidae indet.												
O(Of)					**1**	**14.29**	**1**	**4.35**	**1**	**4.55**	**6**	**1.21**
Columella columella							1				6	
O(Ws)	**1**	**7.69**	**35**	**24.65**	**1**	**14.29**	**6**	**26.09**	**1**	**4.55**	**102**	**20.56**
Vallonia costata			35				6				102	
O(X)	**1**	**7.69**	**1**	**0.70**					**1**	**4.55**	**2**	**0.40**
Truncatellina cylindrica			*1*								*2*	
O(H)												
Vallonia pulchella												
Open total	**6**	**46.15**	**50**	**35.21**	**2**	**28.57**	**7**	**30.43**	**7**	**31.82**	**127**	**25.60**
M	**1**	**7.69**	**32**	**22.54**	**1**	**14.29**	**1**	**4.35**	**1**	**4.55**	**23**	**4.64**
Limacoidea												
Trochulus hispidus			*32*				*1*				*23*	
Mf												
Clausilia rugosa parvula												
M(W)	**1**	**7.69**	**3**	**2.11**					**1**	**4.55**	**1**	**0.20**
Punctum pygmaeum			*3*								*1*	
M(X)	**1**	**7.69**	**7**	**4.93**					**1**	**4.55**	**15**	**3.02**
Succinella oblonga			*7*								*15*	
Succinella oblonga >f. *elongata*												
M(P)												
Deroceras sp.												
Deroceras sp. 1												
Deroceras sp. 2												
Deroceras sp. 3												
Mesic total	**3**	**23.08**	**42**	**29.58**	**1**	**14.29**	**1**	**4.35**	**3**	**13.64**	**39**	**7.86**
H												

sample ID	10-5	10-5	10-5	10-5	10-6	10-6	10-6	10-6	10-7	10-7	10-7	10-7
	S n	S %	I n	I %	S n	S %	I n	I %	S n	S %	I n	I %
Nesovitrea petronella												
H(M)												
Cochlicopa lubrica												
P	**1**	**7.69**	**1**	**0.70**					**1**	**4.55**	**3**	**0.60**
Vertigo antivertigo												
Euconulus praticola			*1*								*3*	
Humid & Wet total	**1**	**7.69**	**1**	**0.70**	**0**	**0.00**	**0**	**0.00**	**1**	**4.55**	**3**	**0.60**
TOTAL	***13***	***100.00***	***142***	***100.00***	***7***	***100.00***	***23***	***100.00***	***22***	***100.00***	***496***	***100.00***

sample ID	10-8	10-8	10-8	10-8	06-1	06-1	06-1	06-1	06-2	06-2	06-2	06-2
	S n	S %	I n	I %	S n	S %	I n	I %	S n	S %	I n	I %
Species/Preferred Type of Habitat												
W	**1**	**5.56**	**1**	**0.55**	**3**	**10.71**	**9**	**2.13**	**7**	**25.93**	**10**	**3.42**
Acanthinula aculeata											*1*	
Ena montana											*2*	
Discus ruderatus							*3*					
Aegopinella nitens												
Aegopis verticillus											*1*	
Limax sp.												
Ruthenica filograna							*1*				*1*	
Semilimax kotulae			*1*				*5*				*2*	
Helicodonta obvoluta											*2*	
Monachoides incarnatus											*1*	
cf. Bulgarica cana												
Causa holosericea												
Wf	**1**	**5.56**	**11**	**6.08**	**2**	**7.14**	**53**	**12.56**	**2**	**7.41**	**24**	**8.22**
Orcula dolium							*4*					
Vertigo alpestris											*1*	
Clausilia dubia			*11*				*49*				*23*	
W(Wf)									**1**	**3.70**	**1**	**0.34**
Helicigona lapicida											*1*	
W(Ws)												
Vertigo pusilla												
Wh												
Perforatella bidentata												
Ws(S)					**1**	**3.57**	**5**	**1.18**	**1**	**3.70**	**2**	**0.68**
Euomphalia strigella							*5*				*2*	
Ws(Of)												
Milacidae (cf., Schaelchen)												
W, Ws(M)												
Helix pomatia												
W(M)	**2**	**11.11**	**3**	**1.66**	**5**	**17.86**	**65**	**15.40**	**5**	**18.52**	**39**	**13.36**
Balea biplicata												
Discus rotundatus											*1*	
Vitrea crystallina							*43*				*11*	
Euconulus fulvus							*1*					
Nesovitrea hammonis			*2*				*4*				*15*	
Fruticicola fruticum							*3*				*3*	
Arianta arbustorum			*1*				*14*				*9*	
W(H)					**2**	**7.14**	**11**	**2.61**	**2**	**7.41**	**6**	**2.05**
Vertigo substriata							*2*					
Semilimax semilimax											*2*	
Petasina unidentata												
Trochulus suberectus							*9*				*4*	
Woodland total	**4**	**22.22**	**15**	**8.29**	**13**	**46.43**	**143**	**33.89**	**18**	**66.67**	**82**	**28.08**
S(Sf)	**2**	**11.11**	**89**	**49.17**	**3**	**10.71**	**54**	**12.80**	**3**	**11.11**	**32**	**10.96**
Pupilla triplicata			*29*				*36*				*27*	
Pupilla sterrii			*60*				*17*				*3*	
Granaria frumentum							*1*				*2*	
SX	**1**	**5.56**	**1**	**0.55**	**1**	**3.57**	**1**	**0.24**				
Chondrula tridens			*1*				*1*					

sample ID	10-8	10-8	10-8	10-8	06-1	06-1	06-1	06-1	06-2	06-2	06-2	06-2
	S n	S %	I n	I %	S n	S %	I n	I %	S n	S %	I n	I %
X												
Monacha cartusiana												
X(Sf)					**1**	**3.57**	**4**	**0.95**				
Cochlicopa lubricella							*4*					
Cochlicopa cf. *lubricella*												
Xeric total	**3**	**16.67**	**90**	**49.72**	**5**	**17.86**	**59**	**13.98**	**3**	**11.11**	**32**	**10.96**
O	**3**	**16.67**	**12**	**6.63**	**2**	**7.14**	**2**	**0.47**	**2**	**7.41**	**17**	**5.82**
Vallonia tenuilabris							1				5	
Vertigo modesta arctica												
Vertigo parcedentata			3									
Pupilla alpicola densegyrata												
Pupilla muscorum			1				1				5	
Pupilla muscorum vel alpicola densegyrata												
Pupilla loessica												
Pupilla sp., apices			8								7	
Pupilla sp. juv.												
Vertigo pygmaea												
Vertiginidae indet.												
O(Of)	**1**	**5.56**	**7**	**3.87**	**1**	**3.57**	**1**	**0.24**				
Columella columella			7				1					
O(Ws)	**1**	**5.56**	**16**	**8.84**	**1**	**3.57**	**37**	**8.77**	**1**	**3.70**	**20**	**6.85**
Vallonia costata			16				37				20	
O(X)	**1**	**5.56**	**1**	**0.55**								
Truncatellina cylindrica			*1*									
O(H)												
Vallonia pulchella												
Open total	**6**	**33.33**	**36**	**19.89**	**4**	**14.29**	**40**	**9.48**	**3**	**11.11**	**37**	**12.67**
M	**1**	**5.56**	**27**	**14.92**	**1**	**3.57**	**149**	**35.31**	**1**	**3.70**	**105**	**35.96**
Limacoidea												
Trochulus hispidus			*27*				*149*				*105*	
Mf												
Clausilia rugosa parvula												
M(W)					**1**	**3.57**	**4**	**0.95**				
Punctum pygmaeum							*4*					
M(X)	**2**	**11.11**	**8**	**4.42**	**1**	**3.57**	**15**	**3.55**	**1**	**3.70**	**30**	**10.27**
Succinella oblonga			*7*				*15*				*30*	
Succinella oblonga >f. *elongata*			*1*									
M(P)	**1**	**5.56**	**1**	**0.55**	**2**	**7.14**	**4**	**0.95**				
Deroceras sp.			*1*									
Deroceras sp. 1							*3*					
Deroceras sp. 2							*1*					
Deroceras sp. 3												
Mesic total	**4**	**22.22**	**36**	**19.89**	**5**	**17.86**	**172**	**40.76**	**2**	**7.41**	**135**	**46.23**
H												

sample ID	10-8	10-8	10-8	10-8	06-1	06-1	06-1	06-1	06-2	06-2	06-2	06-2
	S n	S %	I n	I %	S n	S %	I n	I %	S n	S %	I n	I %
Nesovitrea petronella												
H(M)					**1**	**3.57**	**8**	**1.90**	**1**	**3.70**	**6**	**2.05**
Cochlicopa lubrica							*8*				*6*	
P	**1**	**5.56**	**4**	**2.21**								
Vertigo antivertigo												
Euconulus praticola			*4*									
Humid & Wet total	**1**	**5.56**	**4**	**2.21**	**1**	**3.57**	**8**	**1.90**	**1**	**3.70**	**6**	**2.05**
TOTAL	***18***	***100.00***	***181***	***100.00***	***28***	***100.00***	***422***	***100.00***	***27***	***100.00***	***292***	***100.00***

sample ID	06-3	06-3	06-3	06-3	06-4	06-4	06-4	06-4	06-5	06-5	06-5	06-5
	S n	S %	I n	I %	S n	S %	I n	I %	S n	S %	I n	I %
Species/Preferred Type of Habitat												
W	**5**	**15.15**	**7**	**1.17**	**7**	**20.00**	**12**	**3.08**	**8**	**22.86**	**11**	**3.68**
Acanthinula aculeata												
Ena montana			*1*								*1*	
Discus ruderatus							*1*				*1*	
Aegopinella nitens											*1*	
Aegopis verticillus			*1*				*3*				*1*	
Limax sp.												
Ruthenica filograna			*1*				*1*				*2*	
Semilimax kotulae			*1*				*1*					
Helicodonta obvoluta			*3*				*4*				*2*	
Monachoides incarnatus							*1*				*1*	
cf. Bulgarica cana											*2*	
Causa holosericea							*1*					
Wf	**2**	**6.06**	**54**	**9.03**	**2**	**5.71**	**63**	**16.15**	**2**	**5.71**	**43**	**14.38**
Orcula dolium			*4*				*6*				*5*	
Vertigo alpestris												
Clausilia dubia			*50*				*57*				*38*	
W(Wf)									**1**	**2.86**	**1**	**0.33**
Helicigona lapicida											*1*	
W(Ws)					**1**		**1**					
Vertigo pusilla							*1*					
Wh									**1**	**2.86**	**2**	**0.67**
Perforatella bidentata											*2*	
Ws(S)	**1**	**3.03**	**9**	**1.51**	**1**	**2.86**	**19**	**4.87**	**1**	**2.86**	**17**	**5.69**
Euomphalia strigella			*9*				*19*				*17*	
Ws(Of)					**1**	**2.86**	**1**	**0.26**				
Milacidae (cf., Schaelchen)							*1*					
W, Ws(M)	**1**	**3.03**	**1**	**0.17**								
Helix pomatia			*1*									
W(M)	**4**	**12.12**	**26**	**4.35**	**6**	**17.14**	**30**	**7.69**	**4**	**11.43**	**16**	**5.35**
Balea biplicata							*1*					
Discus rotundatus												
Vitrea crystallina			*11*				*7*				*1*	
Euconulus fulvus							*2*					
Nesovitrea hammonis			*4*				*10*				*1*	
Fruticicola fruticum			*1*				*2*				*2*	
Arianta arbustorum			*10*				*8*				*9*	
W(H)	**1**	**3.03**	**6**	**1.00**	**2**	**5.71**	**15**	**3.85**	**2**	**5.71**	**10**	**3.34**
Vertigo substriata												
Semilimax semilimax												
Petasina unidentata							*4*				*3*	
Trochulus suberectus			*6*				*11*				*7*	
Woodland total	**14**	**42.42**	**103**	**17.22**	**20**	**57.14**	**141**	**36.15**	**19**	**54.29**	**100**	**33.44**
S(Sf)	**2**	**6.06**	**191**	**31.94**	**2**	**5.71**	**56**	**14.36**	**2**	**5.71**	**48**	**16.05**
Pupilla triplicata			*174*				*48*				*42*	
Pupilla sterrii			*17*				*8*				*6*	
Granaria frumentum												
SX	**1**	**3.03**	**2**	**0.33**	**1**	**2.86**	**2**	**0.51**	**1**	**2.86**	**1**	**0.33**
Chondrula tridens			*2*				*2*				*1*	

sample ID	06-3	06-3	06-3	06-3	06-4	06-4	06-4	06-4	06-5	06-5	06-5	06-5
	S n	S %	I n	I %	S n	S %	I n	I %	S n	S %	I n	I %
X					**1**	**2.86**	**3**	**0.77**				
Monacha cartusiana							*3*					
X(Sf)	**1**	**3.03**	**1**	**0.17**					**1**	**2.86**	**4**	**1.34**
Cochlicopa lubricella			*1*									
Cochlicopa cf. *lubricella*											*4*	
Xeric total	**4**	**12.12**	**194**	**32.44**	**4**	**11.43**	**61**	**15.64**	**4**	**11.43**	**53**	**17.73**
O	**6**	**18.18**	**34**	**5.69**	**3**	**8.57**	**9**	**2.31**	**4**	**11.43**	**6**	**2.01**
Vallonia tenuilabris			7				2				1	
Vertigo modesta arctica												
Vertigo parcedentata			2									
Pupilla alpicola densegyrata			2								1	
Pupilla muscorum			9				6				2	
Pupilla muscorum vel alpicola densegyrata												
Pupilla loessica			1									
Pupilla sp., apices			8									
Pupilla sp. juv.												
Vertigo pygmaea			5				1					
Vertiginidae indet.											*2*	
O(Of)	**1**	**3.03**	**3**	**0.50**	**1**	**2.86**	**8**	**2.05**	**1**	**2.86**	**3**	**1.00**
Columella columella			3				8				3	
O(Ws)	**1**	**3.03**	**96**	**16.05**	**1**	**2.86**	**46**	**11.79**	**1**	**2.86**	**41**	**13.71**
Vallonia costata			96				46				41	
O(X)												
Truncatellina cylindrica												
O(H)									**1**	**2.86**	**1**	**0.33**
Vallonia pulchella											*1*	
Open total	**8**	**24.24**	**133**	**22.24**	**5**	**14.29**	**63**	**16.15**	**7**	**20.00**	**51**	**17.06**
M	**1**	**3.03**	**58**	**9.70**	**1**	**2.86**	**59**	**15.13**	**1**	**2.86**	**47**	**15.72**
Limacoidea												
Trochulus hispidus			*58*				*59*				*47*	
Mf	**1**	**3.03**	**1**	**0.17**								
Clausilia rugosa parvula			*1*									
M(W)	**1**	**3.03**	**1**	**0.17**	**1**	**2.86**	**1**	**0.26**	**1**	**2.86**	**1**	**0.33**
Punctum pygmaeum			*1*				*1*				*1*	
M(X)	**1**	**3.03**	**100**	**16.72**	**1**	**2.86**	**54**	**13.85**	**1**	**2.86**	**42**	**14.05**
Succinella oblonga			*100*				*54*				*42*	
Succinella oblonga >f. *elongata*												
M(P)	**1**	**3.03**	**2**	**0.33**	**2**	**5.71**	**5**	**1.28**	**1**	**2.86**	**3**	**1.00**
Deroceras sp.												
Deroceras sp. 1			*2*				*4*					
Deroceras sp. 2							*1*				*3*	
Deroceras sp. 3												
Mesic total	**5**	**15.15**	**162**	**27.09**	**5**	**14.29**	**119**	**30.51**	**4**	**11.43**	**93**	**31.10**
H												

sample ID	06-3	06-3	06-3	06-3	06-4	06-4	06-4	06-4	06-5	06-5	06-5	06-5
	S n	S %	I n	I %	S n	S %	I n	I %	S n	S %	I n	I %
Nesovitrea petronella												
H(M)	**1**	**3.03**	**4**	**0.67**	**1**	**2.86**	**6**	**1.54**	**1**	**2.86**	**2**	**0.67**
Cochlicopa lubrica			*4*				*6*				*2*	
P	**1**	**3.03**	**2**	**0.33**								
Vertigo antivertigo												
Euconulus praticola			*2*									
Humid & Wet total	**2**	**6.06**	**6**	**1.00**	**1**	**2.86**	**6**	**1.54**	**1**	**2.86**	**2**	**0.67**
TOTAL	***33***	***100.00***	***598***	***100.00***	***35***	***100.00***	***390***	***100.00***	***35***	***100.00***	***299***	***100.00***

sample ID	06-6	06-6	06-6	06-6
	S n	S %	I n	I %
Species/Preferred Type of Habitat				
W	**4**	**13.79**	**4**	**0.29**
Acanthinula aculeata				
Ena montana				
Discus ruderatus			*1*	
Aegopinella nitens				
Aegopis verticillus				
Limax sp.				
Ruthenica filograna			*1*	
Semilimax kotulae				
Helicodonta obvoluta				
Monachoides incarnatus			*1*	
cf. Bulgarica cana			*1*	
Causa holosericea				
Wf	**2**	**6.90**	**33**	**2.36**
Orcula dolium			*9*	
Vertigo alpestris				
Clausilia dubia			*24*	
W(Wf)				
Helicigona lapicida				
W(Ws)				
Vertigo pusilla				
Wh	**1**	**3.45**	**2**	**0.14**
Perforatella bidentata			*2*	
Ws(S)	**1**	**3.45**	**2**	**0.14**
Euomphalia strigella			*2*	
Ws(Of)				
Milacidae (cf., Schaelchen)				
W, Ws(M)				
Helix pomatia				
W(M)	**5**	**17.24**	**32**	**2.29**
Balea biplicata				
Discus rotundatus				
Vitrea crystallina			*7*	
Euconulus fulvus			*3*	
Nesovitrea hammonis			*12*	
Fruticicola fruticum			*5*	
Arianta arbustorum			*5*	
W(H)	**1**	**3.45**	**17**	**1.22**
Vertigo substriata				
Semilimax semilimax				
Petasina unidentata				
Trochulus suberectus			*17*	
Woodland total	**14**	**48.28**	**90**	**6.43**
S(Sf)	**2**	**6.90**	**419**	**29.95**
Pupilla triplicata			*409*	
Pupilla sterrii			*10*	
Granaria frumentum				
SX				
Chondrula tridens				

sample ID	06-6	06-6	06-6	06-6
	S n	S %	I n	I %
X				
Monacha cartusiana				
X(Sf)				
Cochlicopa lubricella				
Cochlicopa cf. *lubricella*				
Xeric total	**2**	**6.90**	**419**	**29.95**
O	**3**	**10.34**	**50**	**3.57**
Vallonia tenuilabris			2	
Vertigo modesta arctica				
Vertigo parcedentata			1	
Pupilla alpicola densegyrata				
Pupilla muscorum			47	
Pupilla muscorum vel alpicola densegyrata				
Pupilla loessica				
Pupilla sp., apices				
Pupilla sp. juv.				
Vertigo pygmaea				
Vertiginidae indet.				
O(Of)	**1**	**3.45**	**2**	**0.14**
Columella columella			2	
O(Ws)	**1**	**3.45**	**231**	**16.51**
Vallonia costata			231	
O(X)	**1**	**3.45**	**1**	**0.07**
Truncatellina cylindrica			*1*	
O(H)				
Vallonia pulchella				
Open total	**6**	**20.69**	**284**	**20.30**
M	**1**	**3.45**	**446**	**31.88**
Limacoidea				
Trochulus hispidus			*446*	
Mf				
Clausilia rugosa parvula				
M(W)	**1**	**3.45**	**3**	**0.21**
Punctum pygmaeum			*3*	
M(X)	**1**	**3.45**	**140**	**10.01**
Succinella oblonga			*140*	
Succinella oblonga >f. *elongata*				
M(P)	**3**	**10.34**	**11**	**0.79**
Deroceras sp.				
Deroceras sp. 1			*2*	
Deroceras sp. 2			*8*	
Deroceras sp. 3			*1*	
Mesic total	**6**	**20.69**	**600**	**42.89**
H				

sample ID	06-6	06-6	06-6	06-6
	S n	S %	I n	I %
Nesovitrea petronella				
H(M)	**1**	**3.45**	**6**	**0.43**
Cochlicopa lubrica			*6*	
P				
Vertigo antivertigo				
Euconulus praticola				
Humid & Wet total	**1**	**3.45**	**6**	**0.43**
TOTAL	***29***	***100.00***	***1399***	***100***

Table S7: Willendorf II – Calibrated age ranges and results of Bayesian age modelling for the lower part of the sequence (D2-D1 to C7-1). Calibration curve: IntCal13 atmospheric curve (31), software: OxCal 4.2.3 (32). All ages in cal BP.

	Calibrated age	68.2% probability	Calibrated age	95.4% probability	Modeled Age	68.2% probability	Modeled age	95.4% probability	Convergence
	from	to	from	to	from	to	from	to	%
Boundary end C7-1					39,669	38,108	40,310	36,240	97.8
GrA-38250	39,531	38,650	40,082	38,336	39,722	38,775	40,249	38,420	99.8
Boundary start C7-1					40,876	39,024	42,208	38,689	99.6
Boundary end C8-2					42,909	41,957	43,154	40,589	99.7
GrA-45012	43,001	42,445	43,328	42,179	42,979	42,497	43,247	42,262	99.9
OxA-23520	43,226	42,504	43,764	42,190	43,048	42,515	43,390	42,253	99.9
Boundary start C8-2					43,489	42,649	44,472	42,411	99.8
Boundary end C8-3					45,009	43,155	46,212	42,767	99.8
modelled AH 3					45,800	43,835	46,721	43,133	99.8
Boundary start C8-3					46,524	44,492	47,316	43,492	99.7
Boundary end D1-D2					47,313	45,835	48,122	45,014	99.6
OxA-25836	47,431	45,562	48,755	44,952	47,616	46,270	48,437	45,729	99.8
OxA-25838	47,644	45,737	48,950	45,130	47,624	46,290	48,450	45,771	99.8
OxA-25837	49,570	47,500	...	46,622	47,804	46,409	48,729	45,927	99.8
Boundary start D1-D2					48,296	46,585	49,588	46,087	96.7

Table S8: Willendorf II – AH3 (2006-2011 excavations): Description of lithic artefacts. For definitions of measurements, terms etc. see (16).

(next 8 pages)

ID	raw material	raw material details	patina	Calcareous sinter	Joint plane	Thermal alteration: presence
WII-M20-1	hornstone	light greyish hornstone, smooth cortex	n/a	Yes	No	Yes
WII-M18-25	hornstone	light greyish hornstone, yellowish-beige cortex	No	Yes	No	No
WII-M20-641	hornstone	light greyish hornstone, yellowish-beige cortex	No	Yes	Yes	No
WII-M20-623	hornstone	light greyish hornstone, yellowish-beige cortex	No	Yes	No	No
WII-M20-647	hornstone	light greyish hornstone, yellowish-beige cortex	No	Yes	No	No
WII-M20-617	silicic limestone	n/a (burned)	n/a	Yes	Yes	Yes
WII-M20-635	hornstone	n/a (burned)	n/a	No	No	Yes
WII-M20-646	silicic limestone	dark reddish silici limestone, rose patina, smooth cortex, many joint planes	Yes	Yes	Yes	No
WII-M20-642	silicic limestone	dark reddish silici limestone, rose patina, smooth cortex, many joint planes	No	Yes	Yes	No
WII-M20-620	silicic limestone	grey-greenish, coarse-grained silicic limestone, smooth cortex	Yes	Yes	Yes	No
WII-M19-1626	silicic limestone	grey-greenish, coarse-grained silicic limestone, smooth cortex	Yes	Yes	No	No
WII-M20-619	silicic limestone	n/a (burned)	n/a	Yes	No	Yes
WII-M20-633	silicic limestone	dark brownish silicic limestone	Yes	Yes	Yes	No
WII-M20-639	silicic limestone	reddish silicic limestone	Yes	No	No	No
WII-M20-640	hornstone	grey-greenish, fine-grained hornstone	Yes	No	No	No
WII-M19-1625	hornstone	grey to dark grey hornstone	Yes	Yes	No	No
WII-M20-606	silicic limestone	dark reddish silici limestone, rose patina, smooth cortex, many joint planes	Yes	Yes	No	No
WII-M20-632	hornstone	blackish, fine-grained hornstone	No	Yes	Yes	No
WII-M19-1618	silicic limestone	n/a (burned)	n/a	No	Yes	Yes
WII-M20-598	hornstone	greenish, fein-grained hornstone, structured cortex, joint planes	Yes	Yes	Yes	No

ID	raw material	raw material details	patina	Calcareous sinter	Joint plane	Thermal alteration: presence
WII-M18-593	silicic limestone	reddish, coarse-grained silicic limestone, light reddish patina	Yes	No	No	No
WII-M20-3	silicic limestone	dark reddish silici limestone, rose patina, smooth cortex, many joint planes	Yes	Yes	Yes	No
WII-M20-847	hornstone	grey to dark grey hornstone	Yes	Yes	No	No
WII-M20-851	hornstone	dark brownish, fine-grained hornstone	Yes	Yes	Yes	No
WII-L18-1127	hornstone	hornstone	Yes	Yes	No	No
WII-L19-3074	hornstone	greyish, fine-grained hornstone, brownish cortex	Yes	No	No	No
WII-L19-3091	silicic limestone	dark reddish silici limestone, rose patina, smooth cortex, many joint planes	Yes	Yes	No	No
WII-L19-3385	silicic limestone	grey-greenish, coarse-grained silicic limestone, smooth cortex	Yes	Yes	Yes	No
WII-L19-3357	silicic limestone	dark reddish silici limestone, rose patina, smooth cortex, many joint planes	Yes	No	No	No
WII-L19-3125	silicic limestone	greenish patinated silicic limestone	Yes	Yes	Yes	No
WII-L19-3964	hornstone	brown-greenish, coarse-grained hornstone, brown cortex	Yes	Yes	No	No
WII-L20-2492	silicic limestone	reddish silicic limestone	Yes	No	No	No

ID	Thermal alteration: type	Dataclass	Cortex	Cortex location	length	width	thickness	weight	Fragmened?
WII-M20-1	irregular breakage surface	flake	1-33%	distal	5.46	9.42	1.59	0.10	Yes
WII-M18-25		core tablet	1-33%	sinistrolateral-partial	29.10	32.29	14.19	12.40	No
WII-M20-641		flake	66-99%	prox+sinistro+dist	29.82	24.20	12.45	7.70	No
WII-M20-623		flake	1-33%	dextrolateral-partial	34.07	29.64	5.30	6.00	No
WII-M20-647		bladelet	33-66%	dextrolateral-complete	18.60	9.80	2.31	0.50	Yes
WII-M20-617	craquelation + irregular breakage surface	flake	33-66%	sinistro+distal	26.38	25.25	14.33	9.10	No
WII-M20-635	craquelation + colour change	thermal shatter	0%		13.44	5.08	2.57	0.10	
WII-M20-646		shatter	0%		17.67	11.44	4.23	0.50	
WII-M20-642		< 10 mm frag	0%		7.65	3.48	2.80	0.10	Yes
WII-M20-620		flake	0%		15.79	14.79	3.42	0.60	Yes
WII-M19-1626		flake	0%		10.41	7.75	2.64	0.10	Yes
WII-M20-619	craquelation + colour change + irregular breakage surface	flake	0%		16.20	22.25	4.97	1.90	Yes
WII-M20-633		flake	66-99%	sinistro+distal+dextro	10.55	13.98	2.88	0.40	No
WII-M20-639		flake	1-33%	proximal	9.40	12.03	2.49	0.30	No
WII-M20-640		bladelet	0%		8.12	4.48	0.89	0.10	Yes
WII-M19-1625		chip	0%		7.06	6.62	1.62	0.10	No
WII-M20-606		< 10 mm frag	0%		9.77	3.94	1.00	0.10	Yes
WII-M20-632		< 10 mm frag	33-66%	distal	5.94	6.98	2.00	0.10	Yes
WII-M19-1618	craquelation + irregular breakage surface + potlids	flake	0%		9.56	13.30	2.19	0.20	Yes
WII-M20-598		flake	1-33%	sinistrolateral-partial	32.21	11.76	6.39	3.00	Yes

ID	Thermal alteration: type	Dataclass	Cortex	Cortex location	length	width	thickness	weight	Fragmened?
WII-M18-593		flake	0%		7.83	12.00	1.45	0.20	Yes
WII-M20-3		flake	0%		27.56	33.44	11.12	6.40	Yes
WII-M20-847		flake	0%		0.01	10.77	1.79	0.20	Yes
WII-M20-851		flake	0%		12.58	18.33	4.05	0.70	Yes
WII-L18-1127		flake	0%		12.29	16.98	2.97	0.50	No
WII-L19-3074		< 10 mm frag	1-33%	n/a	7.89	7.97	2.17	0.10	Yes
WII-L19-3091		flake	0%		18.48	16.95	4.28	1.10	No
WII-L19-3385		shatter	33-66%	n/a	48.63	28.59	19.53	14.50	
WII-L19-3357		chip	0%		4.80	5.07	2.62	0.10	No
WII-L19-3125		shatter	0%		9.97	6.31	2.90	0.30	
WII-L19-3964		flake	1-33%	dextrolateral-complete	15.06	7.94	4.37	0.60	Yes
WII-L20-2492		bladelet	0%		8.60	3.24	1.16	0.10	No

ID	Fragmentation: preserved part	Platform type	Platform shape	Platform width	Platform thickness	dorsal reduction: presence?	dorsal reduction: type	Lip	Cone	Bulb	Bulbar scar
WII-M20-1	distal			0.00	0.00						
WII-M18-25	all	plain	irregular	14.66	6.11	No		Yes	No	Yes	Yes
WII-M20-641	all	indeterminable	irregular	17.82	11.64	Yes	hinged scars	No	No	No	No
WII-M20-623	all	plain	irregular	9.13	3.09	Yes	hinged scars + abrasion	Yes	No	Yes	Yes
WII-M20-647	medial			0.00	0.00						
WII-M20-617	all	plain	irregular	10.44	8.42	n/a		Yes	No	No	No
WII-M20-635				0.00	0.00						
WII-M20-646				0.00	0.00						
WII-M20-642	medial			0.00	0.00						
WII-M20-620	medial			0.00	0.00						
WII-M19-1626	proximal	plain	triangular	5.01	2.64	No		No	No	Yes	No
WII-M20-619	distal			0.00	0.00						
WII-M20-633	all	linear	linear	4.36	0.66	Yes	pointed scars	No	No	Yes	No
WII-M20-639	all	cortical	oval	10.75	1.67	Yes	hinged scars + abrasion	Yes	No	No	No
WII-M20-640	medial			0.00	0.00						
WII-M19-1625	all	punctiform	punctiform	0.00	0.00	No		No	No	Yes	No
WII-M20-606	distal			0.00	0.00						
WII-M20-632	medial			0.00	0.00						
WII-M19-1618	proximal	jointSurface	irregular	8.19	1.72	Yes	abrasion	ventral edge not preserved	ventral edge not preserved	No	ventral edge not preserved
WII-M20-598	distal			0.00	0.00						

ID	Fragmentation: preserved part	Platform type	Platform shape	Platform width	Platform thickness	dorsal reduction: presence?	dorsal reduction: type	Lip	Cone	Bulb	Bulbar scar
WII-M18-593	proximal	linear	linear	3.19	0.46	Yes	abrasion	No	No	No	No
WII-M20-3	distal			0.00	0.00						
WII-M20-847	distal			0.00	0.00						
WII-M20-851	distal			0.00	0.00						
WII-L18-1127	all	indeterminable	oval	9.44	2.12	No		No	No	Yes	No
WII-L19-3074	medial			0.00	0.00						
WII-L19-3091	all	plain	irregular	15.16	3.67	No		Yes	No	No	No
WII-L19-3385				0.00	0.00						
WII-L19-3357	all	indeterminable	indeterminate	0.00	0.00	n/a		Yes	No	No	No
WII-L19-3125				0.00	0.00						
WII-L19-3964	proximal	indeterminable	irregular	3.40	0.78	Yes	hinged scars	No	No	Yes	No
WII-L20-2492	all	linear	linear	2.19	0.35	Yes	pointed scars + abrasion	Yes	No	No	No

ID	Exterior Platform Angle	Distal end: top view	Distal end: lateral view	Number of dorsal scars	Orientation of dorsal scars	Lateralisation (only bladelets)	Torsion (only bladelets)	Cross-section	Edge damage	Modification
WII-M20-1	0	straight	pointed	1	indetermined			triangular	No	No
WII-M18-25	72	convex	pointed	4	intersecting			triangular	Yes	No
WII-M20-641	78	pointed	step	1	indetermined			triangular	No	No
WII-M20-623	78	convex	pointed	4	unipolar			irregular	Yes	No
WII-M20-647	0			1	unipolar	no	no	triangular	No	No
WII-M20-617	68	convex	pointed	1	unipolar			triangular	Yes	No
WII-M20-635	0			0					No	No
WII-M20-646	0			0					No	No
WII-M20-642	0			0	indetermined				No	No
WII-M20-620	0			2	indetermined			n/a	No	No
WII-M19-1626	82			1	unipolar			n/a	No	No
WII-M20-619	0	straight	plunging	0	n/a			irregular	No	No
WII-M20-633	0	convex	hinged	0	n/a			lenticular	Yes	No
WII-M20-639	76	convex	hinged	3	indetermined			triangular	No	No
WII-M20-640	0			3	unipolar	no	no	triangular	Yes	No
WII-M19-1625	0	convex	pointed	0					No	No
WII-M20-606	0	pointed	pointed	2	indetermined			triangular	No	No
WII-M20-632	0			2	indetermined			irregular	No	No
WII-M19-1618	84			3	unipolar			n/a	No	No
WII-M20-598	0	straight	hinged	4	irregular			n/a	No	No

ID	Exterior Platform Angle	Distal end: top view	Distal end: lateral view	Number of dorsal scars	Orientation of dorsal scars	Lateralisation (only bladelets)	Torsion (only bladelets)	Cross-section	Edge damage	Modification
WII-M18-593	0			3	indetermined			irregular	No	No
WII-M20-3	0	irregular	plunging	3	indetermined			irregular	Yes	No
WII-M20-847	0	pointed	pointed	2	indetermined			triangular	No	No
WII-M20-851	0	convex	rounded	2	intersecting			irregular	Yes	No
WII-L18-1127	76	convex	pointed	2	indetermined			triangular	Yes	No
WII-L19-3074	0			1	indetermined			triangular	No	No
WII-L19-3091	76	convex	hinged	5	unipolar			trapezoidal	No	No
WII-L19-3385	0			0					Yes	No
WII-L19-3357	0	convex	pointed	0					No	No
WII-L19-3125	0			0					Yes	No
WII-L19-3964	90			2	unipolar			triangular	Yes	No
WII-L20-2492	0	pointed	pointed	5	unipolar	right	no	trapezoidal	Yes	No

Table S9: Willendorf II –list of micromorphology samples studied here.

Sample-ID	year	square	stratigraphic units/sub-units
06-3	2006	R30	C9, C8-2 (stretched in several lenses)
06-4	2006	M25	C9, C8-2
06-5	2006	N27	D1, C9
06-9	2006	M/N27	C9, C8-2
06-19	2006	L25	C9, C8-2, C7-2
07-26	2007	M20	C7-1
07-27	2007	M19	C6, C7-1, C7-2
07-28	2007	M20	C6, C7-1, C7-2
07-38	2007	N22	D2
09-53	2009	M/N30	D1
10-54	2010	M19	C8-2, C8-3
10-55	2010	M19	C8-2, C8-3
10-62	2010	L20	C8-2, C8-3
10-63	2010	L20	C8-2, C8-3, C9

Table S10: Willendorf II – micromorphology: microstructure, b-fabric, Fe-Mn mottles, recalcification features and relict frost lensing for selected stratigraphic units/sub-units/horizons. Abbreviations: Very few = 0-5%, Few= 5-10%, Common=10-15% of the total thin section area (3 X 7 cm). C=Citomorphc calcite, N=Needle-fiber calcite (lubinite), H=Micritic hypocoatings, I=Micritic infillings.

Stratigraphic Unit	***Sample ID***	***Microstructure***	***b-fabric***	***Fe-Mn Mottles***	***Recalcification features***	***Relict frost lensing (<1mm)***
C6	26	Vermicular/granular	Speckled	Very few	Very few (C,N)	
C6	27	Vermicular/granular	Speckled	None	Very few (C,N)	
C6	28	Vermicular/granular	Speckled	None	Very few (C,N,H)	
C7-1	26	Vermicular/granular	Speckled	Very few	Very few (C,N)	
C7-1	27	Vermicular/granular/massive	Speckled	Very few	Very few (C,N)	
C7-1	28	Vermicular/granular	Speckled	Very few	Very few (C,N,H)	
C8-2	3	Vermicular/granular	Speckled	None	Common (C)	
C8-2	9	Vermicular/granular/crumb	Speckled	None	Very few (C,N,I)	
C8-2	19	Vermicular/granular	Speckled	None	Very few (C,N,H)	
C8-3	54	Vermicular/granular	Speckled	Very few	Very few (N,H)	X
C8-3	55	Vermicular/granular	Speckled	Very few	Very few (N,H)	X
C8-3	62	Vermicular/granular	Speckled	Very few	Very few (N,H)	
C8-3	63	Vermicular/granular	Speckled	Very few	Very few (N,H)	
C9	4-2	Vermicular/granular	Speckled	Very few	Very few (C,N,H,I)	X
C9	5-1	Vermicular/granular	Speckled	None	Very few (H,I)	X
C9	9	Vermicular/granular	Speckled	None	Very few (C,N)	
C9	19	Vermicular/granular	Speckled	Very few	Very few (H,I)	
D1	5-2	Vermicular/granular	Grano-striated	Very few	Common (C,N,H)	X
D1	53	Vermicular/granular	Speckled	Few	Few (H)	
D2	38top	Vermicular/granular	Speckled	Few	Few (C,H)	
D2	38base	Vermicular/granular	Speckled	Few	Few (C,H)	

Table S11: Early Aurignacian ages estimations and proposed start dates for the Auirgnacian/Early Aurignacian in Europe used for comparison in Figure S16. Geißenklöstle calibrated and modeled radiocarbon ages after (42). Geißenklöstle weighted mean of TL ages after (60). All other ages have been calibrated using IntCal13 atmospheric curve (31) and OxCal 4.2.3 software (32).

Models for late appearance of the Aurignacian and Early Aurignacian	**^{14}C age**	**1 sigma**	**Cal age max (cal BP)**	**Cal age min (cal BP)**	**Probability**	**Reference**
appearance of Aurignacian (36.5 ka ± 0.5 BP)	36,500	500	41,926	41,179	68.2 %	(56)
Early Auirgnacian after CI (in H4)			39,446	39,344		(57)
Early Aurignacian after 35 ka BP	35,000		40,541	39,972	68.2 %	(58, 59)
Geißenklöstle AH III – modelled age range			**Cal age max (cal BP)**	**Cal age min (cal BP)**	**Probability**	**Reference**
boundary sterile/AH III (start AH III)			42,940	42,180	68.2 %	(42)
boundary AH III/AH II (end AH III)			41,000	39,910	68.2 %	(42)
Geißenklöstle AH III – TL ages	**TL age**	**1 sigma**	**Cal age max (cal BP)**	**Cal age min (cal BP)**	**Probability**	**Reference**
weighted mean TL AH III	40,200	1,500	41,700	38,700	68.2%	(60)
Peskő – bone tool	**^{14}C age**	**1 sigma**	**Cal age max (cal BP)**	**Cal age min (cal BP)**	**Probability**	**Reference**
OxA-17966 – antler split-based point	36,400	800	41,730	40,265	68.2%	(61)

Table S12: Proto-Aurignacian ages estimations used for comparison in Figure S17.

Site	Layer						Modelled age in cal BP Max	Min	Probability	Reference
Riparo Mochi	G			End boundary for Level G (Transistion H/G)			42,500	41,200	68.2 %	(43)
Riparo Mochi	G			Start boundary for Level G (Transistion H/G)			42,800	41,600	68.2 %	(43)
Fumane	A2			End boundary for Level A2 (Boundary A2/A1)			40,280	39,440	68.2 %	(62)
Fumane	A2			Start boundary for Level A2 (Boundary A3/A2)			41,200	40,450	68.2 %	(62)
Abric Romaní	A			End boundary for Level A (Boundary Transition A/AR1 AR4)			41,750	41,180	68.2 %	(63)
Abric Romaní	A			Start boundary for Lavel A (Boundary Transition Trav AR6 AR3/A)			41,900	41,380	68.2 %	(63)
Les Cottés	US 4 lower			End Boundary for Level US 4 lower			39,490	38,850	68.2 %	(64)
Les Cottés	US 4 lower			Start Boundary for Level US 4 lower			40,390	39,440	68.2 %	(64)
Site	**Layer**				**14C age**	**1 sigma**	**Calibrated age in cal BP Max**	**Min**	**Probability**	**Reference**
Isturitz	C 4c4	bone	UF	weighted mean of 31 targets	37,180	420	42,310	41,684	68.2 %	(66)
Site	**Layer**						**Max**	**Min**	**Probability**	**Reference**
Românești-Dumbrăviţa I	GH3	weighted mean	40,600 ±1,500	TL			42,100	39,100	68.2%	(65)

Table S13: Radiocarbon ages and calibrated ages of directly dated modern human remains used for comparison in Figure S18. If several dates for the same specimen exist, only the oldest one was included. Ages younger than 36,000 cal BP at 68.2% probability are not included. Calibration Curve: IntCal13 atmospheric curve (31), Software: OxCal 4.2.3 (32).

Site	Material/sample	Laboratory nr	^{14}C age	1 sigma	Cal age max	Cal age min	Probability	Reference
Pestera cu Oase	Oase 1	GrA-22810	34,290	+970/-870	40,036	37,610	68.2 %	(*67*)
Buran-Kaya III		OxA-13302	32,790	280	37,208	36,328	68.2 %	(*68*)
Buran-Kaya III		GrA-37938	31,900	+240/-220	36,094	35,549	68.2 %	(*69*)
Kostenki 1, III		OxA-15055	32,070	190	36,195	35,762	68.2 %	(*70*)
Kostenki 14	burial	OxA-X-2395-15	33,250	500	38,211	36,816	68.2 %	(*71*)

Table S14: Radiocarbon ages and calibrated ages of directly dated Neanderthal remains used for comparison in Figure S19. If several dates for the same specimen exist, only the oldest one was included. Ages younger than 36,000 cal BP at 68.2% probability are not included. Calibration Curve: IntCal13 atmospheric curve (31), Software: OxCal 4.2.3 (32).

Site	Material/sample	Laboratory nr	^{14}C age	1 sigma	Cal age max	Cal age min	Probability	Reference
Saint-Césaire, SP 28	Neanderthal tibia	OxA-18099	36,200	750	41,544	40,115	68.2 %	(*44*)
Mezmaiskaya, Layer 2	Mezmaiskaya 2 infant	OxA-21839	39,700	1,100	44,425	42,646	68.2 %	(*46*)
Spy	Spy 646a	GrA-35627	32,970	+200/-190	37,398	36,600	68.2 %	(*72*)
Spy	Spy 589a	OxA-17977	34,700	550	39,825	38,650	68.2 %	(*72*)
Spy	Spy 589a	OxA-21610	33,950	550	39,120	37,630	68.2 %	(*72*)
Spy	Spy 572a	GrA-21546	31,810	250	36,024	35,437	68.2 %	(*73*)
Spy	Spy 737a	OxA-10560	36,250	500	41,391	40,388	68.2 %	(*73*)
Spy	Spy 94a	GrA-32623	35,810	+260/-240	40,775	40,120	68.2 %	(*74*)
Spy	Spy 92b	GrA-32626	36,350	+310/-280	41,351	40,672	68.2 %	(*74*)
Spy	Spy 430a	GrA-32630	33,940	+220/-210	38,712	38,241	68.2 %	(*74*)
Neanderthal	NN 1	ETH-19660	39,240	670	43,601	42,541	68.2 %	(*75*)
Neanderthal	NN 4	ETH-19661	40,360	760	44,611	43,287	68.2 %	(*75*)
Neanderthal	Nean 1	ETH-20981	39,900	620	44,124	43,047	68.2 %	(*75*)
Vindija, Layer G1	9663	OxA-X-2089-06	32,400	800	37,575	35,520	68.2 %	(*76*)
Vindija, Layer G1	9665	OxA-X-2089-07	32,400	1,800	38,794	34,735	68.2 %	(*76*)
Okladnikov	OK 1	OxA-15481	37,800	450	42,424	41,808	68.2 %	(*77*)
Rochers-de-Villeneuve		OxA-15257	45,200	1,100	49,664	47,648	68.2 %	(*78*)
El Sidrón, Layer III	500	Beta-192065	40,840	1,200	45,437	43,327	68.2 %	(*79*)
El Sidrón, Layer III	599a	Beta-192066	37,300	830	42,410	41,120	68.2 %	(*79*)
El Sidrón, Layer III	763a	Beta-192067	38,240	890	43,053	41,779	68.2 %	(*79*)
El Sidrón		GifA-99167	48,500	2,600	52,192	45,980	68.2 %	(*80*)
El Sidrón		GifA-99704	49,200	2,500	52,669	46,785	68.2 %	(*80*)